ELASTICITY OF SOME MANTLE

CRYSTAL STRUCTURES

by

HERBERT FAN WANG

B.A., University of Wisconsin
(1966)

A.M., Harvard University
(1968)

SUBMITTED IN
PARTIAL FULFILLMENT
OF THE REQUIREMENTS FOR THE
DEGREE OF DOCTOR OF PHILOSOPHY

at the

MASSACHUSETTS INSTITUTE OF
TECHNOLOGY

September, 1971

Signature of Author..
   Department of Earth and Planetary Sciences, August 23, 1971

Certified by...
                                Thesis Supervisor

Accepted by...
   Chairman, Departmental Committee on Graduate Students

Elasticity of Some Mantle Crystal Structures

by Herbert Fan Wang

Abstract

The elasticity of high-pressure mantle phases may be characterized by crystal chemically similar compounds. Analogue compounds available as single crystals yield the most reliable elastic constant data. The single-crystal elastic constants of pleonaste and hercynite spinel, rutile-structure germanium dioxide, and spessartite-almandine garnet are studied, in most cases as a function of pressure and temperature. High-pressure phases of olivine, silica, and pyroxene occur in the spinel, rutile, and garnet structures, respectively.

The pressure derivative of the shear mode $(C_{11} - C_{12})/2$ is slightly negative for pleonaste. Small shear moduli pressure derivatives are characteristic of the spinel structure and imply a low kinetic barrier to phase transformations and diffusion. The pleonaste and hercynite elastic constant data determine the compressional and shear velocities as a function of mean atomic weight for the spinel phase of olivine. The compressional velocity data indicate an increase in mean atomic weight in the transition zone while the shear velocity data indicate no increase.

The bulk modulus pressure derivative, $\partial K/\partial P$, of rutile-structure germanium dioxide is about 6.2. It is likely that $\partial K/\partial P$ of stishovite is between 6 and 7. The seismic parameter Φ of stishovite is not well-determined at present and its use in a molar averaging scheme to deduce the iron and silicon content of the lower mantle contains inconsistencies. There is no strong evidence for enrichment of either component in the lower mantle.

The elastic constant pressure derivatives of spessartite-almandine garnet are similar to almandine-pyrope. The elastic velocities of garnet-transformed pyroxenes may be estimated from an inverse proportionality relation between the seismic parameter Φ and mean atomic weight $\bar{M}$. The velocity change over the pyroxene $\rightarrow$ garnet transformation is then 20% for compressional waves and 10% for shear waves.

Thesis Supervisor: Gene Simmons

Title: Professor of Geophysics

Acknowledgments

There would have been no thesis without the single-crystal samples. The pleonaste and hercynite were given to me by Dr. Glen Slack of the General Electric Research and Development Center. The GeO_2 crystal was given to me by Capt. John Goodrum and C. Dugger of the Air Force Cambridge Research Laboratories. Several people contributed to the experimental work. Dr. A. Reid of the NASA Manned Spacecraft Center did the microprobe analyses of the pleonaste and garnet samples. P. McFarlin measured the lattice parameter of the pleonaste sample. J. Kalnajs and E. Farrell of the MIT Crystal Physics Laboratory taught me how to determine precision hydrostatic densities and how to orient my crystals. Dr. E. Papadakis used his equipment at Panametrics, Inc. to measure the elastic constants of the extremely small hercynite sample. A.W. England and D.H. Chung showed me how to use the ultrasonic equipment. D. Silversmith helped me understand some of the subtleties of the equipment via telephone conversations. My advisor, Gene Simmons, gave encouragement and advice from the beginning of the study through the preparation of the manuscript. I had many discussions with D. Weidner and T. Todd. C. Sande and R. Fitterman did typing and organizational work. I thank my wife, Rosemary, for her patience and understanding over the last couple of years.

The experimental costs of my study were absorbed by NASA Contract NAS9-8102. Money is not without value.

Table of Contents

Introduction

I. Introduction.

Laboratory ultrasonic experiments on oxides and silicates provide basic data for the interpretation of seismic velocity profiles in the earth's mantle. The mineral phases hypothesized to be stable in the transition zone and lower mantle are usually not available in quantities sufficient for elasticity experiments. Ultrasonic measurements on compounds which are crystal structure analogues to high pressure mineral phases then become important.

A. Statement of thesis problem.

I studied the single-crystal elastic constants of pleonaste spinel and hercynite spinel (Chapter II), rutile-structure germanium dioxide (Chapter III), and spessartite-almandine garnet (Chapter IV). Ringwood [1970] reviewed the depths where these structures are expected. The major phases of the upper mantle are olivine and pyroxene. Between 300 and 450 km depth pyroxene transforms into the garnet structure and olivine transforms into the spinel structure. At 650 km olivine and pyroxene are expected to further transform, possibly into an isochemical mixture of oxides. The stable form of SiO_2 at this depth would be stishovite which has the rutile structure. If SiO_2 were chemically combined with other oxides, the silicon would probably also be in 6-fold coordination like in stishovite.

Introduction

The new elastic constant data lead to a consideration
of aspects of the following questions: Are negative values
of the pressure derivatives of some shear constants related
to phase transformation or diffusion kinetics? Is there
evidence for iron or silicon enrichment in the lower mantle?
Do density - mean atomic weight - velocity relations fit the
data for spinel, rutile, and garnet structure compounds? Can
the velocities of high-pressure mantle phases be estimated?

B. Background literature.

Two comprehensive review papers [Birch, 1952; Ringwood,
1970] provide the basic background for understanding my
thesis study. Birch [1952] reviewed the application of solid
state physics to the elasticity and constitution of the earth's
interior. He concluded that phase transitions to close-packed
oxides such as periclase, rutile, spinel, or corundum were
required to explain the elasticity of the 400 to 1000 km
depth region of the mantle. Direct confirmation of the impor-
tance of phase transitions was made from high pressure and
high temperature phase studies on silicates and their crystal
chemical analogues [reviewed by Ringwood, 1970]. Other useful
review papers on the constitution of the earth's mantle are
Clark and Ringwood [1964], Ringwood [1966], and D.L. Anderson
et al. [1971].

Introduction

References

Anderson, D.L., C. Sammis, and T. Jordan, Composition and evolution of the mantle and core, Science, 171, 1103-1112, 1971.

Birch, F., Elasticity and constitution of the earth's interior, J. Geophys. Res., 57, 227-286, 1952.

Clark, S.P., Jr., and A.E. Ringwood, Density distribution and constitution of the mantle, Rev. Geophys., 2, 35-88, 1964.

Ringwood, A.E., Mineralogy of the mantle, in Advances in Earth Science, edited by P.M. Hurley, pp. 357-399, MIT Press, Cambridge, 1966.

Ringwood, A.E., Phase transformations and the constitution of the mantle, Phys. Earth Planet. Interiors, 3, 109-155, 1970.

Spinel

II. Elastic constants of pleonaste and hercynite spinel.

Pleonaste and hercynite are iron-bearing spinels [see Deer et al., 1962, Vol. 5, p.62] whose elastic properties are of interest for two reasons: (1) Iron-bearing spinel is present as a minor phase in the upper mantle and (2) Iron-bearing spinel serves as an analogue to the spinel phase of olivine. This chapter emphasizes the analogue aspect, particularly in considering the shear behavior of pleonaste as a function of pressure and the effect of iron substitution in the spinel structure.

A. Sample descriptions.

1. Pleonaste.

The natural pleonaste sample was obtained from Dr. Glen Slack of the General Electric Company. Its location of origin was Queensland, Australia and its surface had a stream-worn appearance before cutting. The pleonaste was black and opaque because of the iron content. The polished faces gave mirror-like reflections and no flaws were visible under 3X magnification.

The microprobe analysis shown in Table II.1 was done by A. Reid of the NASA Manned Spacecraft Center. The weight percentages have been recalculated into the molecular formula $Mg_{0.75}Fe_{0.36}Al_{1.90}O_4$, assuming an ideal four oxygens and neglecting the minor elements. If the titanium is Ti^{4+}, then the iron is all Fe^{2+} since the total charge balance is

Spinel

satisfied almost exactly [see also Slack, 1962, p.430].

The pleonaste spinel is essentially $MgAl_2O_4$ with 25% of the

Mg^{2+} and 5% of the Al^{3+} replaced by Fe^{2+}.

The hydrostatically determined density of the pleonaste

was 3.817 g/cm^3 [for a description of the method see Smakula

and Sils, 1955]. A density of 3.836 g/cm^3 was calculated

from the molecular weight based on the microprobe analysis

of Table II.1 and a lattice parameter of 8.1225 Å. An

average value of 3.826 g/cm^3 was used in the determination

of the elastic constants.

A mean atomic weight of 21.9 was calculated directly

from the formula

$$\bar{M} = (\Sigma(x_i/m_i))^{-1} \qquad \text{(Eqn. II.1)}$$

where x_i = wt. % of oxide

and m_i = mean atomic weight of oxide.

On the other hand $\bar{M} = 21.6$ from the approximate chemical

formula. There is an excess of cations compared to the num-

ber expected for 4 oxygens (Σ cations = 3.03 <u>versus</u> ideal

$\Sigma = 3.00$).

After X-ray orientation the pleonaste sample appeared

as sketched in Fig. II.1. Its weight was 1.234 g, the [100]-

path length was 4.933 mm, and the [110]-path length was

6.645 mm.

Spinel

2. Hercynite, $FeAl_2O_4$.

The hercynite sample was also obtained from Dr. Glen Slack of General Electric. The synthetically grown $FeAl_2O_4$ is actually sample R75 described in Slack [1964]. $FeAl_2O_4$ is basically a normal spinel (Fe^{2+} in tetrahedral sites) but Slack found indications for 15% Fe^{2+} in octahedral sites since annealing at 1200°C introduced some disorder.

The $FeAl_2O_4$ sample came as a rectangular bar about 4 x 4 x 10 mm with all sides {100}-faces. The end face of the bar was X-ray oriented and the bar was cut in half. The end {100}-faces of one-half of the bar were then polished flat and parallel. A pair of 45° cuts were then made on the remaining half of the bar to obtain {110}-faces. The cuts are shown in Fig. II.2. The [100]-path length was 4.104 mm and the [110]-path length was just 1.763 mm.

An X-ray density of 4.280 g/cm³ was calculated from a lattice parameter of 8.140 Å [Slack, 1964]. The mean atomic weight $\bar{M} = 24.8$.

Spinel

B. Experimental method and results.

1. Pleonaste.

The elastic constants of the pleonaste spinel were
measured to 5 kb at room temperature (20 °C) by the pulse-
echo-overlap technique [Papadakis, 1967; Chung et al., 1969].
The pleonaste was oriented to 1/2° with a Laue back-reflection
camera in the [110] and [100]-directions. The two sets of
faces were optically polished flat and parallel to 10^{-4} in/in
by the A.D. Jones Optical Works of Burlington, Mass.

For compressional wave modes, the travel time was only
slightly longer than one microsecond and there was a little
difficulty in damping one echo before the next arrived. Also
since the {110} and {100}-faces were mutually perpendicular
and since there were over fifty echoes in a pulse train,
guided-wave mode effects existed, particularly for compres-
sional waves in the [110]-direction at 20 MHz. The measure-
ments in this direction were done at 30 MHz by driving the
third overtone of a 10 MHz transducer. The guided-wave effect
was reduced enough to select a pair of early, unmodulated
echoes. Papadakis [1969] discussed the precautions to be
taken in the pulse-echo-overlap method when guided-wave
effects are present.

Spinel

On the basis of pressure runs for modes (Table II.2 and Fig. II.3) yielding C_{11}, $C_S = 1/2 \ (C_{11} - C_{12})$, C_{44}, and $C_L = 1/2 \ (C_{11} + C_{12} + 2C_{44})$, the C_{ij} are considered to be accurate to 0.5% and the $\partial C_{ij}/\partial P$ accurate to 5%. Temperature runs to 100 °C were made for the two shear constants C_{44} and C_S. No compressional wave temperature runs were successful due to the short path lengths and bonding difficulties. The $\partial C_{ij}/\partial T$ are considered to be accurate to 10%.

The raw frequency versus pressure data were fitted by a least squares linear relation from which the derivative of the "effective elastic constant" [Thurston, 1965a] was obtained either by computing the elastic constant C_{ij} at different pressures and finding the slope, or by differentiating the expression

$$C_{ij} = 4 \ \rho \ l^2 \ f^2 \qquad \text{(Eqn. II.2)}$$

where ρ = density

l = path length

f = reciprocal round trip travel time

with respect to pressure and evaluating it at P = 0. The adiabatic rather than isothermal bulk modulus was used in calculating $\partial C_{ij}/\partial P$ since the difference does not effect the result within the stated 5% accuracy. Temperature derivatives were obtained by the slope method.

Spinel

The results of the single crystal measurements are
tabulated in Table II.3 and calculated aggregate properties
are tabulated in Table II.4. The $\partial S_{ij}/\partial P$ were calculated
from the matrix relation

$$\frac{\partial S}{\partial X} = - S \frac{\partial C}{\partial X} S \qquad \text{(Eqn. II.3)}$$

[see, for example, Finkbeiner, 1960, Theorem 10.8, p.203].
For the cubic case the $\partial S_{ij}/\partial P$ may be obtained from direct
differentiation of formulas for S_{ij} in terms of the C_{ij}. For
lower symmetries the matrix multiplication method becomes most
convenient [see also Thurston, 1965b]. The alternative would
be to compute $S_{ij} = C_{ij}^{-1}$ as a function of pressure and to
obtain $\partial S_{ij}/\partial P$ by finding the slope. Explicit expressions
become quite messy because of the triple matrix product, and
in fact the expressions for the orthorhombic case given by
Kumazawa and Anderson [1969] are not even dimensionally
correct.

The calculated averages are based on the schemes of
Voigt [1928], Reuss [1929], Hashin and Shtrikman [1962a,
1962b], and Kröner [1967]. The larger of the Hashin-Shtrikman
bounds has been called Hashin and the smaller Shtrikman. The
calculated averages for the derivatives are to be considered
simply as the derivatives of the zero pressure formulas
[see Chung, 1967 for "Voigt" and "Reuss" applications to
cubic, hexagonal, trigonal, and tetragonal symmetries] and not

Spinel

an extension of these averaging methods to third order

elastic constants [Barsch, 1968; Hamilton and Parrott, 1968].

No bounds for these derivative averages are implied [for a

discussion see Knopoff and Shapiro, 1969].

2. Hercynite, $FeAl_2O_4$.

Because of the extremely small size of the $FeAl_2O_4$

sample combined with relatively high velocities, the rf-

pulse-echo-overlap method of the previous section could not be

used. The rf-pulse had a nominal 0.5 μsec width but in prac-

tice it was difficult to resolve echoes separated by less than

1.0 μsec. For the longitudinal mode in the [100]-direction,

echoes were separated by about 0.4 μsec.

The velocity measurements were made by E. Papadakis of

Panametrics, Inc., Waltham, Mass. by a digital-pulse-echo-

overlap method using an assembly containing a highly damped

20 MHz ceramic transducer and fused quartz delay line. The

digital pulse width was 25 nsec, which was equivalent to one-

half the transducer resonance width. Echoes every 0.4 μsec

were then clearly resolved and overlapped (Fig. II.4). Mea-

surements were made for all modes shown in Table II.2. The

[110]-direction measurements were more reliable since some

phasing effects occurred in the [100]-direction. Cross checks

were good to 1% and the C_{ij} are considered to be accurate to

1%. The single crystal and calculated aggregate values for

$FeAl_2O_4$ are given in Table II.5.

Spinel

C.   Comparison with other experimental and theoretical work.

Current experimental and theoretical interest exists for the elastic constants of spinel structure compounds, and particularly for various stoichiometries of $MgO:xAl_2O_3$ spinels (Table II.6). Because stoichiometric spinels (x = 1.0) are more difficult to grow, only room condition values for the elastic constants [Lewis, 1966] are presently available. However, during the preparation of this chapter O'Connell and Graham [1971] published an abstract on the elastic constants of stoichiometric spinel to 800 °K and 8 kb. Another paper on the pressure dependence of the elastic constants of stoichiometric spinel is in preparation by Chang and Barsch [Chang, personal communication].

Theoretical work on the elasticity of $MgAl_2O_4$ includes a Born model calculation for the pressure dependence of the elastic constants [Sammis, 1970] and an 11-parameter rigid ion model calculation for both acoustic and optic frequency modes as a function of pressure [Striefler and Barsch, 1971 (abstract)]. Also an oxygen framework model [Leibfried, 1955; O.L. Anderson, 1965; Gieske and Barsch, 1968] may be considered for spinels.

Spinel

1. Effect of stoichiometry.

The elastic constants of the stoichiometric $MgO:1.0Al_2O_3$ are 5 to 10% lower than those with excess alumina xAl_2O_3 $(2.6 \leq x \leq 3.5)$. The elastic constants of the non-stoichiometric spinels agree to 1%.

Suppose the differences between the elastic constants of the stoichiometric and non-stoichiometric spinels are due only to the difference in density. That is, apply a law of corresponding states [O.L. Anderson, 1966] and consider $MgO:2.6Al_2O_3$ $(\rho = 3.62 \text{ g/cm}^3)$ to be $MgO:1.0Al_2O_3$ $(\rho = 3.58 \text{ g/cm}^3)$ compressed 20.2 kb. Decompressing the $MgO:2.6Al_2O_3$ to $\rho = 3.58$ g/cm^3 gives the following values for the elastic constants compared to those for stoichiometric $MgO:1.0Al_2O_3$. Schreiber's [1967] values for the pressure derivatives of the elastic constants of $MgO:2.6Al_2O_3$ are used.

"Decompressed" $MgO:1.0Al_2O_3$
$MgO:2.6Al_2O_3$

$K \quad = 1.935$ Mb $K \quad = 1.950$ Mb

$C_S \quad = 0.716$ Mb $C_S \quad = 0.630$ Mb

$C_{44} = 1.559$ Mb $C_{44} = 1.530$ Mb

where K = bulk modulus

and $C_S = 1/2 \ (C_{11} - C_{12})$

Spinel

The bulk modulus K has been slightly over corrected and the shear moduli C_S and C_{44} have been more significantly under corrected. In other words an excess alumina spinel cannot be regarded as a compressed stoichiometric one, particularly for the shear moduli.

The excess Al_2O_3 structure results in additional cation vacancies in order to maintain charge neutrality within the nearly perfect cubic close packed arrangement of the oxygen anions (Fig. II.5). Jagodzinski and Saalfeld [1958] determined the deviation from a cubic close packed oxygen lattice for natural and synthetic spinels of various $MgO:Al_2O_3$ ratios (Table II.7). The distortion of the cubic close packed oxygen lattice becomes smaller with increasing excess Al_2O_3. Thus on a crystallographic structure basis the non-stoichiometric spinel is expected to be weaker in bulk modulus because of more cation vacancies, yet stronger in shear because there is less distortion of the oxygen framework than a law of corresponding states with stoichiometric spinel would indicate.

2. Born model.

The last line of Table II.6 shows the results of a Born model lattice calculation for the pressure dependence of the elastic constants made by Sammis [1970] who used the method of homogeneous static deformations due to Fuchs [1936]. The

Spinel

elastic energy density was written as the sum of the electro-static energy and the repulsive energy. The repulsive term between nearest neighbors was of the form $\lambda \exp(-r/\rho)$ where λ and ρ were parameters determined from the bulk modulus and lattice parameter (note that ρ is not the density here). Sammis claimed consistency was found in determining the four repulsive parameters for the Mg - O and Al - O interactions from the bulk moduli and lattice parameters of MgO, Al_2O_3, and $MgAl_2O_4$. Two additional adjustable parameters were the shear moduli Madelung constants arising from the electrostatic forces present in a shear static deformation. Their values were chosen to fit the zero pressure moduli.

One feature of Sammis' calculation was that at some pressure greater than 400 kb, $\partial C_{44}/\partial P$ became negative while evidently $\partial C_S/\partial P$ remained positive since no mention was made of it. Since $\partial C_S/\partial P$ is negative for pleonaste while $\partial C_{44}/\partial P$ is about 0.8 for both pleonaste and $MgO:2.6Al_2O_3$, it seems more likely that at high pressure $\partial C_S/\partial P$ will be nega-tive for $MgAl_2O_4$ rather than $\partial C_{44}/\partial P$. Note in Table II.6 that the theoretical $\partial C_S/\partial P$ is greater than $\partial C_{44}/\partial P$, while the inequality is just the other way around for both $MgO:2.6Al_2O_3$ and pleonaste. $\partial C_S/\partial P$ will become negative for $MgAl_2O_4$ when $P \simeq 150$ kb on the assumption it becomes negative when $MgAl_2O_4$ is compressed to the density of pleonaste.

Spinel

3. Oxygen framework model.

Another theoretical approach is to calculate the elastic properties on the assumption that they are determined by the cubic close packed framework of oxygen anions [O.L. Anderson, 1965]. The theory [Leibfried, 1955] predicts ratios C_{ij}/K and $(\partial C_{ij}/\partial P)/(\partial K/\partial P)$. The oxygen framework scheme was applied to Al_2O_3 and MgO by Gieske and Barsch [1968], to Mg_2SiO_4 (olivine) by Graham and Barsch [1969], and to ortho-pyroxene by Frisillo and Barsch [1971].

For the cubic close packing of spinel define $A_{11} = 3/2$, $A_{12} = 3/4$, and $A_{44} = 3/4$, where the A_{ij} have the same matrix properties as the cubic symmetry elastic constants C_{ij}. Then $C_{ij} = K A_{ij}$ and $\partial C_{ij}/\partial P = (\partial K/\partial P) A_{ij}$. First the effective elastic constant derivatives must be converted into thermodynamic elastic constant derivatives [Thurston, 1965a]. The predicted and measured values are shown in Table II.8. As in the previous comparisons on Al_2O_3, MgO, and Mg_2SiO_4, the predicted zero pressure ratios are fairly good for pleonaste ($\pm 10\%$) and excellent for $MgO:2.6Al_2O_3$ ($\pm 4\%$). The agreement of the predicted pressure derivatives corresponds except for a 50% deviation in $(\partial C_{44}/\partial P)/(\partial K/\partial P)$. The lack of agreement can be attributed to many-body forces and the influence of the cations [Gieske and Barsch, 1968].

Spinel

4. Critique of theoretical models.

Though the Born type or oxygen framework lattice calculations based on nearest neighbor interactions yield zeroth order and qualitative results, predictions for pressure derivatives are unreliable. At present, too little is known about solving the full quantum mechanical problem of complex oxides (or "simple" oxides such as MgO [La and Barsch, 1968]). The differences between the experimental and theoretical results indicate the difficulty. Semi-empirical factors to simulate such phenomena as many-body and exchange forces lead to results for which there are no theoretical means of distinguishing between right and wrong results. The reader is also referred to a recent paper by Leigh et al. [1971]. The paper concluded that experimental lattice frequency determinations are never sufficient to determine the atomic force constants uniquely.

Spinel

D.   Lattice modes, crystal stability, and phase transformations.

Shock wave studies on $MgAl_2O_4$ imply that it has undergone
a transition by 700 kb to a phase 2 to 9% denser than an iso-
chemical mixture of MgO and Al_2O_3 [D.L. Anderson and Kanamori,
1968; Ahrens et al., 1969; and Davies and D.L. Anderson, 1971].
The high pressure phase has been interpreted as $MgAl_2O_4$ going
into a $CaFe_2O_4$ or related structure where the Mg^{2+} becomes
8-coordinated [Reid and Ringwood, 1969, p.206]. Static com-
pression of $FeAl_2O_4$ at 120 kb and 1000 °C [Ringwood and Reid,
1969] yielded FeO and Al_2O_3. Therefore, pleonaste which is
intermediate between these end members in composition can also
be expected to undergo some type of spinel → post-spinel tran-
sition. In this section the nature of the spinel → post-spinel
transition will be interpreted from the available information:
thermochemical data, elastic stability criteria, and shock and
static experiments.

1.   Elastic stability criteria.

First the implications of the negative value for the
pressure derivative $\partial C_S/\partial P = -0.05$ of pleonaste will be dis-
cussed in terms of the crystal's shear stability. With in-
creasing pressure the shear modulus decreases so that the
crystal becomes weaker to a C_S-type shear ($\varepsilon_{11} = -\varepsilon_{22}$; all
other strains equal zero). If the shear modulus C_S were to
decrease to a negative value, then the lattice is unstable

Spinel

since $(C_{11} - C_{12}) < 0$. Discussions of lattice stability and particularly shear stability in terms of the Born criteria [$(C_{11} + 2C_{12}) < 0$, $(C_{11} - C_{12}) < 0$, or $C_{44} < 0$] have been the subject of some recent papers [Thomsen, 1971; O.L. Anderson and Demarest, 1971]. Using his fourth-order anharmonic theory and O'Connell's [1970] $MgO:2.6Al_2O_3$ data, Thomsen concluded that none of the Born criteria will be met before megabar pressures. The magnitude of the negative $\partial C_S/\partial P$ in pleonaste is not large enough to bring C_S to zero until megabar pressures, unless $\partial C_S/\partial P$ becomes increasingly negative with pressure. However, the possibility exists that lattice vibrational modes other than those in the long wavelength and non-dispersive elastic region become negative.

2. A case study: rubidium iodide.

Rubidium iodide transforms from the sodium chloride to cesium chloride structure at a pressure of about 4 kb at 300 °K [see, for example, Pistorius, 1965]. The transition is reviewed since it is instructive on the role of lattice modes [Musgrave, 1970, p.274].

Buerger [1948] suggested from crystallographic considerations a C_{44}-type shear along the [111]-direction as the mechanism for the sodium chloride to cesium chloride transition (Fig. II.6). Daniels and Smith [1963] noted that though

Spinel

a negative $\partial C_{44}/\partial P$ was measured for RbI at room pressure,

its magnitude was such as to decrease the initial value of C_{44}

by only 10% at the observed transition pressure. They

suggested, however, that a transverse acoustic (TA) mode

frequency in the [100]-direction became negative and was the

mechanism of instability. This TA mode would be in the dis-

persive region of the spectrum and hence not observable in

the 10 MHz region of elastic measurements. They schematically

pictured the Brillouin zone-boundary frequency dropping off

more rapidly with pressure than the low frequency acoustic

mode (Fig. II.7).

Hardy and Karo [1965] agreed with this conclusion on the

basis of a lattice dynamical calculation which took into

account next-nearest neighbors and non-central forces.

Saunderson [1966] performed a neutron scattering experiment

on RbI that actually measured these zone-boundary modes as a

function of pressure. The decrease with pressure, however,

was still too small to bring the zone-boundary modes to zero

at the transition pressure.

3. Lattice modes, metastability, and activation energy.

In interpreting the neutron scattering experiment

Saunderson [1966] pointed out that the mode instability

theory imposed the stringent condition that at the transi-

tion pressure the sodium chloride phase of rubidium iodide

Spinel

could not exist even metastably. If the mode was not actually
unstable but had a near zero positive value, the implication
would be that a low activation energy was required for the
transition.

Musgrave [1970, p.274] summarized the situation in the
following way: "If phase A effects a transition to phase B,
then phase A must in some way have been able to sample condi-
tion B in order to 'decide' in terms of a free-energy cri-
terion. Consequently, where kinematic paths prove easily
identifiable in terms of lattice modes, the possibility that
the instability of these modes may provide the path to the
new structure has been suggested." The sampling of the new
phase should be regarded on a statistical basis. Thermal
fluctuations of the lattice near a pressure transition en-
able the formation of an "embryo" of the new phase [see, for
example, Smoluchowski, 1948 on the embryo concept].

If a lattice mode is actually unstable, the resistance
to formation of the new phase is zero. If a lattice mode is
stable but weak, the resistance to formation of the new phase
is also weak but the old phase may still exist metastably.
Thus, a zero shear constant is a sufficient but not necessary
condition for a phase transition.

Spinel

4. Shock-wave experiments.

The occurrence of an unstable lattice mode in the microsecond time scale of a shock-wave experiment implies that an instantaneous phase transition will take place, i.e., the transition cannot be overdriven beyond the mode-failure pressure [Barsch, 1965; Roy, 1969]. Roy suggested that in high bond strength materials (such as the alkali halides and oxides) one should look for the correlation of breaks in the shock-wave Hugoniot and predicted mode failures. One might also look for the correlation of limited metastable persistence and weak modes before any mode failure is expected to occur.

Plotted in Figs. II.8 and II.9 are the pressure-density Hugoniots for $MgAl_2O_4$ (ceramic) and Fe_3O_4 which have been taken from Birch's [1966] compilation and D.L. Anderson and Kanamori's [1968] figures. Recall that magnetite has the inverse spinel structure and exhibits negative pressure co-efficients for both shear moduli [England, 1970]. In both figures the spinel structure has gone completely into a new high-pressure phase by pressures of 700 kb. The situation is ambiguous at lower pressures and subject to different inter-pretations. However, the suggestion is that the 200 to 600 kb data represent a mixed-phase region for the $MgAl_2O_4$. The number of data points seems sufficient to say that the

Spinel

Hugoniot is linear between 200 and 500 kb with a possible

negative curvature leading into an inflection at 600 kb.

The linear relation between pressure and density means a

linear relation between bulk modulus and density which is

not consistent with the expected equation of state for

$MgAl_2O_4$.

From thermochemical data the pressure at which $MgAl_2O_4$

would break down to its component oxides may be calculated

through the relation $P = -\Delta G_o/\Delta V$ [Ringwood, 1966]. ΔG_o is

the free energy of the reaction at zero pressure and ΔV is

the molar volume change of the reaction. Approximately,

$\Delta G_o^{1400°C}$ is 8.4 kcal/mole [Rosén and Muan, 1966] and ΔV is

-3 cm^3/mole to give P = 120 kb. Ringwood and Reid [1969] did

not observe any disproportionation of $MgAl_2O_4$ at 120 kb and

1000 °C but the nature of the calculation does not allow

detailed comparison. Several possibilities exist to fill the

gap between the static experiments at 120 kb and the shock-

wave experiments beginning at 200 kb. For example, the

$MgAl_2O_4$ might partially disproportionate and then begin to

transform to a denser state. Or the $MgAl_2O_4$ might remain

metastably and then begin to transform directly to the denser

high-pressure state in the mixed-phase region.

Spinel

Inferences about the nature of the spinel → post-spinel transition may now be drawn in terms of the previous discussion on lattice modes, metastability, and activation energy. By a pressure of 200 kb the shear modulus C_S will have increased a few percent for $MgAl_2O_4$ and it will have decreased a few percent for pleonaste. In either case considering the compression involved, there is evidence of a weak C_S-mode so that in the microsecond duration of the shock wave the activation energy is sufficiently low for transformation to begin. On this microsecond time scale the mixed-phase 200 to 700 kb region represents a metastable range. At 700 kb either the superpressure is sufficient to cause complete transformation, or indeed a lattice mode has gone to zero at this pressure.

The effect of iron substitution is to reduce the value of the elastic constant C_S and apparently also to reduce the value of $\partial C_S / \partial P$. $FeAl_2O_4$ may be expected to have a weaker C_S-mode than $MgAl_2O_4$. Perhaps Ringwood and Reid's [1969] observed disproportionation of $FeAl_2O_4$ compared with no reaction in $MgAl_2O_4$ at 120 kb and 1000 °C is explained by the $FeAl_2O_4$ being more readily able to tunnel (via the C_S-mode) under the kinetic barrier required for unmixing.

Now consider the shock-wave data on olivines as compiled by Ahrens and Petersen [1969] in Fig. II.10. The 200 to

Spinel

780 kb region is one of mixed phase. It is generally agreed that the olivine is in a post-spinel phase above 780 kb and that nowhere is there a clear indication of the presence of just the spinel phase. Note the similarity of the Hugoniots in Fig. II.10 for olivine and Fig. II.8 for $MgAl_2O_4$. The 200 to 700 kb region of both Hugoniots is interpreted as being one of mixed phase. For olivine the possibility exists that the mixed-phase region contains some spinel just as the possibility exists for $MgAl_2O_4$ that the mixed-phase region contains a mixture of MgO and Al_2O_3.

From the pressure derivatives of the elastic constants of olivine [Graham and Barsch, 1969; Kumazawa and Anderson, 1969], Thomsen [1971] tentatively concluded that there will be no failure of the elastic stability criteria. Without a weak mode path for the transformation, the activation energy barrier is sufficiently high that the olivine form remains metastably for a range of superpressures. With the overshoot in pressure the spinel field is also overdriven. The expected shear mode weakness for the spinel form of olivine implies that the spinel phase will tend not to remain metastably above its transition pressure. Thus the high olivine → spinel barrier and the low spinel → post-spinel barrier combine to prevent the observation of the spinel phase in a

Spinel

shock-wave experiment. The combination high/low barriers
are observed as the large mixed-phase region. Other factors
such as the non-hydrostatic nature of shock waves also have
a large influence on whether or not a transformation will
take place, but the above story seems to be consistent with
the ultrasonic data.

Spinel

E. Diffusion kinetics.

Stresses in a descending lithospheric slab depend on the creep behavior of the material in the transition zone. For high temperatures (> 1/2 the melting temperature) the creep rate is determined by the diffusion coefficient of the slowest moving atomic species in the material [see, for example, Weertman, 1970, p.146]. Keyes [1963] has proposed an elastic strain-energy model for diffusion.

$$K \frac{V^*}{G^*} = \frac{K}{\mu} \frac{\partial \mu}{\partial P} - 1 \qquad\qquad \text{(Eqn. II.4)}$$

where G^* = activation energy for diffusion

V^* = activation volume for diffusion = $\partial G^* / \partial P$

K = bulk modulus

μ = shear modulus

Eqn. II.4 is plotted in Fig. II.11 for several values of K/μ. The model gives the result that for small or negative values of the shear modulus pressure derivative, the diffusion rate increases with pressure ($V^* < 0$). Such behavior is not intuitive. The strain-energy model is a semi-empirical theory which considers the activation energy for diffusion as work done against the elastic forces. The model does a fair job of explaining existing diffusion data.

Spinel

Other diffusion theories might give a conflicting result. Weertman [1970] advocates the theory where the diffusion coefficient

$$D = D_o \exp(-gT_m/T) \qquad \text{(Eqn. II.5)}$$

is an implicit function of pressure through the melting temperature $T_m(P)$. D_o and g are constants and T is the temperature. The activation volume in this theory is negative only if $dT_m(P)/dP < 0$ and there is no clear correlation between the signs of $dT_m(P)/dP$ and $\partial\mu/\partial P$ [Keyes, 1963]. No conflict occurs for rutile-GeO_2 (next chapter). $dT_m(P)/dP$ does not seem to be available for $MgAl_2O_4$ to check.

A negative activation volume for the spinel structure implies a decrease in viscosity with depth in the transition region of the mantle rather than the increase usually calculated [Gordon, 1965; Weertman, 1970]. Postglacial uplift calculations do not resolve the viscosity profile within the transition zone. The calculations show a slightly lower viscosity for the lower mantle (below 1000 km) than for the transition zone [Cathles, 1971].

If the viscosity in the transition zone is constant or decreasing, a mechanism other than increasing strength is needed to explain the compressional axis parallel to the lithospheric slab for deep focus earthquakes [Isacks and Molnar, 1971]. For example, the density of the slab might remain lighter than the surrounding mantle.

Spinel

F. Iron substitution and the Jahn-Teller effect.

The ground state spin configuration of Fe^{2+} ($3d^6$) in a tetrahedral site is degenerate. The Jahn-Teller effect is the distortion of the site which lowers the energy. The degeneracy is removed by the splitting of the t_2 and e orbital groups.

The soft mode $C_S = 1/2$ $(C_{11} - C_{12})$ in ulvöspinel, Fe_2TiO_4, was attributed to the Jahn-Teller effect for tetrahedral Fe^{2+} by Ishikawa and Syono [1971] and Syono et al. [1971]. Syono [personal communication, 1971] suggested that the "acoustic" Jahn-Teller effect should also be present in pleonaste and $FeAl_2O_4$. Previously, the elastic properties of the Jahn-Teller ions Mn^{3+} and Ni^{3+} in YIG:Mn^{3+} and Al_2O_3:Ni^{3+} were studied by Gyorgy et al. [1966] and Sturge et al. [1967], respectively.

Syono et al. [1971] found values of $C_{11} = 1.39$, $C_{12} = 1.12$, and $C_{44} = 0.396$ Mb for Fe_2TiO_4. Fe_2TiO_4 is an inverse spinel in which one-half of the Fe^{2+} ions are in tetrahedral sites and one-half are in octahedral sites. The measured values for $C_S = 0.132$ Mb and $C_{44} = 0.396$ Mb are smaller than other spinels by a factor of five (Table II.6). Such a drastic reduction in C_S and C_{44} is not the case for $FeAl_2O_4$ which has the same molar concentration of tetrahedral

Spinel

Fe^{2+} as Fe_2TiO_4. Rather there is only a gradual decrease in C_S and C_{44} with increasing iron substitution. Since the decrease in C_{11} is smaller than the decrease in C_S, C_{12} increases and so does the bulk modulus K.

Thus there is a gradual softening of the C_S-mode with increasing iron content which may be due to a Jahn-Teller effect. However, with 100% iron substitution in the $MgAl_2O_4$ - $FeAl_2O_4$ system, the reduction is about 35% and not a factor of five as found in Fe_2TiO_4. The great reduction in the elastic constants of Fe_2TiO_4 is not due solely to the presence of Jahn-Teller Fe^{2+} ions in the tetrahedral site. Perhaps magnetoelastic coupling between the Jahn-Teller distortion and the long-range magnetic ordering in Fe_2TiO_4 [Ishikawa and Syono, 1971] is responsible for the difference. $FeAl_2O_4$ shows no signs of magnetic ordering down to 11 °K [and probably 1.9 °K, Slack, 1964] while Fe_2TiO_4 becomes weakly ferromagnetic below 142 °K. The low temperature dependence of the elastic constants of $FeAl_2O_4$ will be needed to resolve the theoretical discussion since the effect is enhanced as 1/T [Gyorgy et al., 1966; Syono et al., 1971].

Spinel

G. Iron substitution, velocity-density relations, and the
transition zone.

A variety of velocity-density relations [for a critical
review see Simmons and England, 1969] have appeared since
Birch [1961] proposed his linear relation

$$V_p = a(\bar{M}) + b\rho \qquad \text{(Eqn. II.6)}$$

where V_p = compressional wave velocity

ρ = density

$\bar{M}$ = mean atomic weight

$a(\bar{M})$, b = constants .

Birch used his velocity-density relation in the mantle's
transition zone to test density models for consistency [1961],
to examine the question of a change in iron content [1961],
and to construct density models [1964]. The necessary
parameters to know were $dV_p/d\bar{M}$, $(\partial V_p/\partial \rho)_{\bar{M}}$, and $(\partial \rho/\partial \bar{M})_y$
where y represents a constant phase and Δy is the change of
density arising from a phase transition. Birch [1961] used
values: $dV_p/d\bar{M} = -0.36$, $(\partial V_p/\partial \rho)_{\bar{M}} = 3.31$, and $(\partial \rho/\partial \bar{M})_y =$
0.13.* These values were also applied to the question of
iron content in the transition zone by D.L. Anderson [1968,
p.92] and Press [1970, p.18].

---

*All numbers given in this section are based on units where
V_p or V_s is in km/sec, ρ is in g/cm^3, and $\bar{M}$ is in g/mole/atom.

Spinel

The new data in the $MgAl_2O_4$ - $FeAl_2O_4$ system allow redetermination of the parameters

$$dV_p/d\overline{M} = (\partial V_p/\partial \rho)_{\overline{M}}(\partial \rho/\partial \overline{M})_y + (\partial V_p/\partial \overline{M})_\rho \qquad \text{(Eqn. II.7)}$$

and $(\partial V_p/\partial \rho)_{\overline{M}}$ for use in considering the olivine → spinel transition which is one of the major phase changes in the 300 to 1000 km region. Also the data determine the corresponding parameters $dV_s/d\overline{M}$ and $(\partial V_s/\partial \rho)_{\overline{M}}$ for shear wave velocities.

1. Velocity-density relation for spinels.

First the $MgAl_2O_4$ - $FeAl_2O_4$ system will be tested in a velocity-density relation proposed for spinel structure compounds [Liebermann, 1970].

$$V_p = 15.66 - 1.59 \rho \qquad \text{(Eqn. II.8a)}$$

$$V_s = 9.88 - 1.17 \rho \qquad \text{(Eqn. II.8b)}$$

V_p and V_s are in km/sec and ρ is in g/cm^3. The heavy lines in Fig. II.12 represent Eqns. II.8. The newly measured values for V_p and V_s on pleonaste and hercynite fall 5 to 10% below the predicted values. The slope of the light line connecting $MgAl_2O_4$ to $FeAl_2O_4$ for V_p is the same as Liebermann's. However, the slope of the light line connecting $MgAl_2O_4$ to $FeAl_2O_4$ for V_s is steeper than Liebermann's, and in fact is the same as the slope of both V_p lines.

Spinel

It appears as if V_p and V_s might be linear with composition in the $MgAl_2O_4$ - $FeAl_2O_4$ system. The $MgAl_2O_4$ - $FeAl_2O_4$ system would be expected to serve as a better elastic analogue to the spinel phase of the Mg_2SiO_4 - Fe_2SiO_4 system than the assortment of spinels used in Liebermann's relation. The densities, mean atomic weights, and molar volumes of $(Mg_{1-x}Fe_x)Al_2O_4$ and $(Mg_{1-z}Fe_z)_2SiO_4$ where $z = x/2$ are compared in Table II.9. Note that 100% Fe substitution for Mg in $MgAl_2O_4$ is equivalent to about 50% Fe substitution for Mg in Mg_2SiO_4. For example, 100% Fe substitution in $MgAl_2O_4$ increases $\bar{M}$ by 4.5 which is exactly one-half the increase in $\bar{M}$ for 100% Fe substitution in spinel-Mg_2SiO_4. The densities for $(Mg_{1-x}Fe_x)Al_2O_4$ and spinel-$(Mg_{1-z}Fe_z)_2SiO_4$ were calculated from a linear volume versus composition relation. The molar volumes for spinel-Mg_2SiO_4 and spinel-Fe_2SiO_4 were taken from Ringwood and Major [1970].

Assume that V_p and V_s are linear with composition in the $(Mg_{1-x}Fe_x)Al_2O_4$ and $(Mg_{1-z}Fe_z)_2SiO_4$ systems and that the elastic properties in the two systems are exactly similar for $z = x/2$. Then

$$V_p = 9.73 - 1.03 x \qquad \text{(Eqn. II.9a)}$$

$$V_s = 5.49 - 1.03 x \qquad \text{(Eqn. II.9b)}$$

where V_p and V_s are in km/sec and $0 \leq x \leq 1$. Uncertainties are about 3%.

Spinel

2. Redetermination of Birch's parameters.

The parameters $dV_p/d\overline{M}$, $(\partial V_p/\partial\rho)_{\overline{M}}$, and $(\partial\rho/\partial\overline{M})_y$ will now be considered in turn.

a. The value of $dV_p/d\overline{M}$ is $-1.03/4.5 = -0.23$ based on the $MgAl_2O_4$ - $FeAl_2O_4$ data (Eqns. II.9). Birch's value for $dV_p/d\overline{M}$ was -0.36. For reference, $dV_s/d\overline{M}$ is -0.23 based on the $MgAl_2O_4$ - $FeAl_2O_4$ data. Recall that V_p and V_s are in km/sec, ρ is in g/cm^3, and $\overline{M}$ is in g/mole/atom.

b. For consideration of the olivine → spinel transition, it seems proper to consider the value of $(\partial V_p/\partial\rho)_{\overline{M}}$ to be

$$(\partial V_p/\partial\rho)_{\overline{M}} = \frac{V_p^{spinel} - V_p^{olivine}}{\rho^{spinel} - \rho^{olivine}} \qquad \text{(Eqn. II.10)}$$

where the superscripts "spinel" and "olivine" refer to the respective phases of Mg_2SiO_4. The Hill averages for olivine-Mg_2SiO_4 [Graham and Barsch, 1969; Kumazawa and Anderson, 1969] are used to obtain $(\partial V_p/\partial\rho)_{\overline{M}} = 3.45$ and for reference $(\partial V_s/\partial\rho)_{\overline{M}} = 1.41$. Birch's value for $(\partial V_p/\partial\rho)_{\overline{M}}$ was 3.31. Neither $(\partial V_p/\partial\rho)_{\overline{M}}$ nor $(\partial V_s/\partial\rho)_{\overline{M}}$ calculated over the transition by Eqn. II.10 is consistent with that calculated from the pressure or temperature derivatives of olivine-Mg_2SiO_4 or $MgO:2.6Al_2O_3$ [C. Wang, 1970, p.3265; England, 1970, p.95].

Spinel

c. The parameter $(\partial\rho/\partial\overline{M})_y$ for different Mg/Fe solid solution series is given below.

System	$(\partial\rho/\partial\overline{M})_y$
Olivine- $(Mg_{1-z}Fe_z)_2SiO_4$	0.130
Spinel- $(Mg_{1-z}Fe_z)_2SiO_4$	0.143
$(Mg_{1-x}Fe_x)Al_2O_4$	0.156

3. Transition zone.

a. To indicate the vagaries that remain on the question of iron content change in the transition zone, I will rework Birch's [1961] example where he used Jeffreys' 1939 seismic velocities and Bullen's Model A. I use the values

$$(\partial\rho/\partial\overline{M})_y = 0.14 \ , \quad (\partial V_p/\partial\rho)_{\overline{M}} = 3.45 \ , \quad dV_p/d\overline{M} = -0.23$$

which were determined in the previous section. The equations to be solved are [Birch, 1961, p.308]:

	Seismic change		Adiabatic compression		Phase change		Iron content change
ΔV_p =	2.32	=	1.14	+	3.45 Δy	-	0.23 $\Delta\overline{M}$
$\Delta\rho$ =	0.95	=	0.33	+	Δy	+	0.14 $\Delta\overline{M}$

The solution is $\Delta\overline{M} = 1.4$ and $\Delta y = 0.43$ g/cm^3. Birch obtained $\Delta\overline{M} = 1.0$ and $\Delta y = 0.48$ g/cm^3.

Spinel

However, if shear velocity values are used, the equations become:

$$\Delta V_s = 1.33 = 0.46 + 1.41 \Delta y - 0.23 \Delta \overline{M}$$

$$\Delta \rho = 0.95 = 0.33 + \Delta y + 0.14 \Delta \overline{M}$$

The solution is $\Delta \overline{M} = 0$ and $\Delta y = 0.62$ g/cm^3. Thus the V_p solution indicates some iron increase while the V_s solution indicates that phase changes account for the entire density increase.

b. Some recent seismic shear velocity profiles have either a constant velocity gradient [Ibrahim and Nuttli, 1967] or a negative velocity gradient [D.L. Anderson and Julian, 1969] between 500 and 650 km. The small positive and slightly negative pressure derivatives of V_s for MgO:2.6Al$_2$O$_3$ and pleonaste, respectively, suggest that the seismically deter-mined V_s versus depth are indicative of the spinel structure.

The smaller value of $\partial V_s / \partial P$ obtained on pleonaste com-pared to MgO:2.6Al$_2$O$_3$ suggests this reduction in $\partial V_s / \partial P$ may generally be true for iron substitution. When more con-fidence is gained in seismic shear wave gradients as well as in laboratory data on the effects of iron substitution, changes in the FeO/(FeO + MgO) ratio in the transition zone may be estimated. An observed decrease in the slope of the shear wave gradient might mean an increase in the FeO/ (FeO + MgO) ratio.

Spinel

References

Ahrens, T.J., and C.F. Petersen, Shock wave data and the study of the earth, in The Application of Modern Physics to the Earth and Planetary Interiors, edited by S.K. Runcorn, pp. 449-461, Wiley-Interscience, London, 1969.

Ahrens, T.J., D.L. Anderson, and A.E. Ringwood, Equations of state and crystal structures of high-pressure phases of shocked silicates and oxides, Rev. Geophys., 7, 667-707, 1969.

Anderson, D.L., Chemical inhomogeneity of the mantle, Earth Planet. Sci. Letters, 5, 89-94, 1968.

Anderson, D.L., and B. Julian, Shear velocities and elastic parameters of the mantle, J. Geophys. Res., 74, 3281-3286, 1969.

Anderson, D.L., and H. Kanamori, Shock-wave equations of state for rocks and minerals, J. Geophys. Res., 73, 6477-6502, 1968.

Anderson, O.L., Determination and some uses of isotropic elastic constants of polycrystalline aggregates using single-crystal data, in Physical Acoustics, Vol. III - Part B edited by W.P. Mason, pp. 43-95, Academic Press, New York, 1965.

Anderson, O.L., A proposed law of corresponding states for oxide compounds, J. Geophys. Res., 71, 4963-4971, 1966.

Spinel

Anderson, O.L., and H.H. Demarest, Jr., Elastic constants of
the central force model for cubic structures: polycrystalline
aggregates and instabilities, J. Geophys. Res., 76, 1349-1369,
1971.

Barsch, G.R., Material instability of initially stressed
crystals (abstract), Bull. Am. Phys. Soc., II, 10, 452, 1965.

Barsch, G.R., Relation between third-order elastic constants
of single crystals and polycrystals, J. Appl. Phys., 39,
3780-3793, 1968.

Birch, F., Composition of the earth's mantle, Geophys. J.,
4, 295-311, 1961.

Birch, F., Density and composition of mantle and core, J.
Geophys. Res., 69, 4377-4388, 1964.

Birch, F., Compressibility: elastic constants, in Handbook
of Physical Constants -- Revised Edition, edited by S.P.
Clark, Jr., pp. 97-173, Geological Society of America Memoir
97, New York, 1966.

Brugger, K., Pure modes for elastic waves in crystals, J.
Appl. Phys., 36, 759-768, 1965.

Buerger, M.J., Crystallographic aspects of phase transforma-
tions, in Phase Transformations in Solids, edited by R.
Smoluchowski, J.E. Mayer, and W.A. Weyl, pp. 183-211, John
Wiley and Sons, New York, 1951.

Burns, R.G., Mineralogical Applications of Crystal Field
Theory, 224 pp., Cambridge University Press, London, 1970.

Spinel

Cathles, L.M., III, Lower mantle viscosity inferred from postglacial adjustment of the ocean basins and Canada (abstract), Trans. Am. Geophys. Union, 52, 353, 1971.

Chung, D.H., First pressure derivatives of polycrystalline elastic moduli: their relation to single-crystal acoustic data and thermodynamic relations, J. Appl. Phys., 38, 5104-5113, 1967.

Chung, D.H., D.J. Silversmith, and B.B. Chick, A modified ultrasonic pulse-echo-overlap method for determining sound velocities and attenuation of solids, Rev. Sci. Inst., 40, 718-720, 1969.

Daniels, W.B., and C.S. Smith, The pressure variation of the elastic constants of crystals, in The Physics and Chemistry of High Pressures, pp. 50-63, Society of Chemical Industry, London, and Gordon and Breach, New York, 1963.

Davies, G.F., and D.L. Anderson, Revised shock-wave equations of state for high-pressure phases of rocks and minerals, J. Geophys. Res., 76, 2617-2627, 1971.

Deer, W.A., R.A. Howie, and J. Zussman, Rock-forming Minerals, Vol. 5, Non-silicates, 371 pp. Longmans, London, 1962.

England, A.W., Equations of state of oxides and silicates and new data on the elastic properties of spinel, magnetite, and cadmium oxide, Ph.D. thesis, Massachusetts Institute of Technology, Cambridge, 1970.

Spinel

Finkbeiner, D.T., II, Introduction to Matrices and Linear
Transformations, 246 pp., W.H. Freeman and Company, San
Francisco, 1960.

Frisillo, A.L., and G.R. Barsch, The pressure dependence of
the elastic coefficients of orthopyroxene (abstract), Trans.
Am. Geophys. Union, 52, 359, 1971.

Fuchs, K., A quantum mechanical calculation of the elastic
constants of monovalent metals, Proc. Roy. Soc. (London),
A153, 622-639, 1936.

Fyfe, W.S., Geochemistry of Solids, 199 pp., McGraw-Hill,
New York, 1964.

Gieske, J.H., and G.R. Barsch, Pressure dependence of the
elastic constants of single crystalline aluminum oxide,
Phys. Status Solidi, 29, 121-131, 1968.

Gordon, R.B., Diffusion creep in the earth's mantle, J. Geo-
phys. Res., 70, 2413-2418, 1965.

Graham, E.K., Jr., and G.R. Barsch, Elastic constants of
single-crystal forsterite as a function of temperature and
pressure, J. Geophys. Res., 74, 5949-5960, 1969.

Gyorgy, E.M., R.C. LeCraw, and M.D. Sturge, Influence of
Jahn-Teller ions on the acoustic and magnetic properties of
YIG, J. Appl. Phys., 37, 1303-1309, 1966.

Hamilton, R.A.H., and J.E. Parrott, The third-order elastic
constants of quasi-isotropic materials, J. Phys. C (Proc.
Phys. Soc.), Ser. 2, Vol. 1, 829-834, 1968.

Spinel

Hardy, J.R., and A.M. Karo, Lattice dynamics of rubidium iodide in relation to the NaCl-CsCl phase transition, in Lattice Dynamics, edited by R.F. Wallis, pp. 195-201, Pergamon Press, Oxford, 1965.

Hashin, Z., and S. Shtrikman, On some variational principles in anisotropic and nonhomogeneous elasticity, J. Mech. Phys. Solids, 10, 335-342, 1962a.

Hashin, Z., and S. Shtrikman, A variational approach to the theory of the elastic behavior of polycrystals, J. Mech. Phys. Solids, 10, 343-352, 1962b.

Ibrahim, A.K., and O.W. Nuttli, Travel-time curves and upper-mantle structure from long-period S waves, Bull. Seismol. Soc. Am., 57, 1063-1092, 1967.

Isacks, B., and P. Molnar, Distribution of stresses in the descending lithosphere from a global survey of focal-mechanism solutions of mantle earthquakes, Rev. Geophys. Space Phys., 9, 103-174, 1971.

Ishikawa, Y., and Y. Syono, Giant magnetostriction due to Jahn-Teller distortion in Fe_2TiO_4, Phys. Rev. Letters, 26, 1335-1338, 1971.

Jagodzinski, H., and H. Saalfeld, Kationenverteilung und Strukturbeziehungen in Mg-Al-Spinellen, Z. Krist., 110, 197-218, 1958.

Spinel

Keyes, R.W., Continuum models of the effect of pressure on activated processes, in Solids Under Pressure, edited by W. Paul and D.M. Warschauer, pp. 71-99, McGraw - Hill, New York, 1963.

Knopoff, L., and J.N. Shapiro, Comments on the inter-relationships between Grüneisen's parameter and shock and isothermal equations of state, J. Geophys. Res., 74, 1439-1450, 1969.

Kröner, E., Elastic moduli of perfectly disordered composite materials, J. Mech. Phys. Solids, 15, 319-329, 1967.

Kumazawa, M., and O.L. Anderson, Elastic moduli, pressure derivatives, and temperature derivatives of single-crystal olivine and single-crystal forsterite, J. Geophys. Res., 74, 5961-5972, 1969.

La, S.Y., and G.R. Barsch, Pressure derivatives of second-order elastic constants of MgO, Phys. Rev., 172, 957-966, 1968.

Leibfried, G., Gittertheorie der mechanischen und thermischen Eigenschaften der Kristalle, in Encyclopedia of Physics, VII, Part 1, edited by S. Flügge, pp. 104-324, Springer-Verlag, Berlin, 1955.

Leigh, R.S., B. Szigeti, and V.K. Tewary, Force constants and lattice frequencies, Proc. Roy. Soc. (London), A320, 505-526, 1971.

Lewis, M.F., Elastic constants of magnesium aluminate spinel, J. Acoust. Soc. Am., 40, 728-729, 1966.

Spinel

Liebermann, R.C., Velocity-density systematics for the olivine and spinel phases of Mg_2SiO_4 - Fe_2SiO_4, $\underline{J}$. $\underline{Geophys}$. $\underline{Res}$., $\underline{75}$, 4029-4034, 1970.

Musgrave, M.J.P., $\underline{Crystal}$ $\underline{Acoustics}$, 288 pp., Holden-Day, San Francisco, 1970.

O'Connell, R.J., Equation of state of spinel to 10 kbar and 800°K (abstract), $\underline{Trans}$. $\underline{Am}$. $\underline{Geophys}$. $\underline{Union}$, $\underline{51}$, 419, 1970.

O'Connell, R.J., and E.K. Graham, Equation of state of stoichiometric spinel to 10 kbar and 800°K (abstract), $\underline{Trans}$. $\underline{Am}$. $\underline{Geophys}$. $\underline{Union}$, $\underline{52}$, 359, 1971.

Papadakis, E.P., Ultrasonic phase velocity by the pulse-echo-overlap method incorporating diffraction phase corrections, $\underline{J}$. $\underline{Acoust}$. $\underline{Soc}$. $\underline{Am}$., $\underline{42}$, 1045-1051, 1967.

Papadakis, E.P., Effect of multimode guided-wave propagation on ultrasonic phase velocity measurements: problem and remedy, $\underline{J}$. $\underline{Acoust}$. $\underline{Soc}$. $\underline{Am}$., $\underline{45}$, 1547-1555, 1969.

Pistorius, C.W.F.T., Polymorphic transitions of the alkali bromides and iodides at high pressures to 200°C, $\underline{J}$. $\underline{Phys}$. $\underline{Chem}$. $\underline{Solids}$, $\underline{26}$, 1003-1011, 1965.

Press, F., Earth models consistent with geophysical data, $\underline{Phys}$. $\underline{Earth}$ $\underline{Planet}$. $\underline{Interiors}$, $\underline{3}$, 3-22, 1970.

Reid, A.F., and A.E. Ringwood, Newly observed high pressure transformations in Mn_3O_4, $CaAl_2O_4$, and $ZrSiO_4$, $\underline{Earth}$ $\underline{Planet}$. $\underline{Sci}$. $\underline{Letters}$, $\underline{6}$, 205-208, 1969.

Spinel

Reuss, A., Berechnung der Fliessgrenze von Mischkristallen auf Grund der Plastizitätsbedingung für Einkristalle, Z. Angew. Math. Mech., 9, 49-58, 1929.

Ringwood, A.E., Mineralogy of the mantle, in Advances in Earth Science, edited by P.M. Hurley, pp. 357-399, MIT Press, Cambridge, 1966.

Ringwood, A.E., and A. Major, The system Mg_2SiO_4 - Fe_2SiO_4 at high pressures and temperatures, Phys. Earth Planet. Interiors, 3, 89-108, 1970.

Ringwood, A.E., and A.F. Reid, High pressure transformations of spinels (I), Earth Planet Sci. Letters, 5, 245-250, 1969.

Rosen, E., and A. Muan, Stability of $MgAl_2O_4$ at 1400 °C as derived from equilibrium measurements in $CoAl_2O_4$ - $MgAl_2O_4$ solid solutions, J. Am. Ceram. Soc., 49, 107-108, 1966.

Roy, R., Neglected role of metastability in high pressure research, in Reactivity of Solids, edited by J.W. Mitchell, R.C. DeVries, R.W. Roberts, and P. Cannon, pp. 777-788, Wiley-Interscience, New York, 1969.

Sammis, C.G., The pressure dependence of the elastic constants of cubic crystals in the NaCl and spinel structures from a lattice model, Geophys. J., 19, 285-297, 1970.

Saunderson, D.H., Pressure dependence of the TA [100] zone-boundary phonon frequency in rubidium iodide, Phys. Rev. Letters, 17, 530-533, 1966.

Spinel

Schreiber, E., Elastic moduli of single-crystal spinel at 25 °C and to 2 kbar, $\underline{J}$. $\underline{Appl}$. $\underline{Phys}$., $\underline{38}$, 2508-2511, 1967.

Simmons, G., and A.W. England, Universal equations of state for oxides and silicates, $\underline{Phys}$. $\underline{Earth}$ $\underline{Planet}$. $\underline{Interiors}$, $\underline{2}$, 69-76, 1969.

Slack, G.A., Thermal conductivity of MgO, Al_2O_3, $MgAl_2O_4$, and Fe_3O_4 crystals from 3° to 300 °K, $\underline{Phys}$. $\underline{Rev}$., $\underline{126}$, 427-441, 1962.

Slack, G.A., $FeAl_2O_4$ - $MgAl_2O_4$: Growth and some thermal, optical, and magnetic properties of mixed single crystals, $\underline{Phys}$. $\underline{Rev}$., $\underline{134}$, A1268-A1280, 1964.

Smakula, A., and V. Sils, Precision density determination of large single crystals by hydrostatic weighing, $\underline{Phys}$. $\underline{Rev}$., $\underline{99}$, 1744-1746, 1955.

Smoluchowski, R., Nucleation theory, in $\underline{Phase}$ $\underline{Transformations}$ $\underline{in}$ $\underline{Solids}$, edited by R. Smoluchowski, J.E. Mayer, and W.A. Weyl, pp. 149-182, John Wiley and Sons, New York, 1951.

Striefler, M.E., and G.R. Barsch, Pressure dependence of elastic constants and infrared optical frequencies of spinel (abstract), $\underline{Trans}$. $\underline{Am}$. $\underline{Geophys}$. $\underline{Union}$., $\underline{52}$, 359, 1971.

Sturge, M.D., J.T. Krause, E.M. Gyorgy, R.C. LeCraw, and F.R. Merritt, Acoustic behavior of the Jahn-Teller ion Ni^{3+} in Al_2O_3, $\underline{Phys}$. $\underline{Rev}$., $\underline{155}$, 218-224, 1967.

Spinel

Syono, Y., Y. Fukai, and Y. Ishikawa, Anomalous elastic

properties of Fe_2TiO_4, J. Phys. Soc. Japan, 31, 1971, in

press.

Thomsen, L., Elastic shear moduli and crystal stability at high

P and T, J. Geophys. Res., 76, 1342-1348, 1971.

Thurston, R.N., Effective elastic coefficients for wave

propagation in crystals under stress, J. Acoust. Soc. Am.,

37, 348-356, 1965a.   Erratum, J. Acoust. Soc. Am., 37,

1147, 1965a.

Thurston, R.N., Ultrasonic data and the thermodynamics of

solids, Proc. IEEE, 53, 1320-1336, 1965b.

Verma, R.K., Elasticity of some high-density crystals, J.

Geophys. Res., 65, 757-766, 1960.

Voigt, W., Lehrbuch der Krystallphysik, 962 pp., B.G. Teubner,

Leipzig, 1928.

Wang, C., Density and constitution of the mantle, J. Geophys.

Res., 75, 3264-3284, 1970.

Weertman, J., The creep strength of the earth's mantle,

Rev. Geophys. Space Phys., 8, 145-168, 1970.

Table II.1

Pleonaste microprobe analysis* (wt. %).

Approximate chemical formula: $(Mg_{0.75}Fe_{0.36})Al_{1.90}O_4$.

	Wt. % oxide
SiO_2	0.1
TiO_2	0.5
Al_2O_3	63.8
Cr_2O_3	0.3
FeO	17.2
MnO	0.1
MgO	19.9
	101.9

* Microprobe analysis by A. Reid of the NASA Manned Spacecraft Center, Houston, Texas.

ρ, g/cm^3	3.826
a_o, Å	8.1225
$\overline{M}$, g/mole/atom	21.8

Table II.2

Elastic constants determined from different
propagation modes shown
in Fig. II.3 for a cubic crystal.

Propagation direction	Path length (mm)	Vibration direction	Vibration mode	Elastic constant
α or [100]	4.933	[100]	L	C_{11}
α or [100]	4.933	Any	T	C_{44}
γ or [110]	6.645	[110]	L	C_L
γ or [110]	6.645	[1$\bar{1}$0]	T	C_s
γ or [110]	6.645	[001]	T	C_{44}

where $C_L = 1/2 \, (C_{11} + C_{12} + 2C_{44})$

$C_s = 1/2 \, (C_{11} - C_{12})$

Also   L = longitudinal

T = transverse

Table II.3

Pleonaste single crystal elastic constants.

(Based on density ρ = 3.826 g/cm^3)

	11	12	44
C_{ij} (Mb)	2.695	1.633	1.435
$\partial C_{ij}/\partial P$	4.85	4.95	0.75
S_{ij} (Mb^{-1})	0.684	-0.258	0.697
$\partial S_{ij}/\partial P$ (Mb^{-2})	-0.079	-0.168	-0.364

Shear mode temperature derivatives:

$$\partial C_S/\partial T = +0.067 \text{ kb/}°K \quad \text{and} \quad \partial C_{44}/\partial T = -0.080 \text{ kb/}°K$$

$$\text{where } C_S = 1/2 \; (C_{11} - C_{12})$$

Based on thermal expansion $\alpha = 22 \times 10^{-6}$ / °C used also by

Schreiber [1967].

Table II.4

Pleonaste calculated aggregate elastic constants.
(Based on density $\rho = 3.826$ g/cm^3)

	Zero pressure aggregate constants						
	E	μ	σ	K	β	V_s	V_p
Voigt	2.729	1.073	0.271	1.987	0.503	5.297	9.452
Hashin	2.546	0.990	0.286	1.987	0.503	5.086	9.296
Kröner	2.509	0.973	0.290	1.987	0.503	5.042	9.265
Shtrikman	2.448	0.946	0.295	1.987	0.503	4.972	9.214
Reuss	2.240	0.854	0.312	1.987	0.503	4.724	9.038

	Aggregate pressure derivatives						
	$\partial E/\partial P$	$\partial\mu/\partial P$	$\partial\sigma/\partial P$	$\partial K/\partial P$	$\partial\beta/\partial P$	$\partial V_s/\partial P$	$\partial V_p/\partial P$
"Voigt"	1.96	0.43	4.02	4.92	-1.25	-0.27	5.21
"Hashin"	1.64	0.34	3.90	4.92	-1.25	-0.41	5.21
"Kröner"	1.55	0.31	3.90	4.92	-1.25	-0.47	5.18
"Shtrikman"	1.37	0.24	3.93	4.92	-1.25	-0.61	5.11
"Reuss"	0.94	0.11	3.86	4.92	-1.25	-0.89	5.04

(continued)

Table II.4

Pleonaste calculated aggregate elastic constants.

(Based on density $\rho = 3.826$ g/cm^3.)

(continued)

Symbol	Elastic constant units	
	Unit	Pressure derivative unit $(\partial/\partial P)$
E, Young's modulus	Mb	None
μ, Shear modulus	Mb	None
σ, Poisson's ratio	None	10^{-4}/kb
K, Bulk modulus	Mb	None
β, Compressibility	Mb^{-1}	Mb^{-2}
V_s, Shear velocity	km/sec	(km/sec)/Mb
V_p, Compressional velocity	km/sec	(km/sec)/Mb

Table II.5

Elastic constants of $FeAl_2O_4$.

	Single crystal constants		
	11	12	44
C_{ij} (Mb)	2.660	1.825	1.335
S_{ij} (Mb^{-1})	0.851	-0.346	0.749

	Calculated aggregate constants						
	E (Mb)	μ (Mb)	σ	K (Mb)	β (Mb^{-1})	V_s (km/sec)	V_p (km/sec)
Voigt	2.518	0.968	0.300	2.103	0.475	4.756	8.905
Hashin	2.305	0.875	0.317	2.103	0.475	4.521	8.740
Kröner	2.253	0.853	0.322	2.103	0.475	4.463	8.701
Shtrikman	2.163	0.814	0.329	2.103	0.475	4.361	8.631
Reuss	1.916	0.711	0.348	2.103	0.475	4.074	8.442

Table II.6

Elastic constants of various spinels.

Spinel	ρ	$\overline{M}$	K	C_S	C_L	C_{11}	C_{12}	C_{44}	V_p^*	V_s^*	Ref.
						Elastic constants					
$MgO:3.5Al_2O_3$	3.630	20.4	2.026	0.734	3.857	3.005	1.537	1.585	9.939	5.676	(1)
$MgO:3.0Al_2O_3$	3.624	20.4	2.026	0.723	3.847	2.990	1.544	1.580	9.929	5.658	(2)
$MgO:2.6Al_2O_3$	3.619	20.4	2.020	0.724	3.838	2.986	1.537	1.576	9.926	5.660	(3)
$MgO:1.0Al_2O_3$	3.581	20.3	1.950	0.630	3.690	2.790	1.530	1.530	9.727	5.489	(4)
Pleonaste	3.826	21.8	1.987	0.531	3.599	2.695	1.633	1.435	9.265	5.042	(5)
$FeAl_2O_4$	4.280	24.8	2.103	0.418	3.588	2.660	1.825	1.335	8.701	4.463	(5)
Fe_2TiO_4	4.836	31.9	1.210	0.135	1.651	1.390	1.120	0.396	5.681	2.332	(6)
Fe_3O_4	5.163	33.1	1.596	0.810	2.819	2.676	1.056	0.953	7.349	4.162	(2)
						Elastic constant pressure derivatives $(\partial/\partial P)$					
$MgO:3.0Al_2O_3$	3.624	20.4	4.59	0.57	5.67	5.35	4.21	0.89	5.34	0.46	(2)
$MgO:2.6Al_2O_3$	3.619	20.4	4.23	0.50	5.25	4.90	3.90	0.85	4.74	0.32	(3)
Pleonaste	3.826	21.8	4.92	-0.05	5.65	4.85	4.95	0.75	5.18	-0.47	(5)
Theoretical $MgO:1.0Al_2O_3$	3.581	20.3	3.20	1.30	4.00	4.90	2.30	0.34	3.96	1.13	(7)

*Kröner average

References	Symbol	Unit	Pressure derivative $(\partial/\partial P)$ unit
1. Verma, 1960	C_{ij}, elastic stiffnesses	Mb	None
2. England, 1970	K, bulk modulus	Mb	None
3. Schreiber, 1967	V_p, compressional velocity	km/sec	(km/sec)/Mb
4. Lewis, 1966	V_s, shear velocity	km/sec	(km/sec)/Mb
5. Present study	ρ, density	g/cm^3	Not used
6. Syono et al., 1971	$\overline{M}$, mean atomic weight	g/mole/atom	Not used
7. Sammis, 1970			

$$C_S = 1/2 \ (C_{11} - C_{12}) \qquad C_L = 1/2 \ (C_{11} + C_{12} + 2C_{44})$$

Table II.7

Deviation from oxygen cubic close packing for various spinel stoichiometries [Jagodzinski and Saalfeld, 1958]. Define $\Delta = u - 0.375$, where u establishes the oxygen location. For perfect cubic close packing $u = 0.375$.

Spinel	Δ	u
Natural $MgO:1.0Al_2O_3$	0.012	0.387
Synthetic $MgO:1.0Al_2O_3$	0.011	0.386
$MgO:2.0Al_2O_3$	0.008	0.383
$MgO:3.5Al_2O_3$	0.006	0.381

Table II.8

Comparison of oxygen framework results with

experimental values for pleonaste and $MgO:2.6Al_2O_3$.

The $\partial C_{ij}/\partial P$ are thermodynamic elastic constant derivatives.

	Pleonaste		$MgO:2.6Al_2O_3$		Theoretical ratio
	C_{ij}/K	$\dfrac{(\partial C_{ij}/\partial P)}{(\partial K/\partial P)}$	C_{ij}/K	$\dfrac{(\partial C_{ij}/\partial P)}{(\partial K/\partial P)}$	A_{ij}
ij = 11	1.36	1.30	1.48	1.51	1.50
ij = 12	0.82	0.86	0.76	0.75	0.75
ij = 44	0.72	0.41	0.78	0.50	0.75

$$\left(\frac{\partial C_{11}}{\partial P}\right)^{thermo} = \left(\frac{\partial C_{11}}{\partial P}\right)^{effective} + 1 + \frac{C_{11}}{3K}$$

$$\left(\frac{\partial C_{12}}{\partial P}\right)^{thermo} = \left(\frac{\partial C_{12}}{\partial P}\right)^{effective} - 1 + \frac{C_{12}}{3K}$$

$$\left(\frac{\partial C_{44}}{\partial P}\right)^{thermo} = \left(\frac{\partial C_{44}}{\partial P}\right)^{effective} + 1 + \frac{C_{44}}{3K}$$

Table II.9

Comparisons between $(Mg_{1-x}Fe_x)Al_2O_4$ and $(Mg_{1-z}Fe_z)_2SiO_4$.

$(Mg_{1-x}Fe_x)Al_2O_4$				$(Mg_{1-z}Fe_z)_2SiO_4$			
x	ρ	$\overline{M}$	V	$z = x/2$	ρ	$\overline{M}$	V
0.00	3.58	20.3	39.7	0.00	3.56	20.1	39.6
0.25	3.76	21.4	40.0	0.12	3.73	21.2	39.9
0.50	3.93	22.6	40.2	0.25	3.89	22.4	40.2
0.75	4.11	23.7	40.4	0.38	4.06	23.5	40.5
1.00	4.28	24.8	40.6	0.50	4.22	24.6	40.8

Symbol	Unit
ρ, density	g/cm^3
$\overline{M}$, mean atomic weight	g/mole/atom
V, molar volume	cm^3/mole

Spinel

Figure Captions

Fig. II.1.   Sketch of pleonaste sample.

Fig. II.2.   Sketch of hercynite sample.

Fig. II.3.   Pure mode directions in cubic crystals. :The elastic constants determined are shown in Table II.2 [after Brugger, 1965].

Fig. II.4.   (a) Echo train in hercynite for a compressional wave in the [110]-direction. The first echo on the left is the reflection from the interface between the quartz buffer rod and the sample. Later echoes that have made round trips in the sample are inverted in phase with respect to the reflection from the end of the buffer rod. The time scale is 0.2 µsec/cm. (b) Overlap of two echoes. The overlap frequency is 2.60 MHz for a sample path length of 1.763 mm.

Fig. II.5.   Spinel structure [after Fyfe, 1964, p.106]. The unit cell contains 32 oxygens in cubic closest packing with cations in (a) 16 of the 32 octahedral sites and (b) 8 of the 64 tetrahedral sites. For the general formula, AB_2O_4, the spinel is termed normal when the A ions occupy the tetrahedral sites and the B ions occupy the octahedral sites. When the A ions and 1/2 the B ions occupy the tetrahedral sites, the spinel is termed inverse.

Spinel

Fig. II.6. C_{44}-type crystallographic shear mechanism for the
NaCl → CsCl structure transformation [after Buerger, 1948,
p. 204].

Fig. II.7. Schematic representation of transverse acoustic
(TA) mode dispersion curve under pressure. The horizontal
line represents a cutoff frequency at low temperatures. The
LA curve represents the longitudinal acoustic mode dispersion
curve. ν is the frequency, κ is the wavevector, and a is the
lattice parameter [figure after Daniels and Smith, 1963].

Fig. II.8. Pressure-density Hugoniots for spinel. Two fits
to the high-pressure data are shown for two assumed starting
densities. The range of metastable Hugoniots P_H corresponds
to the range of assumed zero-pressure densities indicated by
the heavy bar above the zero-pressure axis. P_K is the 0°K
isotherm. The crosses represent the zero-pressure densities
found by D.L. Anderson and Kanamori [1968, p. 6489] from
whom the figure was taken. The 200 to 600 kb data is con-
sidered to be a region of mixed phase.

Fig. II.9. Pressure-density Hugoniots for magnetite. The
symbols are as in Fig. II.8. Again the figure is from
D.L. Anderson and Kanamori [1968, p. 6489]. The 200 to
600 kb data is considered to be a region of mixed phase.

Spinel

Fig. II.10. Pressure-volume Hugoniots for various olivines
[after Ahrens and Petersen, 1969]. The 200 to 700 kb data
is considered to be a region of mixed phase.

Fig. II.11. Keyes' [1963] strain-energy model for diffusion
under pressure. V* is the activation volume, G* is the
activation energy, K is the bulk modulus, and μ is the shear
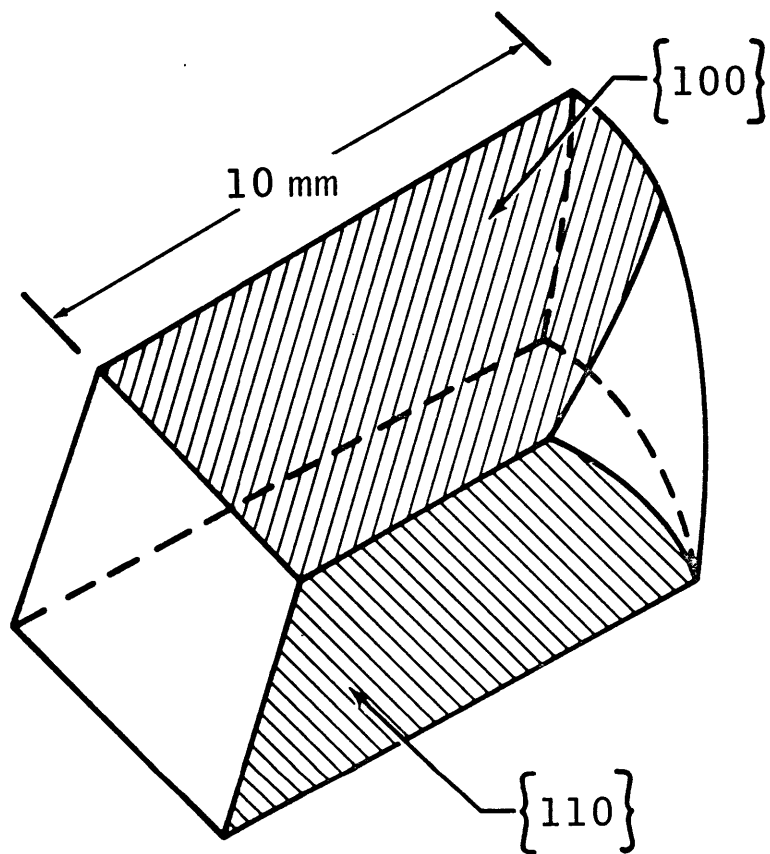modulus.

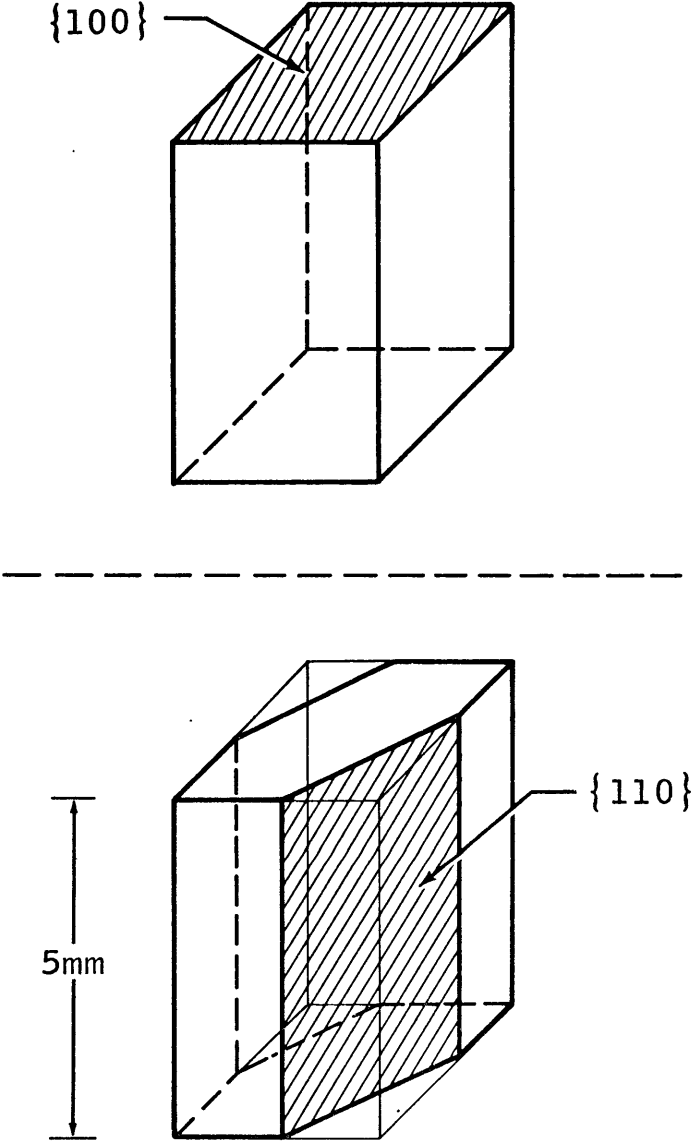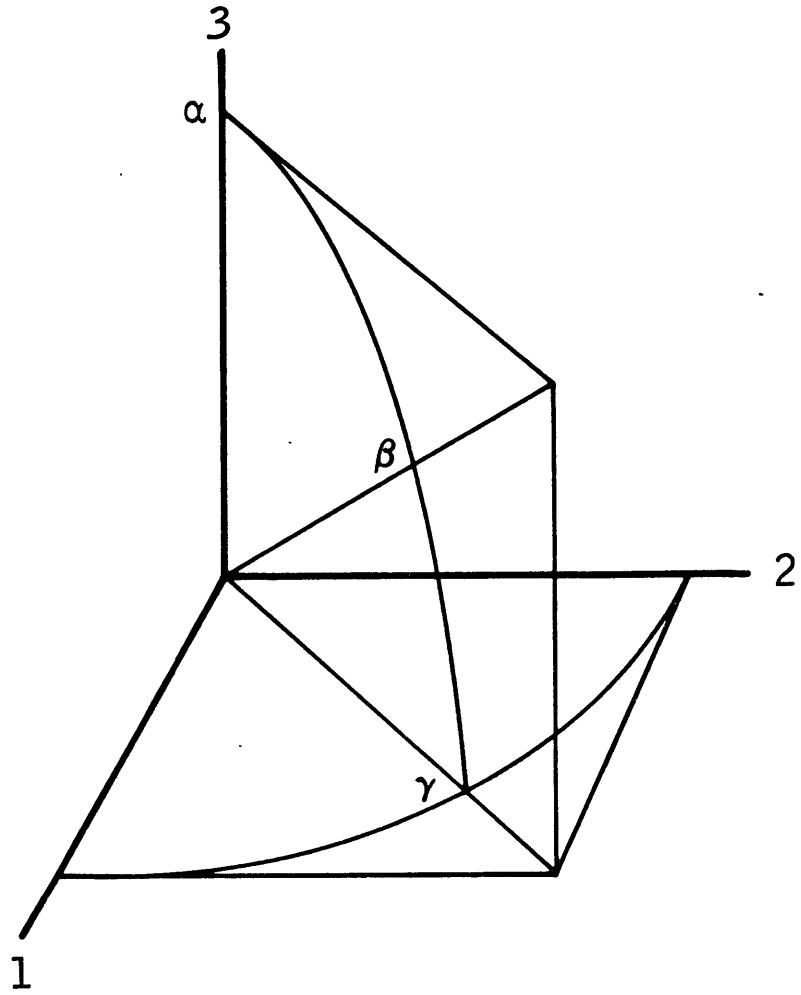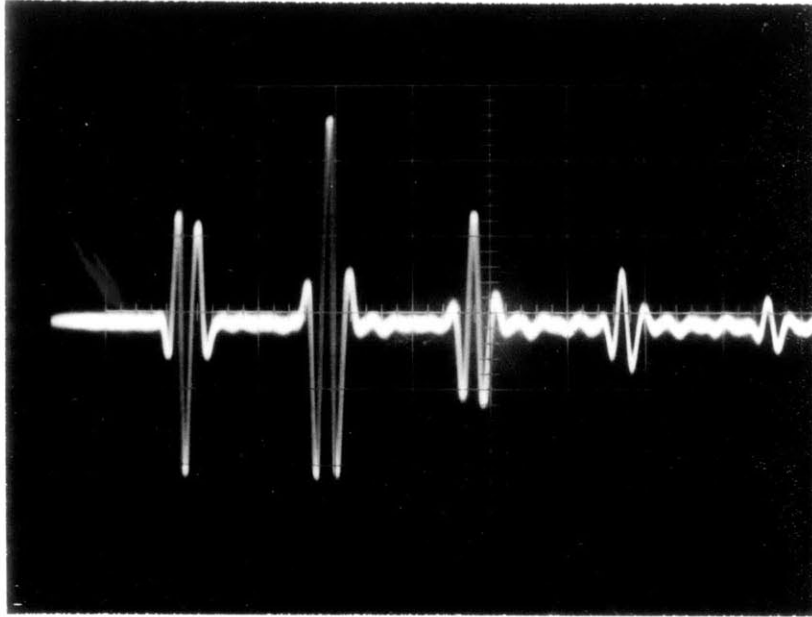Fig. II.12. Velocity-density relations for spinels.

Fig. II.1

{100}

{110}
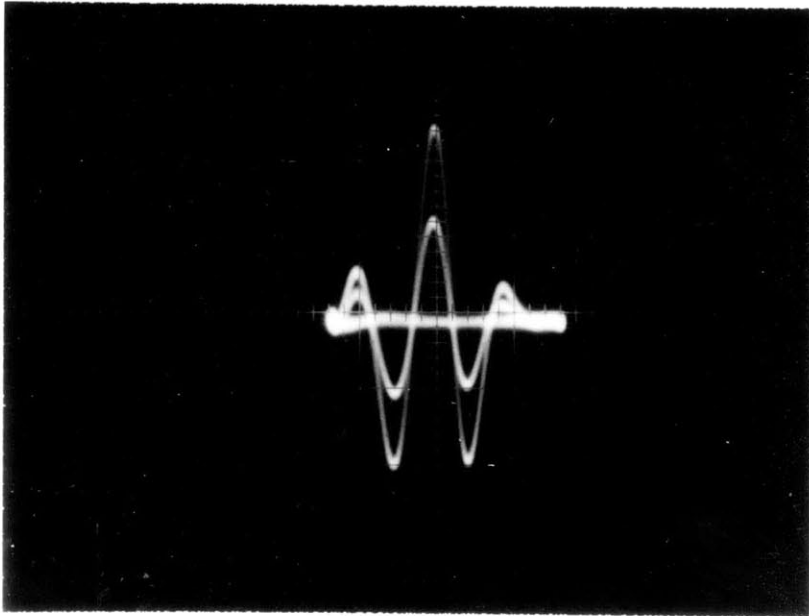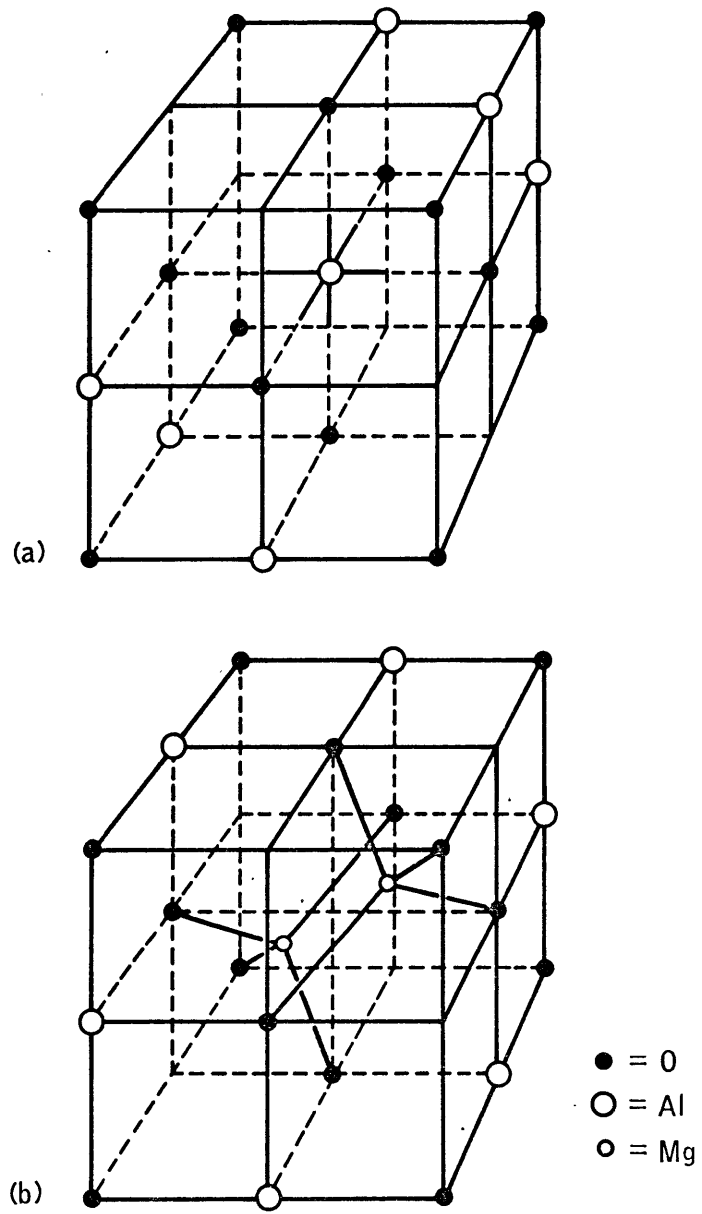
5mm

Fig. II.2

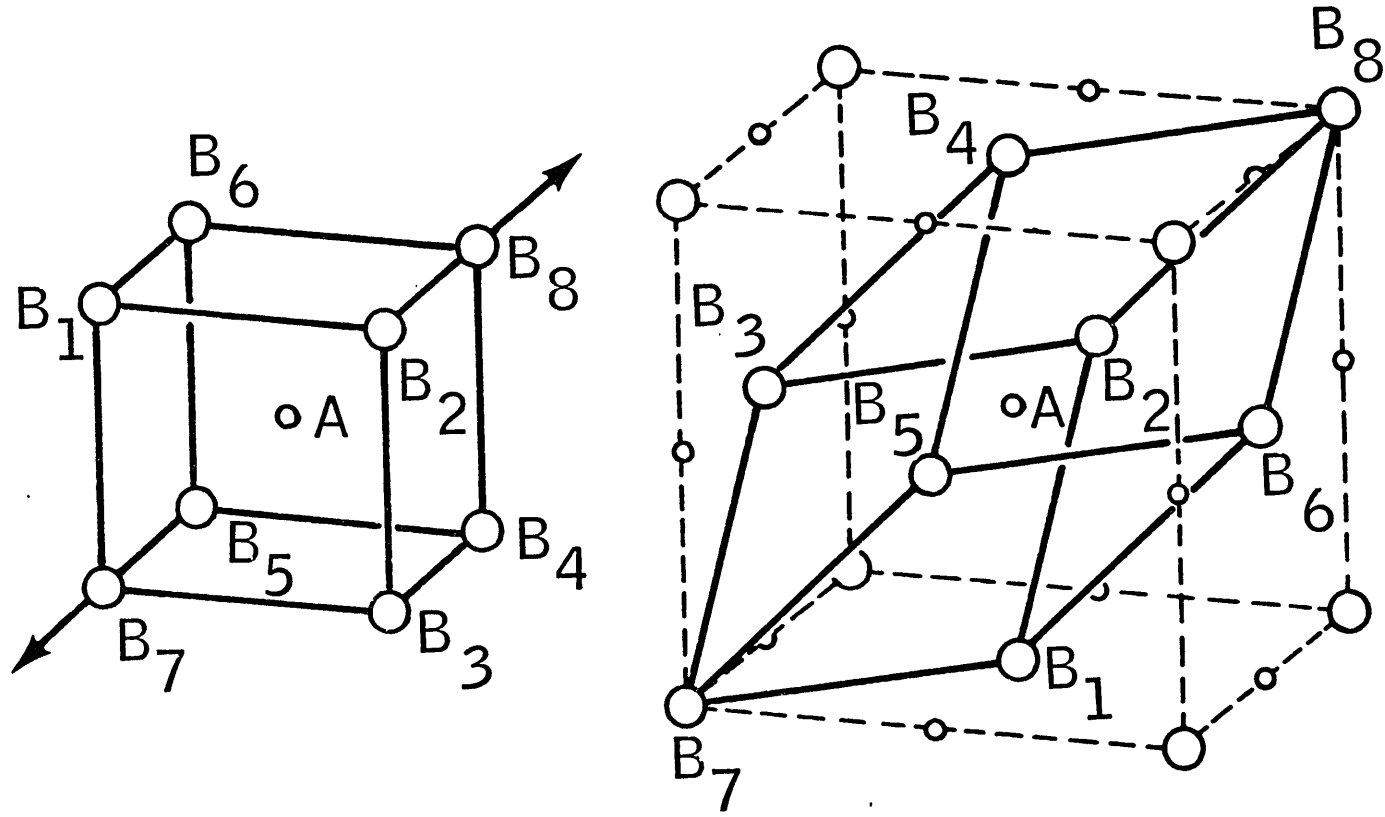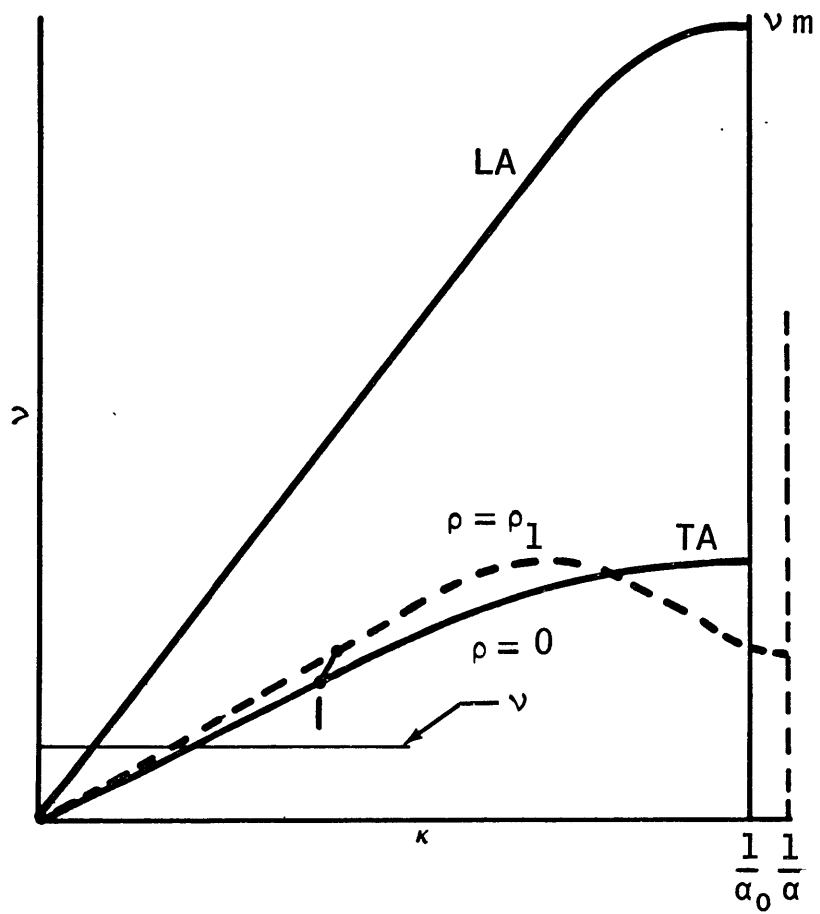Fig. II.3

(a)

(b)

Fig. II.4

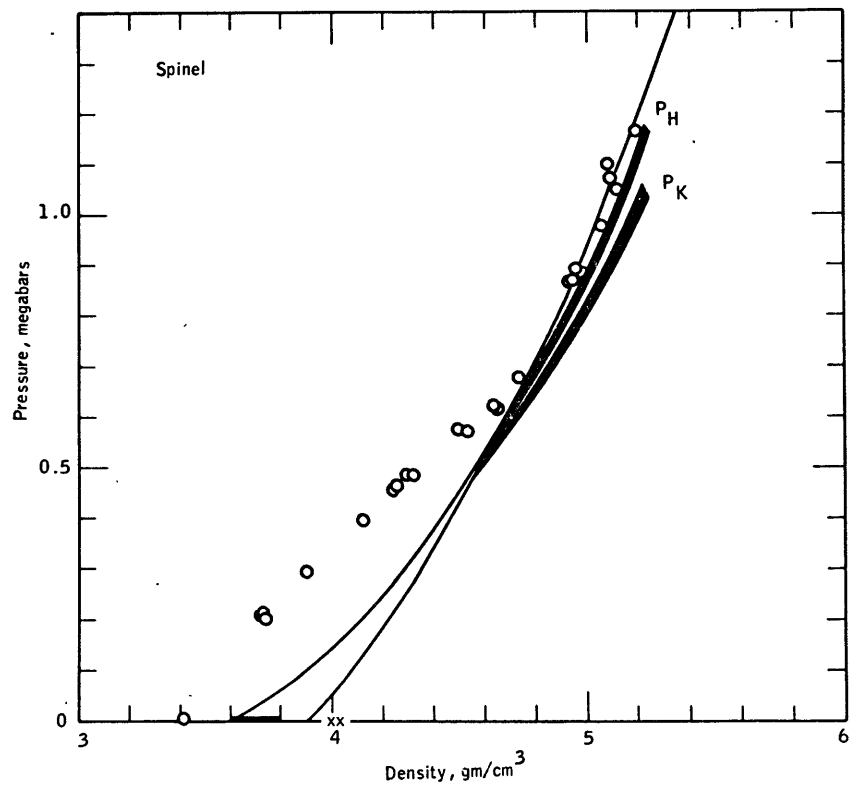● = 0
O = Al
o = Mg

Fig. II.5

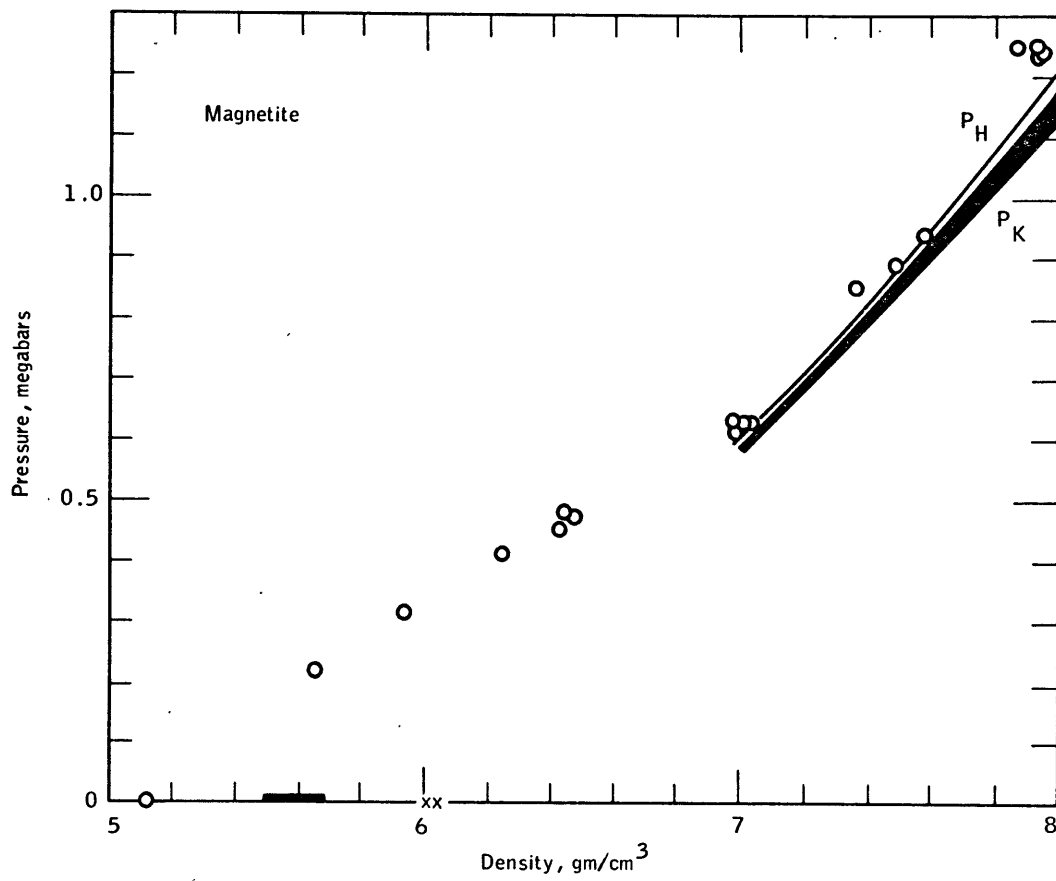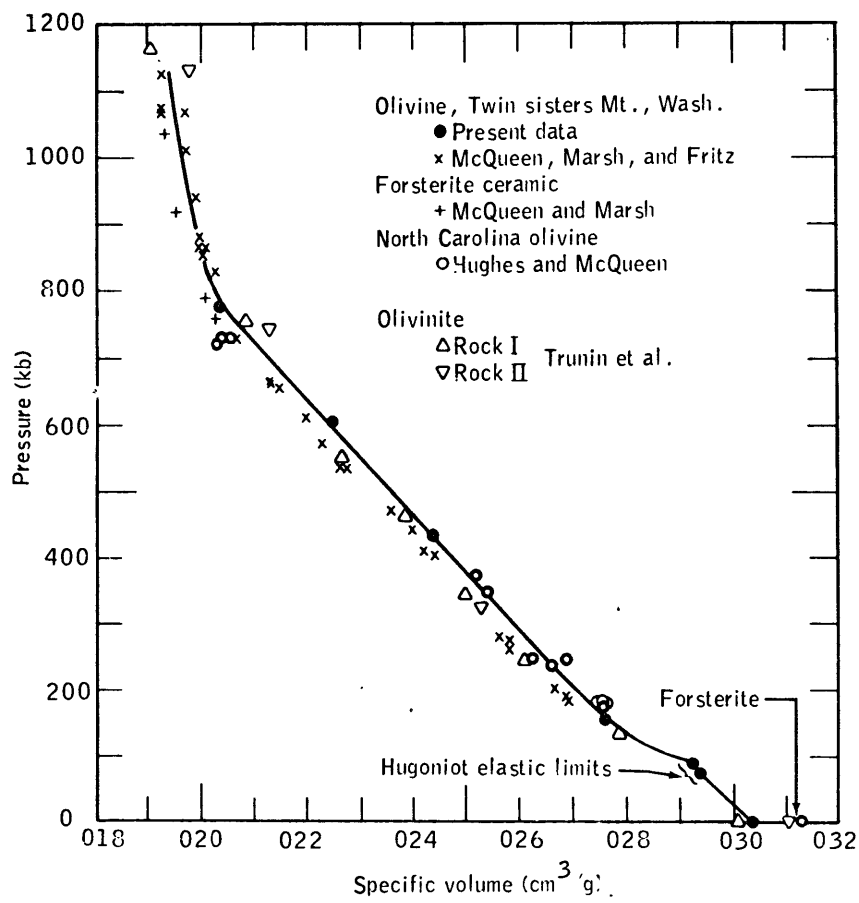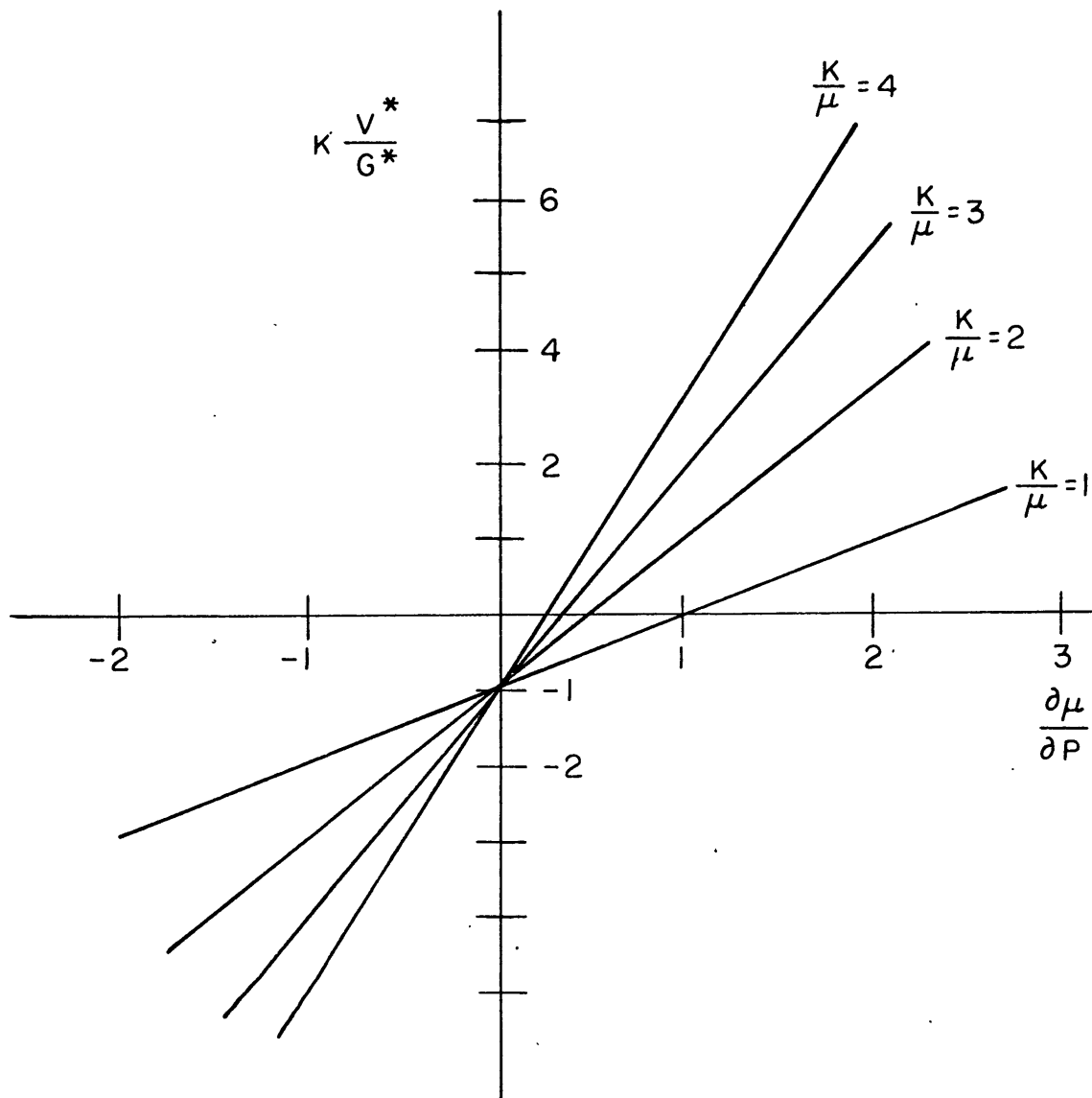Fig. II.6

70

Fig. II.7

Fig. II.8

Fig. II.9

Fig. II.10

$$K \frac{V^*}{G^*} = \frac{K}{\mu} \frac{\partial \mu}{\partial P} - 1$$
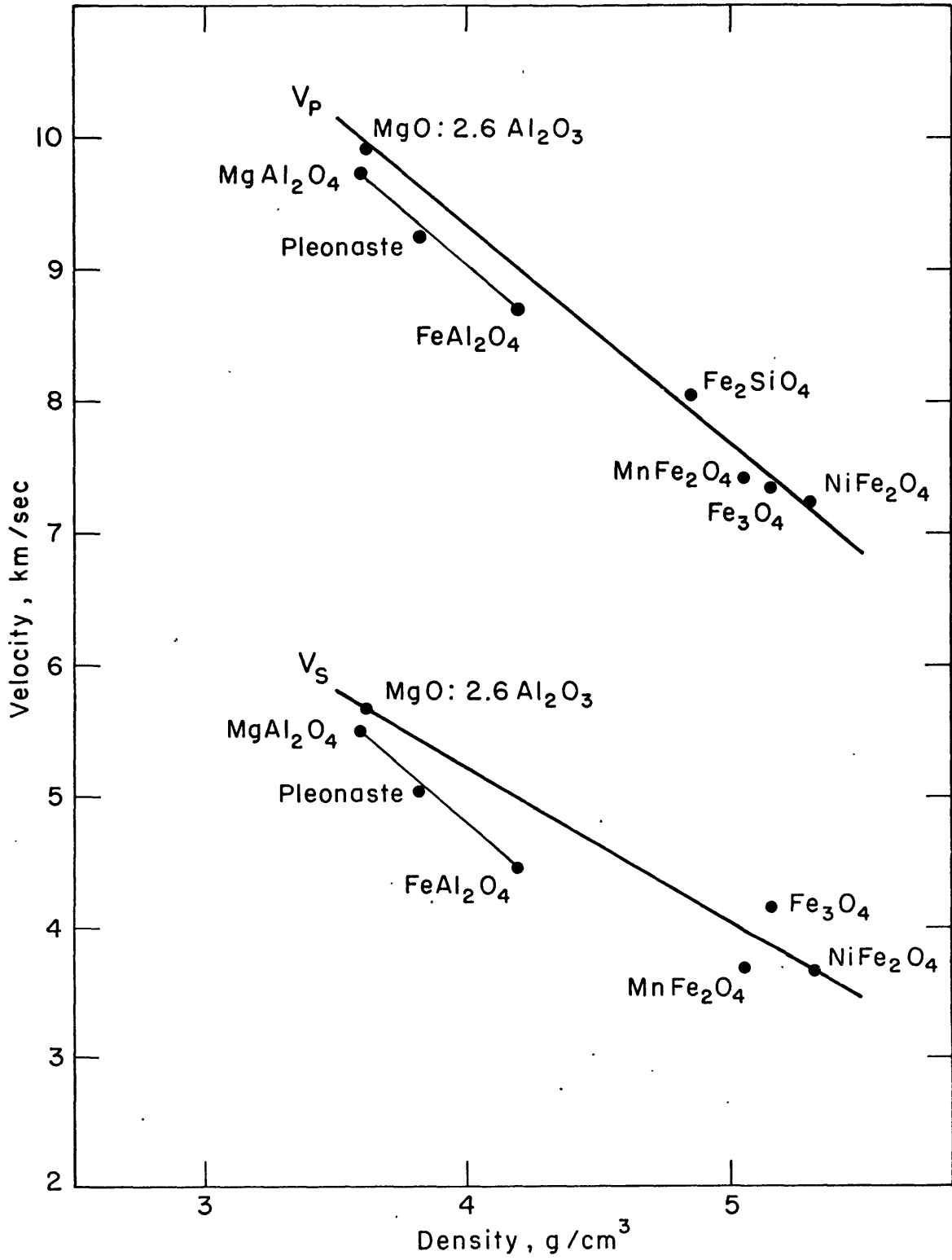
Fig. II.11

Fig. II.12

Rutile-GeO$_2$

III. Elastic constants of rutile-structure GeO$_2$.

Germanium dioxide (germania) and germanate compounds have been used in geochemistry as a means of studying high pressure structures of silica and silicates [see reviews by Ringwood, 1966, 1970].* The germanium ion (radius = 0.40 Å) is somewhat larger than the silicon ion (radius = 0.26 Å) when both are in tetrahedral coordination [radii from Shannon and Prewitt, 1969]. The germanate crystal isostructural to a silicate crystal is expected to go into a high pressure modification at a pressure below that of the silicate (see Table III.1 [after Ringwood, 1970]), because the oxygen framework will collapse around the germanium ion relatively sooner than around the silicon ion [Bernal, 1936]. The chemical similarity has been exploited by geochemists to estimate phase boundaries of the corresponding silicate through extrapolation in systems such as Mg$_2$GeO$_4$ - Mg$_2$SiO$_4$ [Dachille and Roy, 1960], Ni$_2$GeO$_4$ - MgSiO$_4$ [Ringwood and Seabrook, 1962], and presently Mn$_2$GeO$_4$ - Mg$_2$SiO$_4$ [Ringwood, 1970, p. 116]. The Mg$_2$GeO$_4$ - Mg$_2$SiO$_4$ and Ni$_2$GeO$_4$ - Mg$_2$SiO$_4$ systems gave early estimates of the olivine-spinel phase boundary which

---

* I have thought that this similarity between germanates and silicates could be exploited in the following examination question: "Describe the evolution and present state of the earth if the abundances of germanium and silicon were reversed."

Rutile-GeO$_2$

has recently been determined directly [Ringwood and Major,

1970]. The Mn$_2$GeO$_4$ - Mg$_2$SiO$_4$ system is in early stages of

study to estimate the boundary of the spinel → post-spinel

(strontium plumbate) transition [Ringwood, 1970].

Even though some of these high-pressure silicate phases

are being synthesized, they are recovered in milligram pro-

portions. Present ultrasonic techniques require close to

one gram of material for polycrystalline samples. Single

crystals are out of the question (unless General Electric

becomes interested). So the germanium analogue technique

may also be used to understand the elasticity of high-pressure

silicate phases.

I add that though grams of stishovite are recoverable

from Meteor Crater, phase studies [Holm et al., 1967] show

that stishovite spontaneously transforms to a glass indis-

tinguishable from ordinary SiO$_2$ glass at 800 °K in 15 to 20

minutes. Sample synthesis by hot-pressing might lead to an

undesired finished product.

Quite recently some elastic property work on germanate

compounds was reported by Soga [1969, 1971] and Mizutani

[1970]. Soga measured the pressure dependence of the elas-

tic moduli on germania glass and he measured the room condi-

tion values on a series of nearly dense polycrystalline

samples of quartz-structure GeO$_2$, rutile-structure GeO$_2$, and

Rutile-GeO$_2$

olivine-structure Mg$_2$GeO$_4$. Mizutani [1970] reported in abstract form shear velocity measurements on very thin samples of Mn$_2$GeO$_4$ (olivine, spinel, and strontium plumbate structures) and MnGeO$_3$ (ilmenite structure).

In this chapter I report the pressure and temperature dependence of the single crystal elastic constants of rutile-structure (Fig. III.1) GeO$_2$. This form of GeO$_2$ is isostructural to stishovite [Stishov and Popova, 1961], the 6-coordinated polymorph of SiO$_2$. Similar measurements for the elastic constants as a function of pressure and temperature have been made for rutile (TiO$_2$) by Manghnani [1969]. Since silica constitutes 33 to 50 mole percent of the transition zone and lower mantle, information gained from analogue studies will be important.

Rutile-GeO_2

A. GeO_2 phase diagram and thermochemical data.

Germanium dioxide can exist at room conditions in either the low-quartz or rutile structure [for an early comprehensive paper, see Laubengayer and Morton, 1932]. The densities of the two polymorphs are shown in Table III.2. The cation/anion ratio is right on the boundary between 4:2 and 6:3 coordination. At room conditions the rutile form of GeO_2 is the thermodynamically stable phase. At zero pressure the rutile-GeO_2 transforms to quartz-GeO_2 at 1002 °C. The quartz form is quite stable at room conditions, however. In fact when one buys GeO_2 one obtains the quartz phase. It is made at high temperatures from the ignition of $GeCl_4$ and maintains this metastable state. Thus the quartz-GeO_2 → rutile-GeO_2 transformation is quite sluggish in the absence of catalysts. A hydrothermally determined phase diagram is shown in Fig. III.2 [Hill and Chang, 1968].

The thermochemical data for germania is fairly complete (Table III.2). I have included the values for the analogous but metastable transition SiO_2 (quartz) → SiO_2 (stishovite) [Holm et al., 1967].

Rutile-GeO$_2$

B. Sample description.

The synthetically grown rutile-GeO$_2$ sample was obtained from Capt. John Goodrum and C. Dugger of the Air Force Cambridge Research Laboratories, Bedford, Mass. The sample was slightly less than 1 cm^3 in size and weighed 4.94 g. It was transparent and yellow. A sketch of the sample as grown is shown in Fig. III.3a. The four vertical sides were {110}-faces and the pyramid top pointed in the C-axis direction. The crystal was grown by a top-seeding method in an Na$_2$O flux [Goodrum, 1970, 1971]. The only noticeable internal flaw was some small bubbles near the seed. Comparison of the X-ray density (6.2857 g/cm^3) and hydrostatic weighing density (6.2718 g/cm^3) showed less than 0.2% deviation and the bubbles were ignored. An average density of 6.279 g/cm^3 was used in the determination of the elastic constants. The only other flaw was that the initial {110}-faces showed apparent dislocation etch pits in reflected light. This caused some difficulty in the optical polishing of these faces until enough of the surface was ground away to remove the pits. The {110}-faces as grown were within 1/2° of the true orientation. Since the symmetry of Laue back-reflection photographs does not distinguish between {100} and {110}-faces for tetragonal symmetry, the distinction was made by means of a diffraction scan. When compared against the powder pattern, the scan showed missing {100}-peaks which confirmed the {110}-orientation.

Rutile-GeO$_2$

C. Experimental method and results.

In order to obtain a complete set of six elastic con-
stants with reasonable cross checks, four sets of parallel
faces were required. The normals to the four sets of faces
are shown in Fig. III.4. Polarization directions for shear
modes are also indicated and each mode is labelled. The
exact combination of elastic constants determined for each
mode is indicated in Table III.3.

1. Sample cutting procedure.

The four sets of parallel faces were obtained from the
single sample described in the previous section. Initially
one pair of {110}-faces was polished and pressure and temper-
ature runs were made. Since the two shear modes were non-
degenerate, three independent elastic constant combinations
were determined. Then the pyramid was cut off and the set of
{001}-faces polished. The pressure and temperature dependence
of C_{33} and C_{44} were obtained from this direction. Note that
C_{44} had previously been determined from the [110]-direction.
At this point it was necessary to lose the {110}-faces. Name-
ly, in order to obtain {100}-faces, cuts had to be made at a
45° angle to the {110}-face. Though the {110}-faces were not
completely destroyed, a perpendicular path connecting them
was lost. With the {100}-faces the crystal looked as in

Rutile-GeO$_2$

Fig. III.3b.   The pressure and temperature dependence of C_{11},
C_{66}, and C_{44} were obtained from the [100]-direction.   At this
point five of the six elastic constants had been determined.
Only C_{13} remained.   It could be obtained from a set of
{101}-faces, i.e., a cut had to be made at 45° to both the
{100} and {001}-faces.   The {001}-face was oriented so that
the spots representing the mirror planes pointed in the [100]-
direction.   Then swinging the goniometer 45° in the horizon-
tal plane and making a pair of vertical saw cuts yielded the
{101}-faces(Fig. III.3c).   The [001]-path direction was now
lost.   However, the [100]-path direction remains and in theory
all six elastic constants may still be determined from just
the [100] and [101]-directions.   Table III.3 summarizes the
final path lengths in the different directions.   All the
pairs of faces were optically polished flat and parallel to
10^{-4} in/in by the A.D. Jones Optical Works, Burlington, Mass.

Rutile-GeO$_2$

2. Ultrasonic measurements.

The elastic constants of rutile-GeO$_2$ were measured to 5 kb at room temperature (20 °C) and to 100 °C at zero pressure by the pulse-echo-overlap technique [Papadakis, 1967; Chung et al., 1969]. The measurements were mostly made at 20 MHz with coaxially plated X-cut and AC-cut quartz transducers. Some measurements were made at 30 MHz by driving the third harmonic of a 10 MHz transducer to reduce the beam spreading and guided-wave mode effects. A total of 22 pressure runs and 20 temperature runs were made. A summary of the average values for each mode is shown in Table III.4. The cross checks for the room condition elastic constants are all good to better than 0.2%. The values shown for C_{44} are the average of runs in different directions. Mode cross checks for the pressure derivatives show agreement within 5% and mode cross checks for the temperature derivatives show agreement within 10%. The pressure and temperature derivatives are considered accurate to 5% and 10%, respectively.

Since the different modes listed in Table III.4 over-determine the six independent elastic constants, an arithmetic average weighted by the number of runs was used in some cases. C_{33}, C_{44}, and C_{66} were taken simply as their value in Table III.4. C_{11} and C_{12} were determined from the three modes C_{11}, C_s, and C_{L_1}. Finally C_{13} was determined from the difference $1/2$ $(C_{L_2} - C_{T_2})$ and from the values for C_{11}, C_{33},

Rutile-GeO$_2$

and C_{44}. Since $1/2 \, (C_{L_2} - C_{T_2}) = 1/4 \, [(C_{11} - C_{13})^2 +$

$4 \, (C_{13} + C_{44})^2]^{1/2}$, the magnitude of $(C_{13} + C_{44})$ was deter-

mined but not its sign. The two choices for C_{13} were

$C_{13} = 1.874$ Mb or $C_{13} = -5.104$ Mb. The proper choice was

$C_{13} = 1.874$ Mb in order to satisfy the inequality $C_{11}C_{33} >$

C_{13}^2. The inequality comes from the requirement that the

strain energy density be positive definite, i.e.,

$$\sum_{i=1}^{6} \sum_{j=1}^{6} C_{ij}\varepsilon_i\varepsilon_j > 0.$$

A theorem of linear algebra [see, for example, Hausner, 1965,

p.127] says the energy density will be positive definite if

all the determinants

$$\left| C_{11} \right| \, , \quad \begin{vmatrix} C_{11} & C_{12} \\ C_{12} & C_{11} \end{vmatrix} \, , \quad \begin{vmatrix} C_{11} & C_{12} & C_{13} \\ C_{12} & C_{11} & C_{13} \\ C_{13} & C_{13} & C_{33} \end{vmatrix} \, , \cdots$$

are greater than zero. The inequality $C_{11}C_{33} > C_{13}^2$ follows

after some algebra. The resulting final values for the

single crystal elastic constants, their pressure derivatives,

and their termperature derivatives are tabulated in Table

III.5. In addition the linear compressibilities and the

volume compressibility are tabulated. Calculated aggregate

properties are tabulated in Table III.6.

Rutile-GeO$_2$

D. Comparison with other work.

In this section the present results will be compared with the polycrystalline rutile-GeO$_2$ values of Soga [1971], the single crystal TiO$_2$ values of Manghnani [1969], the stishovite shock-wave reductions of Ahrens et al. [1970], and the stishovite isothermal compression measurements of Bassett and Barnett [1970]. Soga's values for the bulk modulus and compressional wave velocity of rutile-GeO$_2$ appear to be 20% and 7% too low, respectively. The pressure derivative of the bulk modulus, $\partial K/\partial P$, for rutile-GeO$_2$ is about 10% lower than for TiO$_2$. The values are close enough that it is probable $\partial K/\partial P$ for stishovite is between 6 and 7.

1. Comparison with polycrystalline rutile-GeO$_2$.

Soga studied the elastic properties of polycrystalline quartz-GeO$_2$, rutile-GeO$_2$, and olivine-Mg$_2$GeO$_4$. He synthesized four rutile-GeO$_2$ polycrystalline samples of different porosity, the densest of which was 96% theoretical density. He then estimated the following values for the compressional wave velocity V_p and the shear wave velocity V_s. The corresponding values for the bulk modulus K and seismic parameter Φ are also given.

Polycrys-talline values	V_p = 7.90 km/sec	V_s = 4.85 km/sec
	K = 1.950 Mb	Φ = 31.0 km^2/sec^2

Rutile-GeO$_2$

The values for K and V_p fall considerably outside the calculated Voigt and Reuss bounds shown in Table III.6. The Hill averages for the single crystal rutile-GeO$_2$ measurements are shown below.

Hill	V_p = 8.55 km/sec	V_s = 4.90 km/sec
	K = 2.576 Mb	Φ = 41.0 km^2/sec^2
averages		

The cause of the discrepancies is in Soga's value for V_p. His Table 1 is plotted in Fig. III.5. Perhaps the type of porosity present in the sample reduced the compressional wave velocity but not the shear wave velocity.

2. Comparison with single crystal rutile-TiO$_2$.

a. Both GeO$_2$ and TiO$_2$ exhibit a negative value for the pressure derivative of the shear modulus $C_S = 1/2 (C_{11} - C_{12})$.

b. Both compounds show marked anisotropy. The ratio of linear compressibilities parallel and perpendicular to the C-axis are 0.449 for TiO$_2$ and 0.369 for GeO$_2$.

c. The "Hill" averages for the bulk modulus pressure derivatives are $(\partial K/\partial P)_{TiO_2}$ = 6.76 and $(\partial K/\partial P)_{GeO_2}$ = 6.16. Although the value is about 10% lower for GeO$_2$ than for TiO$_2$, it is still relatively higher than those for other oxides and silicates.

Rutile-GeO$_2$

d. The "Hill" averages for the shear modulus pressure deriva-
tives are $(\partial\mu/\partial P)_{TiO_2}$ = 0.78 and $(\partial\mu/\partial P)_{GeO_2}$ = 1.22. Note
that the individual "Voigt" and "Reuss" values are far apart.
For TiO$_2$ the "Voigt" and "Reuss" values for $\partial\mu/\partial P$ are 1.88
and -0.34, respectively. For GeO$_2$ the "Voigt" and "Reuss"
values for $\partial\mu/\partial P$ are 1.78 and 0.67, respectively. The shear
modulus pressure derivative for GeO$_2$ is apparently larger
than for TiO$_2$.

e. The "Hill" averages for the bulk modulus temperature
derivatives are $(\partial K/\partial T)_{TiO_2}$ = -0.41 kb/°K and $(\partial K/\partial T)_{GeO_2}$ =
-0.36 kb/°K. As for $\partial K/\partial P$, the value of $\partial K/\partial T$ is about
10% lower (in magnitude) for GeO$_2$ than for TiO$_2$, but it is
still relatively higher (in magnitude) than those for other
oxides and silicates.

3. Comparison with stishovite (shock-wave and isothermal
compression measurements).

   Stishovite is the rutile modification of SiO$_2$. Its
bulk modulus has been determined from shock-wave [Wackerle,
1962; McQueen et al., 1963; D.L. Anderson and Kanamori, 1968;
Ahrens et al., 1970; Davies and D.L. Anderson, 1971] and iso-
thermal compression measurements [Ida et al., 1967; Liu et al.,
1969; Bassett and Barnett, 1970]. In some cases a value for

Rutile-GeO$_2$

the pressure derivative of the bulk modulus is quoted. The more recent (1970 - 1971) determinations will be considered in this section.

a. Shock-wave measurements.

Ahrens et al. [1970] fitted the raw high pressure (> 400 kb) Hugoniot points of quartz to a third-order Birch-Murnaghan equation. The Hugoniot was reduced to a room-condition stishovite adiabat, where the adiabat was also given a Birch-Murnaghan form. The initial volume of quartz, the initial volume of stishovite, and the internal energy of the quartz → stishovite transformation were assumed to be known (Table III.3). The volume dependence V/V_O of the thermodynamic Grüneisen ratio, $\gamma = \alpha K_s/C_p \rho_O$, was given the form $\gamma = \gamma_O (V/V_O)^A$. α is the thermal expansion, K_s is the adiabatic bulk modulus, C_p is the specific heat at constant pressure, ρ_O is the initial density, and A is an adjustable parameter. The preferred solution of Ahrens et al. [1970] was

$$\gamma_O = 1.58 \qquad\qquad A = 6$$

$$C_O \equiv \sqrt{\Phi} = 8.37 \text{ km/sec} \qquad\qquad K_O = 3.0 \text{ Mb}$$

$$(\partial K/\partial P)_{P=0} = 6.86 \qquad\qquad \partial K_O/\partial T = -0.50 \text{ kb/}^\circ K.$$

Rutile-GeO$_2$

The distinction between adiabatic and isothermal values
is not indicated since the differences are more than ade-
quately covered by uncertainties. Previously, Ahrens et al.
[1969] obtained K$_0$ = 3.6 Mb and $\partial K/\partial P$ = 3 by using the
Dugdale-MacDonald relation for the volume dependence of γ
along the Hugoniot. The 1970 reduction yielding $\partial K/\partial P$ = 6.86
seems appropriate in keeping with similar values found
ultrasonically for TiO$_2$ and rutile-GeO$_2$.

b. Grüneisen's ratio.

Grüneisen's ratio γ is an important parameter in the
reduction of shock-wave data. It is generally regarded to be
only a function of volume and not explicitly a function of
temperature. There is evidence that the room condition γ
(1.5 ± 0.3) for stishovite determined from thermodynamic
data is much higher than the high temperature γ (0.8 to 0.9)
determined from the pressure offsets of fused quartz and por-
ous quartz (Coconino sandstone) Hugoniots [Ahrens et al., 1970].

Because both Grüneisen's ratio and pressure derivatives
of elastic constants are a measure of the anharmonicity of
lattice vibrations, various relationships exist between them.
Acoustic Grüneisen parameters associated with shear and longi-
tudinal modes may be defined by [Schuele and Smith, 1964]:

$$\gamma_s = 1/3 + K_T \ (\partial \ln V_s \ / \ \partial P)_T \qquad \text{(Eqn. III.1)}$$

$$\gamma_p = 1/3 + K_T \ (\partial \ln V_p \ / \ \partial P)_T \qquad \text{(Eqn. III.2)}$$

Rutile-GeO$_2$

The definitions are for the case of an isotropic solid.
If Hill averages are used, Eqns. III.1 and III.2 may also
be applied to single crystal elastic constants.

For high temperatures when all modes are excited

$$\gamma_{HT} = (\gamma_p + 2\gamma_s)/3 \qquad \text{(Eqn. III.3)}$$

since there exist twice as many shear modes as longitudinal
modes. The low temperature (where the specific heat associ-
ated with each mode is inversely proportional to the velocity
cubed) value is given by

$$\gamma_{LT} = \frac{V_p^{-3}\gamma_p + 2V_s^{-3}\gamma_s}{V_p^{-3} + 2V_s^{-3}} . \qquad \text{(Eqn. III.4)}$$

For reference purposes, the various γ's for GeO$_2$ are
given below:

$$\gamma_s = 0.87 \qquad\qquad \gamma_p = 2.02$$

$$\gamma_{LT} = 0.97 \qquad\qquad \gamma_{HT} = 1.25$$

$$\gamma_{thermo} = 1.16 \qquad\qquad \gamma_{elastic} = 1.06$$

The room condition thermodynamic $\gamma_{thermo} = \alpha K/C_p \rho_o = 1.16$
based on $\alpha = 13.6 \times 10^{-6}/°K$ [Rao et al., 1968] and $C_p =$
12 cal/mole°K [Counsell and Marin, 1967]. Since the

Rutile-GeO$_2$

Debye temperature for GeO$_2$ calculated from V_p and V_s is 773 °K, γ_{HT} and γ_{LT} may be averaged to obtain $\gamma_{elastic}$ = 1.06 for room conditions (300 °K). The value compares favorably with γ_{thermo} but is lower. Manghnani found that for TiO$_2$, $\gamma_{elastic}$ = 0.88 while γ_{thermo} = 1.28.

c. Static compression measurements.

Bassett and Barnett [1970] measured the change in X-ray lattice parameter of stishovite to 85 kb at 25 °C in a tetrahedral press. NaCl mixed with the stishovite was used to calibrate the pressure. The compressibilities parallel to the a-axis and c-axis are given below when linear fits were made to the lattice parameter versus pressure data.

$$\beta_a = \frac{-1}{a_o} \frac{\Delta a}{\Delta P} = 0.138 \ \text{Mb}^{-1}$$

$$\beta_c = \frac{-1}{c_o} \frac{\Delta c}{\Delta P} = 0.057 \ \text{Mb}^{-1}$$

The ratio β_c/β_a is equal to 0.41 which is intermediate between the ratios found for TiO$_2$ and rutile-GeO$_2$. The volume compressibility β_V is 0.333 Mb^{-1} which gives a bulk modulus K = 3.0 Mb. However, if the volume versus pressure data were fit by the Birch-Murnaghan equation, K = 2.76 Mb for $\partial K/\partial P$ = 4 and K = 2.69 Mb for $\partial K/\partial P$ = 6. The different values suggest that a 10% uncertainty may be placed on the value for the bulk modulus.

Rutile-GeO$_2$

d. Discussion.

A value of $(\partial K/\partial P)_{P=0}$ between 6 and 7 should be used in reductions of shock-wave or isothermal compression data for stishovite which involve that parameter. The similar $\partial K/\partial P$ values for TiO$_2$ and rutile-GeO$_2$ make such a requirement reasonable and seem to rule out the possibility that the high $\partial K/\partial P$ for TiO$_2$ is due to some peculiarity of the electronic structure. In fact the Ti^{4+} ion is 3p^6 in its outermost shell and is exactly isoelectronic to Si^{4+} which is 2p^6. Ge^{4+} is 3d^{10} and hence might be considered more likely to show any electronic structure bonding differences. Recall, however, that the silicon atom and the germanium atom are isoelectronic, and that in oxides they show more crystal chemical similarities because their ionic radii are closer. Thus TiO$_2$ and rutile-GeO$_2$ together indicate that stishovite will have a value of $\partial K/\partial P$ between 6 and 7 because of their similar crystal structures.

e. Some suggestions.

Much effort has gone into the shock-wave work on quartz. Some of the assumptions used in the reduction of the data may perhaps be checked by performing shock-wave experiments on polycrystalline GeO$_2$, both in the quartz and rutile structures. The synthesis of such samples to a density between 90 and 95% theoretical density should provide no special difficulty. Such synthesis has been done by Soga [1971].

Rutile-GeO_2

The thermochemical data for both the quartz and rutile structures are fairly complete. Reliable single crystal elastic constants, their pressure derivatives, and their temperature derivatives for rutile-GeO_2 have been presented. Single crystal data for quartz-GeO_2 may also be expected to be available in the future. Single crystal quartz-GeO_2 samples of limited size have been grown already [Roy and White, 1967; Finch and Clark, 1968; Theokritoff, 1970]. A 1 cm^3 size sample would be sufficient for an ultrasonic study. Complete sets of elastic constants for both structures along with shock-wave measurements would be an opportunity to study the lattice dynamics over this geophysically interesting phase transition.

Rutile-GeO$_2$

E. Phase transformation and diffusion kinetics.

The kinetics of the quartz-GeO$_2$ → rutile-GeO$_2$ transformation as a function of pressure (10 to 30 kb) and temperature (380 to 600 °C) were studied by Zeto and Roy [1969]. The transformation is of the metastable-to-stable type with a large volume decrease (50%) and thus is of the type one might associate with a phase transformation source for deep focus earthquakes [Evison, 1963; Randall, 1964; Holstrom, 1968].

The experimentally determined rate curves are shown in Fig. III.6. Zeto and Roy in their discussion of the rate curves divided the transformation kinetics into three stages.

Stage 1. The initial growth of the rutile phase was relatively rapid and was increased by both pressure and temperature. This stage was interpreted as the nucleation of rutile growth sites over the surfaces of individual grains.

Stage 2. After the formation of nuclei on grain surfaces, the growth of the nuclei took place preferentially over further nucleation. This mechanism represented the rate curve up to the "knee."

Stage 3. Beyond the knee of the curve the rate behavior was somewhat unusual. The interpretation was that inhibition of the growth of the rutile phase occurred due to the formation of a product layer of the phase surrounding the individual grains.

Rutile-GeO$_2$

Zeto and Roy continued their discussion by writing the rate of transformation in the general form:

$$\alpha = 1 - \exp(-bt^n) \qquad \text{(Eqn. III.5)}$$

where α = volume fraction transformed

t = time

b, n = constants

The portion of the rate curves before the knee yielded $n = 0.5$. A value of $n = 0.5$ had been suggested for diffusion controlled growth. An empirical activation energy of 29 ± 9 kcal/mole and an activation volume between -15 and -25 cm^3/ mole were obtained for the transformation before the knee. The negative activation volume meant that the activation energy decreased as a function of pressure, i.e., the rate constants increased as a function of pressure. Since diffu- sion rate constants normally are decreased by pressure, a diffusion mechanism for the transformation became questionable. Zeto and Roy did not rule out the possibility since they indicated that pressure might have reduced the particle size and hence increased the transformation rate.

Rutile-GeO$_2$

a. Keyes' strain energy model.

In terms of Keyes' [1963] strain energy model presented
in the previous chapter, the diffusion rate constant might
actually be expected to increase a little with pressure.
Keyes' relation is

$$V^* = \frac{G^*}{K} \left[\frac{K}{\mu} \frac{\partial \mu}{\partial P} - 1 \right] \qquad \text{(Eqn. III.6)}$$

where V^* = activation volume for diffusion

   G^* = activation energy for diffusion

   K = bulk modulus

   μ = shear modulus.

From Soga's values of V_p = 4.1 km/sec and V_s = 2.55 km/sec for
quartz-GeO$_2$, the bulk modulus K is 0.348 Mb and the shear
modulus μ is 0.278 Mb so that K/μ = 1.25. The ratio K/μ is
0.82 for α-quartz [based on Hill averages for K and μ from the
single crystal values of McSkimin et al., 1965]. α-quartz is
apparently the only oxide known for which the bulk modulus is
smaller than the shear modulus. Soga's quartz-GeO$_2$ does not
show such behavior. Single crystal elastic constants to con-
firm the K/μ ratio for quartz-GeO$_2$ would be desirable.

Since the pressure derivative $\partial \mu / \partial P$ for quartz-GeO$_2$ is
not available, a value of 0.5 is estimated from the quartz-SiO$_2$
data [McSkimin et al., 1965]. Then the factor in brackets in
Eqn. III.6 is negative and so is V^*.

Rutile-GeO$_2$

b. Empirical melting temperature relationship.

Now consider the empirical diffusion relationship

advocated by Weertman [1970].

$$D = D_o \exp(-gT_m/T) \qquad \text{(Eqn. III.7)}$$

where   D = diffusion coefficient

D$_o$ = constant

g = constant

T$_m$ = melting temperature as function

of pressure

T = temperature

The general relationship for the diffusion coefficient under

pressure is given by

$$D = D_o \exp(-G^*/kT) \exp(-PV^*/kT) \qquad \text{(Eqn. III.8)}$$

where   G* = activation energy for diffusion

V* = activation volume for diffusion

k = Boltzmann's constant.

For small pressures $T_m = T_{m_o} + (dT_m/dP)_o P$, where T_{m_o} =

melting temperature at P = 0.   Then near P = 0 the constant g

of Eqn. III.7 should satisfy both $g = G^*/kT_{m_o}$ and

$g = V^*/(k(dT_m/dP)_o)$ [Weertman, 1970].   If the two expressions

for g are assumed to be equal, then

Rutile-GeO$_2$

$$V^* = G^* \, (dT_m/dP)_o \, / \, T_{m_o} \, . \qquad \text{(Eqn. III.9)}$$

A value of $(dT_m/dP)_o = -0.5$ °C/bar is obtained from the

GeO$_2$ phase diagram (Fig. III.2). Then V* is negative.

Quantitative agreement between Eqn. III.6 and III.9 is lack-

ing (V*/G* $\simeq$ -1.0 Mb^{-1} and V*/G* $\simeq$ -0.5 kb^{-1}, respectively)

but the signs do agree.

c. Summary.

The negative sign of the experimentally determined

activation volume for the quartz-GeO$_2$ → rutile-GeO$_2$ trans-

formation is predicted by Keyes' strain energy model for

diffusion and the empirical melting temperature relation

favored by Weertman. For quartz-GeO$_2$ there does not seem to

be a conflict between the two theories. Since the theories

predict an increase in diffusion rate with pressure, it may

not be necessary to suppose a particle size effect in order

to have the quartz → rutile transformation kinetics be

controlled by a diffusion process.

Rutile-GeO$_2$

F. FeO and SiO$_2$ in the lower mantle.

The composition of the lower mantle was inferred from
seismic data and ultrasonic, shock wave, isothermal compres-
sion, petrologic, crystal chemical, and high-pressure/high-
temperature phase equilibria studies by Ringwood [1970] and
D.L. Anderson [1970]. Ringwood concluded that the mineral
assemblage was denser than an isochemical mixture of oxides
due to phase transitions and that no change in chemical
composition was required. D.L. Anderson concluded that the
lower mantle was richer in FeO and SiO$_2$ than in the upper
mantle.

In my opinion the discussion of the lower mantle given
by Ringwood [1970] was well-reasoned and consistent with the
available data. The reader is referred to his paper for the
details. The methods by which D.L. Anderson reached his con-
clusions on the composition of the lower mantle will be cri-
tically reviewed in this section.

1. D.L. Anderson's three methods for estimating the composi-
tion of the lower mantle.

Method 1. Since the lower mantle (1000 to 2900 km) is basi-
cally homogeneous and adiabatic, the third-order Birch-
Murnaghan equation and its density derivative may be least
squares fit to different density and seismic velocity models.

Rutile-GeO$_2$

The final parameters determined are a room condition density ρ_o and seismic parameter Φ_o. The mean atomic weight $\overline{M}$ (i.e., iron content) is determined from the seismic equation of state [D.L. Anderson, 1967].

Method 2. The assumption is made that the room condition molar volumes and seismic parameters of the high-pressure phases of olivine, pyroxene, and garnet are molar sums and molar averages of the constituent oxides, respectively. Then the ρ_o and Φ_o found for the lower mantle determine molar percentages of the oxides MgO, FeO, and SiO$_2$ (stishovite).

Method 3. A direct comparison is made between the lower mantle's pressure versus density curve and that of shocked dunites of different FeO/(FeO + MgO) ratios.

2. Discussion.

Methods 1 and 3 marginally favored the case for iron-enrichment. The uncertainties in the seismic equation of state were duly noted [D.L. Anderson and Jordan, 1970]. Ringwood [1970] discussed the shock-wave evidence with the conclusion that iron-enrichment was possible but not required. My discussion then concentrates on Method 2 -- the molar averaging scheme.

Rutile-GeO$_2$

a.   Assumption of an isochemical mixture of oxides.

Note immediately that an isochemical mixture of oxides has been assumed since the molar volumes of the high-pressure phases of olivine, pyroxene, and garnet are considered to be the molar sum of the oxides.   The lower mantle density referred to room conditions is generally conceded to be greater than an isochemical mixture of oxides of upper mantle composition.   Is the greater density due to phase transitions and/or iron enrichment?   Assuming an isochemical mixture of oxides begs the question in favor of iron enrichment since phase transformations to a denser state are precluded.   (Previously, D.L. Anderson [1968] also made the assumption of an isochemical mixture of oxides.   In that paper (p. 94) he explicitly stated that his conclusions involved only the region between the top of the mantle and 800 km depth and that he did not rule out the possibility of further phase changes below 800 km. In D.L. Anderson and Jordan [1970], however, their discussion dealt only with the lower mantle at depths greater than 1000 km.)

b.   Uncertainties in $\Phi(SiO_2)$.

Anderson and Jordan [1970] apparently used a value $\Phi(SiO_2) = 85$ km^2/sec^2 while Anderson et al. [1971] used $\Phi(SiO_2) = 70$ km^2/sec^2.   One wonders, of course, what the effect is of the change in values.   The change is summarized in Fig. III.7.   In Fig. III.7 the dashed lines represent the

Rutile-GeO$_2$

original figure from Anderson and Jordan [1970] while the

solid lines represent the revision to $\Phi(SiO_2) = 70$ km^2/sec^2.

The garnet line has not been reproduced for simplicity.

In the figure's original form the lower mantle ρ_o and Φ_o

solutions fell between the dashed "pyroxene" and "olivine"

lines. The molar averaging scheme gave a composition (in

mole percent):

$$\text{Model 200204} \qquad 0.38 \text{ MgO} + 0.16 \text{ FeO} + 0.46 \text{ SiO}_2$$
$$\text{(82\% "pyroxene")}$$

$$\text{Birch 2} \qquad 0.49 \text{ MgO} + 0.12 \text{ FeO} + 0.39 \text{ SiO}_2$$
$$\text{(43\% "pyroxene")}$$

By way of comparison Ringwood's pyrolite [Ringwood, 1966] is:

$$\text{Pyrolite} \qquad 0.54 \text{ MgO} + 0.06 \text{ FeO} + 0.40 \text{ SiO}_2$$
$$\text{(50\% "pyroxene")}$$

However, in its revised form, the lower mantle solutions no

longer fall between the "pyroxene" and "olivine" lines.

But now the triangle determined by the points SiO_2,

Mg_2SiO_4, and $(Mg_{0.5}Fe_{0.5})_2SiO_4$ is almost the same as that in

Fig. 4 of Anderson et al. [1971]. They evidently used this

triangle in the sense of a petrologic composition indicator.

For example, a perpendicular is dropped to the ρ-axis from

the point representing Model 200204. The point at which the

perpendicular to the ρ-axis intersects the Mg_2SiO_4 -

Rutile-GeO_2

$(Mg_{0.5}Fe_{0.5})_2SiO_4$ base side determines the MgO/FeO ratio. The (MgO + FeO)/SiO_2 ratio is determined by the ratio of lengths along the vertical between $\Phi(SiO_2)$ and the "olivine" line with Model 200204 as the dividing point. The triangle of Fig. III.7 gives a 100% "pyroxene" component $(Mg_{0.7}Fe_{0.3})SiO_3$ with 15% excess silica. D.L. Anderson et al. [1971] found a 100% "pyroxene" component $(Mg_{0.64}Fe_{0.36})SiO_3$.

c. Summary.

Consistency of the petrologic triangle interpolation scheme with the molar averaging scheme is lacking when the same $\Phi(SiO_2)$ is used in both cases. All the lower mantle solutions fall above the revised "pyroxene" and "olivine" lines (Fig. III.7). Presumably, no one will consider the revised figure to be an argument for a lower mantle richer in silica than "pyroxene."

Rutile-GeO$_2$

References

Ahrens, T.J., D.L. Anderson, and A.E. Ringwood, Equations of state and crystal structures of high-pressure phases of shocked silicates and oxides, Rev. Geophys., 7, 667-707, 1969.

Ahrens, T.J., T. Takahashi, and G. Davies, A proposed equation of state of stishovite, J. Geophys. Res., 75, 310-316, 1970.

Anderson, D.L., A seismic equation of state, Geophys. J., 13, 9-30, 1967.

Anderson, D.L., Chemical inhomogeneity of the mantle, Earth Planet. Sci. Letters, 5, 89-94, 1968.

Anderson, D.L., Petrology of the mantle, in Special Paper No. 3, edited by B.A. Morgan, pp. 85-93, Mineralogical Society of America, Washington, D.C., 1970.

Anderson, D.L., and T. Jordan, The composition of the lower mantle, Phys. Earth Planet. Interiors, 3, 23-35, 1970.

Anderson, D.L., and H. Kanamori, Shock-wave equations of state for rocks and minerals, J. Geophys. Res., 73, 6477-6502, 1968.

Anderson, D.L., C. Sammis, and T. Jordan, Composition and evolution of the mantle and core, Science, 171, 1103-1112, 1971.

Bassett, W.A., and J.D. Barnett, Isothermal compression of stishovite and coesite up to 85 kilobars at room temperature by X-ray diffraction, Phys. Earth Planet. Interiors, 3, 54-60, 1970.

Bernal, J.D., Discussion, Observatory, 59, 268, 1936.

Rutile-GeO$_2$

Chung, D.H., D.J. Silversmith, and B.B. Chick, A modified ultrasonic pulse-echo-overlap method for determining sound velocities and attenuation of solids, Rev. Sci. Inst., 40, 718-720, 1969.

Counsell, J.F., and J.F. Martin, The entropy of tetragonal germanium dioxide, J. Chem. Soc. (A), 560-561, 1967.

Dachille, F., and R. Roy, High pressure studies of the system Mg$_2$GeO$_4$ - Mg$_2$SiO$_4$ with special reference to the olivine-spinel transition, Am. J. Sci., 258, 225-246, 1960.

Davies, G.F., and D.L. Anderson, Revised shock-wave equations of state for high-pressure phases of rocks and minerals, J. Geophys. Res., 76, 2617-2627, 1971.

Evison, F.F., Earthquakes and faults, Bull. Seismol. Soc. Am., 53, 873-891, 1963.

Finch, C.B., and G.W. Clark, Flux growth and characterization of hexagonal germanium dioxide single crystals, Am. Mineral., 53, 1394-1398, 1968.

Fyfe, W.S., Geochemistry of Solids, 199 pp., McGraw-Hill, New York, 1964.

Goodrum, J.W., Top-seeded flux growth of tetragonal GeO$_2$, J. Crystal Growth, 7, 254-256, 1970.

Goodrum, J.W., Growth and characterization of tetragonal (rutile) GeO$_2$ crystals, Phys. Sci. Res. Pap. No. 449, 25 pp., Air Force Cambridge Research Laboratories, Bedford, Mass., 1971.

Rutile-GeO$_2$

Hausner, M., A Vector Space Approach to Geometry, 397 pp.,
Prentice-Hall, Englewood Cliffs, N.J., 1965.

Hill, V.G., and L.L.Y. Chang, Hydrothermal investigation of
GeO$_2$, Am. Mineral., 53, 1744-1748, 1968.

Holm, J.L., O.J. Kleppa, and E.F. Westrum, Jr., Thermodynamics
of polymorphic transformations in silica. Thermal properties
from 5 to 1070°K and pressure-temperature stability fields
for coesite and stishovite, Geochim. Cosmochim. Acta, 31,
2289-2307, 1967.

Holstrom, G.B., Elastic radiation from a propagating phase
boundary, Phys. Earth Planet. Interiors, 1, 181-195, 1968.

Ida, Y., Y. Syono, and S. Akimoto, Effect of pressure on the
lattice parameters of stishovite, Earth Planet. Sci. Letters,
3, 216-218, 1967.

Keyes, R.W., Continuum models of the effect of pressure on
activated processes, in Solids under Pressure, edited by W.
Paul and D.M. Warschauer, pp. 71-99, McGraw-Hill, New York,
1963.

Laubengayer, A.W., and D.S. Morton, Germanium. XXXIX. The
polymorphism of germanium dioxide, J. Am. Chem. Soc., 54,
2303-2320, 1932.

Liu, L.G., T. Takahashi, and W.A. Bassett, Compression of
stishovite and magnesian ilmenite at 25°C, Trans. Am. Geophys.
Union, 50, 312, 1969.

Rutile-GeO$_2$

Manghnani, M.H., Elastic constants of single-crystal rutile under pressure to 7.5 kilobars, J. Geophys. Res., 74, 4317-4328, 1969.

McQueen, R.G., J.N. Fritz, and S.P. Marsh, On the equation of state of stishovite, J. Geophys. Res., 68, 2319-2322, 1963.

McSkimin, H.J., P. Andreatch, Jr., and R.N. Thurston, Elastic moduli of quartz versus hydrostatic pressure at 25° and -195.8°C, J. Appl. Phys., 36, 1624-1632, 1965.

Mizutani, H., Shear wave velocities of mantle minerals and their geophysical implications, paper presented at the International Symposium on Mechanical Properties and Processes in the Mantle, Flagstaff, Arizona, 24 June - 3 July 1970.

Papadakis, E.P., Ultrasonic phase velocity by the pulse-echo-overlap method incorporating diffraction phase corrections, J. Acoust. Soc. Am., 42, 1045-1951, 1967.

Randall, M.J., Seismic energy generated by a sudden volume change, Bull. Seismol. Soc. Am., 54, 1291-1298, 1964.

Rao, K.V.K., S.V.N. Naidu, and L. Iyengar, Thermal expansion of rutile-type GeO$_2$ by the X-ray method, J. Am. Ceram. Soc., 51, 467-468, 1968.

Rayne, J.A., and B.S. Chandrasekhar, Elastic constants of β tin from 4.2°K to 300°K, Phys. Rev., 120, 1658-1663, 1960.

Ringwood, A.E., Mineralogy of the mantle, in Advances in Earth Science, edited by P.M. Hurley, pp. 357-399, MIT Press, Cambridge, 1966.

Rutile-GeO$_2$

Ringwood, A.E., Phase transformations and the constitution of the mantle, Phys. Earth Planet. Interiors, 3, 109-155, 1970.

Ringwood, A.E., and A. Major, The system Mg$_2$SiO$_4$ - Fe$_2$SiO$_4$ at high pressures and temperatures, Phys. Earth Planet. Interiors, 3, 89-108, 1970.

Ringwood, A.E., and M. Seabrook, Olivine-spinel equilibria at high pressure in the system Ni$_2$GeO$_4$ - Mg$_2$SiO$_4$, J. Geophys. Res., 67, 1975-1985, 1962.

Roy, R., and W.B. White, High temperature solution (flux) and high pressure solution (hydrothermal) crystal growth, J. Crystal Growth, 3,4, 33-42, 1968.

Schuele, D.E., and C.S. Smith, Low temperature thermal expansion of RbI, J. Phys. Chem. Solids, 25, 801-814, 1964.

Shannon, R.D., and C.T. Prewitt, Effective ionic radii in oxides and fluorides, Acta Cryst., B25, 925-946, 1969.

Soga, N., Pressure derivatives of the elastic constants of vitreous germania at 25°, -78.5°, and -195.8°C, J. Appl. Phys., 40, 3382-3385, 1969.

Soga, N., Sound velocity of some germanate compounds and its relation to the law of corresponding states, J. Geophys. Res., 76, 3983-3989, 1971.

Stishov, S.M., and S.V. Popova, New dense polymorphic modification of silica, Geokhimiya, English Transl., no. 10, 837-839, 1961.

Rutile-GeO$_2$

Theokritoff, S., Hetero-epitaxial growth of large crystals of

  a metastable phase: germania [quartz], M.S. thesis, The

  Pennsylvania State University, University Park, 1970.

Wackerle, J., Shock-wave compression of quartz, J. Appl. Phys.,

  33, 922-937, 1962.

Weertman, J., The creep strength of the earth's mantle, Rev.

  Geophys. Space Phys., 8, 145-168, 1970.

Zeto, R.J., and R. Roy, Kinetics of the GeO$_2$(quartz) → GeO$_2$

  (rutile) transformation at pressure to 30 kbar, in Reactivity

  of Solids, edited by J.W. Mitchell, R.C. DeVries, R.W. Roberts,

  and P. Cannon, pp. 803-815, Wiley-Interscience, New York,

  1969.

Table III.1

Comparison of some isostructural germanates and silicates.

[after Ringwood's Table 1, 1970]

Structure	Germanate	Stability conditions	Silicate	Stability conditions
Rutile	GeO_2	$P = 0$ $T < 1007\ °C$	SiO_2	$P > 100\ kb$ $T = 1000\ °C$
Garnet	$Ca_3Al_2Ge_3O_{12}$	$P = 0$ $T \sim 1000\ °C$	$Ca_3Al_2Si_3O_{12}$	$P > 15\ kb$ $T = 800\text{-}1000\ °C$
Spinel	Ni_2GeO_4	$P = 0$ $T = 650\ °C$	Ni_2SiO_4	$P > 18\ kb$ $T = 650\ °C$
Spinel	Fe_2GeO_4	$P = 0$ $T = 600\ °C$	Fe_2SiO_4	$P > 38\ kb$ $T = 600\ °C$
Spinel	$(Mg_{0.8}Fe_{0.2})_2GeO_4$	$P = 0$ $T = 800\ °C$	$(Mg_{0.8}Fe_{0.2})_2SiO_4$	$P > 110\ kb$ $T = 800\ °C$

Table III.2

Densities and thermochemical data for germania and silica.

	GeO_2(qtz)	GeO_2(rut)	SiO_2(qtz)	SiO_2(stish)
Density (g/cm^3)	4.28	6.28	2.65	4.28
Molecular wt.	104.6	104.6	60.1	60.1
Vol. (cm^3/mole)	24.44	16.66	22.70	14.04

	GeO_2(qtz→rut)	SiO_2(qtz→stish)
$(\Delta H)^\circ_{298}$(kcal/mole)	-4.85 ± 0.7	11.8 ± 0.3
$(\Delta S)^\circ_{298}$(cal/mole°K)	-3.5 ± 0.6	-3.24
$(\Delta V)^\circ_{298}$(cm^3/mole)	-8.0	-8.7

Qtz = Quartz

Rut = Rutile

Stish = Stishovite

Table III.3

Elastic constants determined from different

propagation modes shown in Fig. III.4.

Propagation direction	Path length (mm)	Vibration direction	Vibration mode	Elastic constant
[110]	9.5225	[110]	L	C_{L_1}
[110]	9.5225	[1$\bar{1}$0]	T	C_s
[110]	9.5225	[001]	T	C_{44}
[001]	6.7686	[001]	L	C_{33}
[001]	6.7686	Any	T	C_{44}
[100]	6.8669	[100]	L	C_{11}
[100]	6.8669	[010]	T	C_{66}
[100]	6.8669	[001]	T	C_{44}
[101]	4.9878	[101]	L	C_{L_2}
[101]	4.9878	[010]	T	C_{T_1}
[101]	4.9878	[10$\bar{1}$]	T	C_{T_2}

where $C_{L_1} = 1/2 \ (C_{11} + C_{12} + 2C_{66})$

$C_s = 1/2 \ (C_{11} - C_{12})$

$C_{L_2} = A + B$

$C_{T_1} = 1/2 \ (C_{44} + C_{66})$

$C_{T_2} = A - B$

$A = 1/4 \ (C_{11} + C_{33} + 2C_{44})$

$B = 1/4 \ [(C_{11} - C_{33})^2 + 4 \ (C_{13} + C_{44})^2]^{1/2}$

Also   L = longitudinal, T = transverse

Table III.4

Average values for C_{ij}, $\partial C_{ij}/\partial P$, and $\partial C_{ij}/\partial T$ for different

modes. Since the values for C_{44} as determined from different

modes showed no systematic error, the values below are

arithmetic averages of all runs for it.

Elastic constant designation (see Table III.3)	Velocity from $C_{ij} = \rho v^2$ (km/sec)	C_{ij} (Mb)	$\partial C_{ij}/\partial P$	$\partial C_{ij}/\partial T$ (kb/°K)
C_{11}	7.328	3.372	6.50	−0.40
C_{33}	9.770	5.994	6.63	−0.38
C_{44}	5.072	1.615	1.78	−0.15
C_{66}	6.415	2.584	4.10	−0.38
C_{s}	3.445	0.745	−0.69	+0.02
C_{L_1}	9.109	5.210	11.62	−0.90
C_{L_2}	8.949	5.029	7.16	-----
C_{T_1}	5.784	2.100	----	-----
C_{T_2}	4.554	1.302	1.55	−0.11

----- indicates that a pressure or temperature

run was not made.

Table III.5

Rutile-GeO$_2$ single crystal elastic constants.

(Based on density ρ = 6.279 g/cm^3)

	11	12	13	33	44	66
C_{ij}	3.372	1.882	1.874	5.994	1.615	2.584
S_{ij}	0.458	-0.213	-0.077	0.215	0.619	0.387
$\partial C_{ij}/\partial P$	6.65	8.05	4.10	6.63	1.78	4.10
$\partial S_{ij}/\partial P$	-0.01	-0.64	0.12	-0.21	-0.68	-0.61
$\partial C_{ij}/\partial T$	-0.42	-0.46	-0.23	-0.38	-0.15	-0.38
$\partial S_{ij}/\partial T$	0.11	0.29	-0.08	0.13	0.58	0.57

$$\frac{\partial S}{\partial X} = -S \frac{\partial C}{\partial X} S$$

$\partial C_{ij}/\partial T$ are based on the following thermal expansion values [Rao et al., 1968]:

α_a = linear thermal expansion parallel to a-axis

= 6.3 x 10^{-6}/°C

α_c = linear thermal expansion parallel to c-axis

= 2.1 x 10^{-6}/°C

Table III.5

Rutile-GeO$_2$ single crystal elastic constants.

Based on density ρ = 6.279 g/cm^3

(continued)

$$\beta_a = S_{11} + S_{12} + S_{13} = 0.168 \text{ Mb}^{-1}$$

$$\beta_c = S_{33} + 2S_{13} = 0.062 \text{ Mb}^{-1}$$

$$\beta_V = 2S_{11} + S_{33} + 2S_{12} + 4S_{13} = 0.398 \text{ Mb}^{-1}$$

where β_a = linear compressibility parallel to a-axis

β_c = linear compressibility parallel to c-axis

β_V = volume compressibility = $2\beta_a + \beta_c$

Symbol	Unit	Pressure derivative ($\partial/\partial P$) Unit	Temperature derivative ($\partial/\partial T$) Unit
C_{ij}, elastic stiffnesses	Mb	None	Kb/°K
S_{ij}, elastic compliances	Mb^{-1}	Mb^{-2}	10^{-4}Mb^{-1}/°K

Table III.6

Rutile-GeO$_2$ calculated aggregate elastic constants.

(Based on density ρ = 6.279 g/cm^3)

Zero pressure aggregate constants

	E	μ	σ	K	β	V$_s$	V$_p$
Voigt	4.076	1.637	0.245	2.666	0.375	5.106	8.788
Reuss	·3.500	1.381	0.268	2.511	0.398	4.689	8.325

Aggregate pressure derivatives

	∂E/∂P	∂μ/∂P	∂σ/∂P	∂K/∂P	∂β/∂P	∂V$_s$/∂P	∂V$_p$/∂P
"Voigt"	5.19	1.78	2.32	5.83	-0.82	1.82	5.78
"Reuss"	2.83	0.67	4.12	6.48	-0.91	0.20	5.40

(continued)

Table III.6.   (continued)

Rutile-GeO$_2$ calculated aggregate elastic constants.

(Based on density ρ = 6.279 g/cm^3)

	Aggregate temperature derivatives						
	$\partial E/\partial T$	$\partial \mu/\partial T$	$\partial \sigma/\partial T$	$\partial K/\partial T$	$\partial \beta/\partial T$	$\partial V_s/\partial T$	$\partial V_p/\partial T$
"Voigt"	-0.41	-0.16	-0.07	-0.34	0.48	-0.21	-0.44
"Reuss"	-0.25	-0.08	-0.19	-0.38	0.54	-0.10	-0.41

	Symbol	Unit	Pressure derivative $(\partial/\partial P)$ unit	Temperature derivative $(\partial/\partial T)$ unit
E,	Young's modulus	Mb	None	kb/°K
μ,	Shear modulus	Mb	None	kb/°K
σ,	Poisson's ratio	None	Mb^{-1}	10^{-4}/°K
K,	Bulk modulus	Mb	None	kb/°K
β,	Compressibility	Mb^{-1}	Mb^{-2}	10^{-4}Mb^{-1}/°K
V_s,	Shear velocity	km/sec	(km/sec)/Mb	10^{-3}(km/sec)/°K
V_p,	Compressional velocity	km/sec	(km/sec)/Mb	10^{-3}(km/sec)/°K

Rutile-GeO$_2$

Figure Captions

Fig. III.1. Rutile structure [after Fyfe, 1964, p. 47]. The cation is octahedrally coordinated and the oxygen is surrounded by a trigonal-planar group of three cations.

Fig. III.2. Phase diagram of GeO$_2$ [after Hill and Chang, 1968].

Fig. III.3. Sketch of GeO$_2$ sample at different stages of the measurements.

Fig. III.4. Propagation and polarization directions for the different modes used in determining the elastic constants of tetragonal crystals [after Rayne and Chandrasekhar, 1960]. The mode designations are shown in Table III.3.

Fig. III.5. Polycrystalline rutile-GeO$_2$ values for V$_p$ compared to the single-crystal Voigt and Reuss bounds.

Fig. III.6. (a) Quartz-GeO$_2$ → rutile-GeO$_2$ transformation rate curves for different temperatures at 20.4 kb. (b) Quartz-GeO$_2$ → rutile-GeO$_2$ transformation rate curves for different pressures at 480°C [after Zeto and Roy, 1969].

Fig. III.7. Molar averaging scheme for estimating composition of lower mantle from seismic Φ and ρ solutions [revised from D.L. Anderson and Jordan, 1970, p. 32].
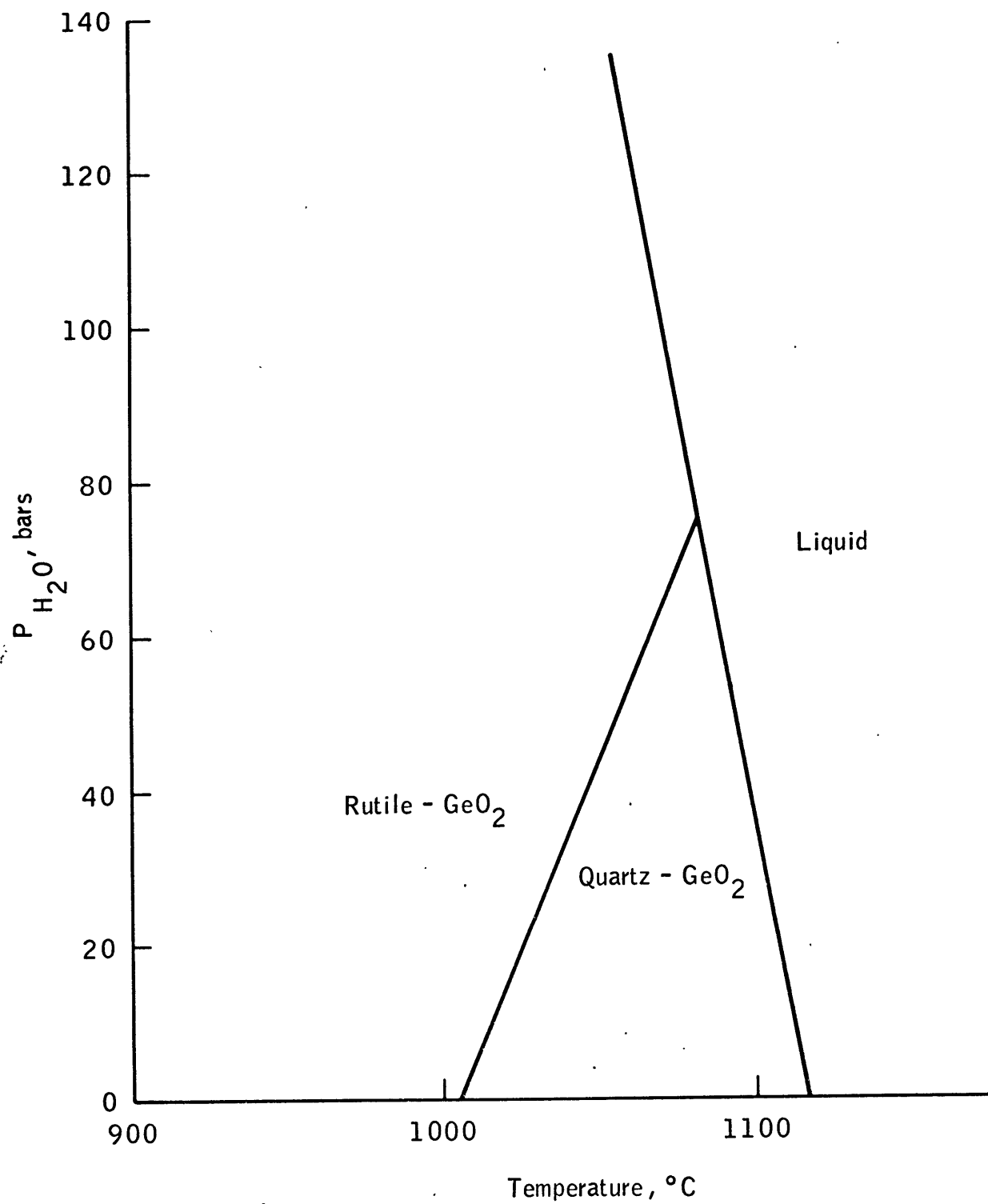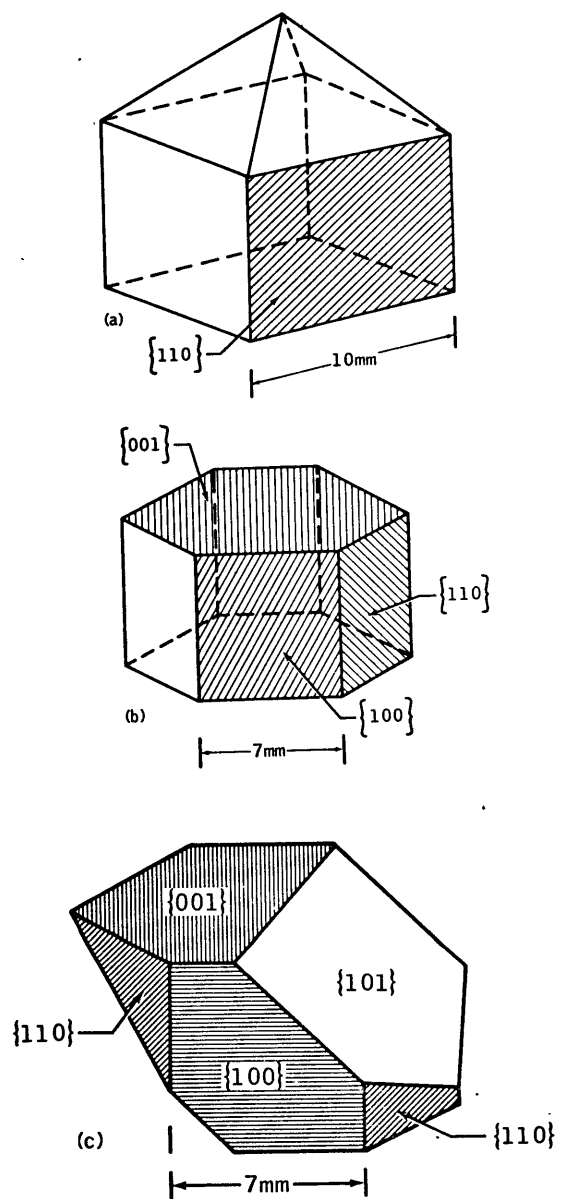
Fig. III.1

● = Ti^{4+}

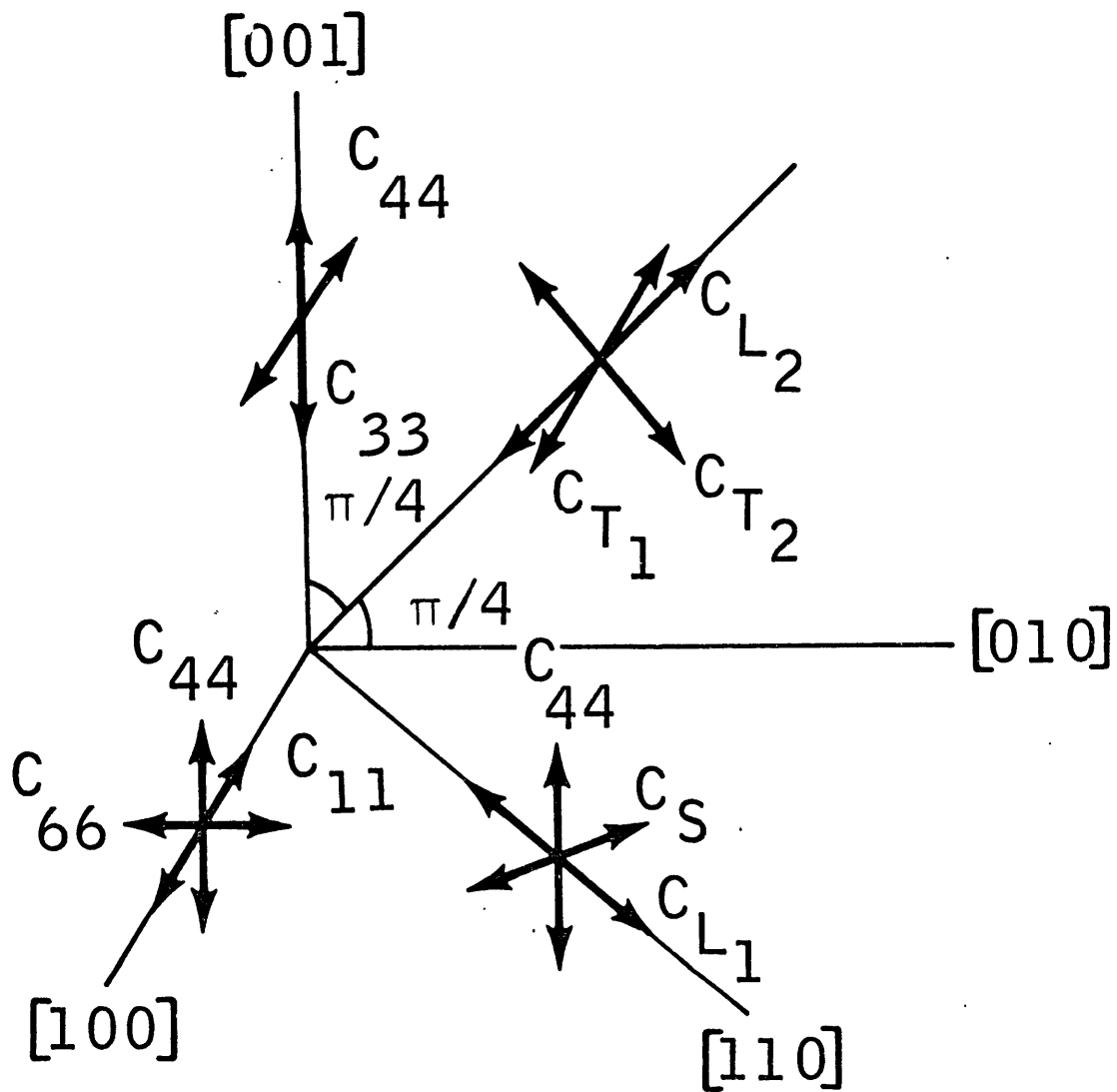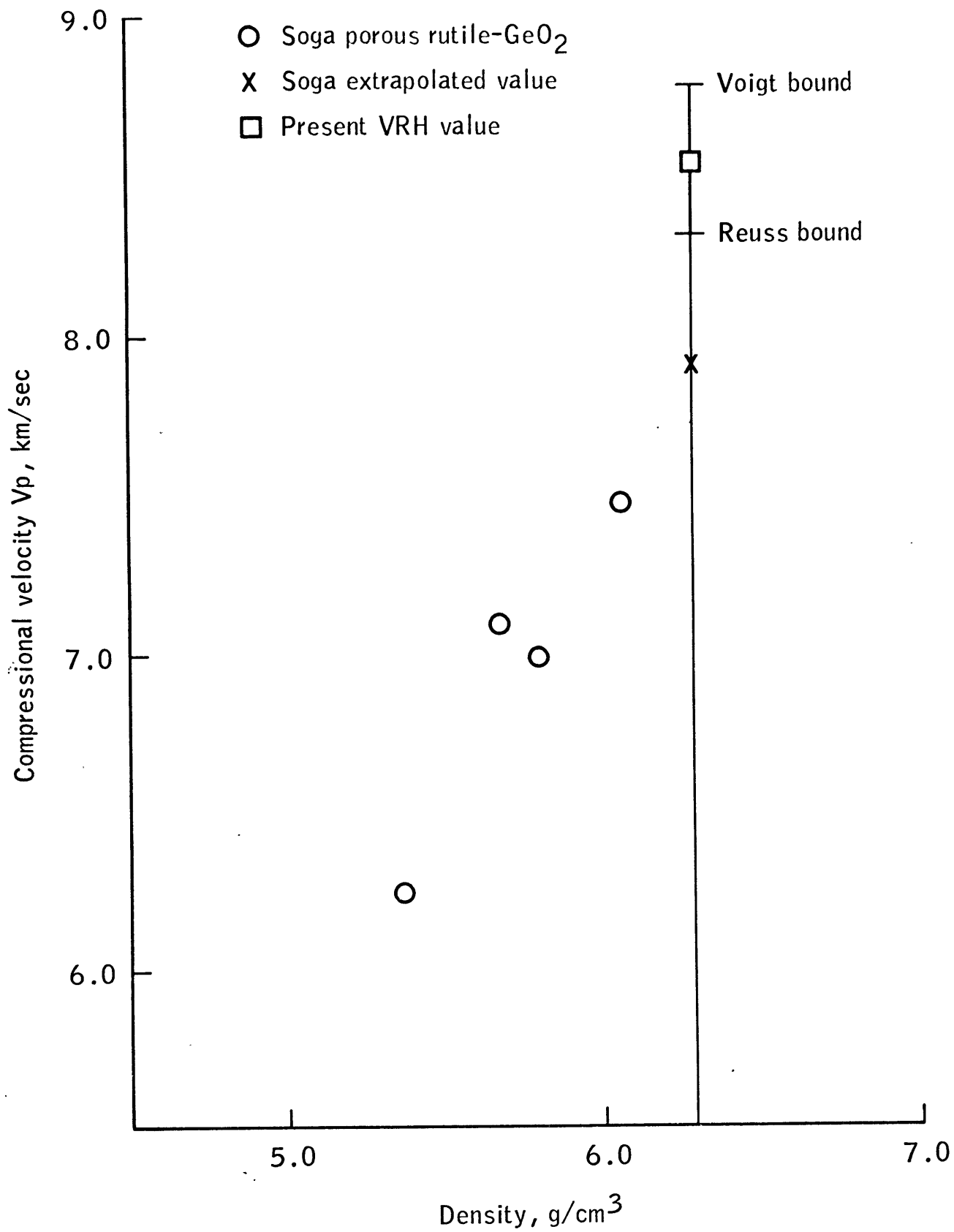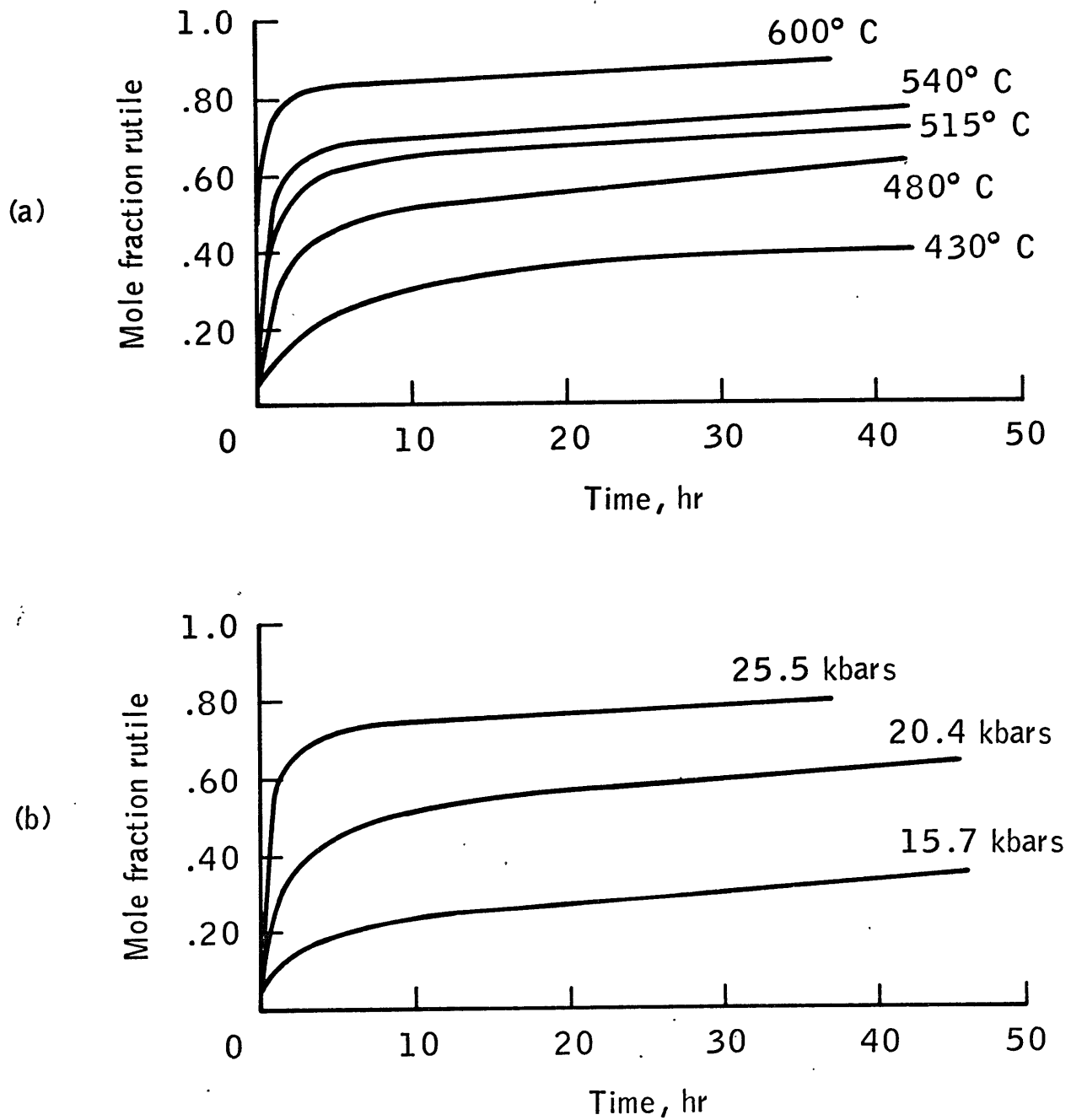O = O^{--}
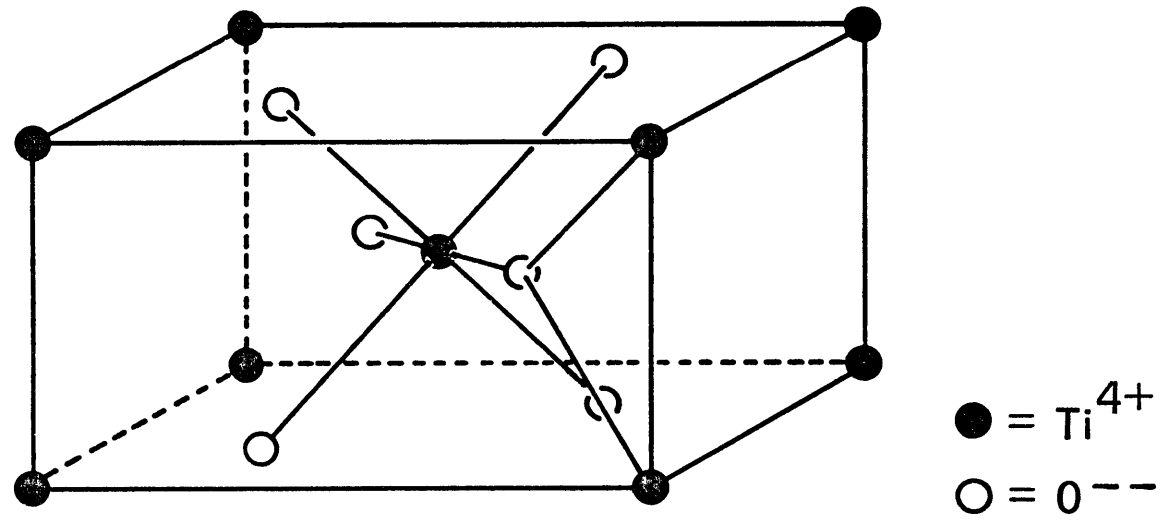
Fig. III.2

Fig. III.3

Fig. III.4

Fig. III.5

(a)

(b)
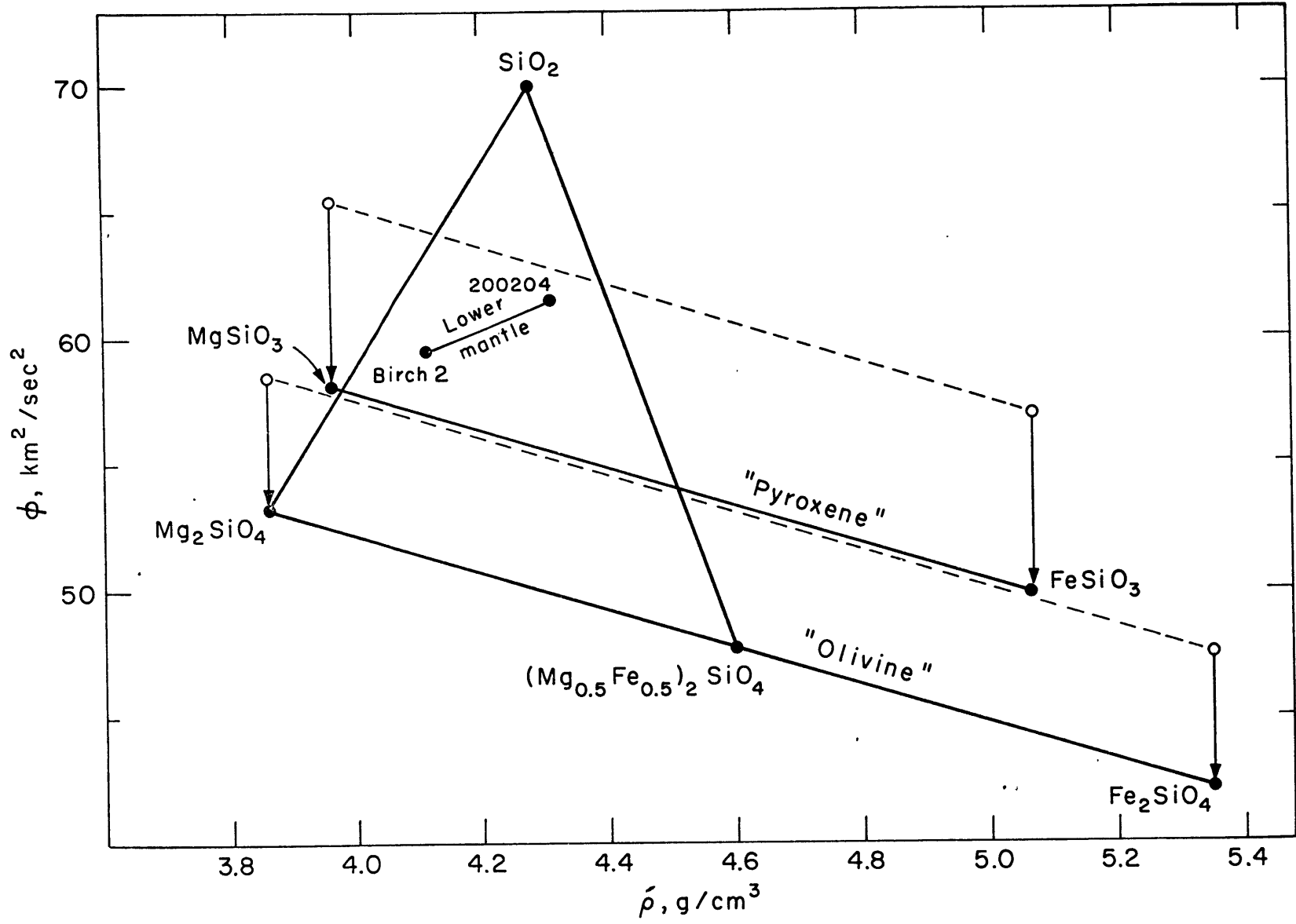

Fig. III.6

Fig. III.7

IV. Elastic constants of spessartite-almandine garnet.

The word "garnet" is used in two different ways. First,

it represents the six natural silicate garnets with the

general formula $A_3^{VIII}B_2^{VI}Si_3^{IV}O_{12}$* (Table IV.1). Second, it

represents the complex structure (Fig. IV.1) which these

natural garnets possess. The context in which the word

"garnet" is used should keep the meaning clear.

The elastic properties of garnet are of geophysical

interest in both senses of the word. (1) Garnet is important

in distinguishing between a peridotitic (olivine + pyroxene)

or eclogitic (pyroxene + garnet) upper mantle. Even for the

predominant view of a peridotitic upper mantle, garnet is an

important accessory phase. For example, if garnet pyrolite

is taken to represent the upper mantle at a depth of 150 to

250 km, then garnet represents 14 weight percent [Ringwood,

1970]. (2) Beginning at about 350 km depth pyroxene

gradually transforms into the garnet structure [Ringwood,

1967]. For example, $MgSiO_3$ has the garnet structural formula

$Mg_3^{VIII}(Mg,Si)^{VI}Si_3^{IV}O_{12}$. "Such garnets, characterized by par-

tial octahedral coordination of silicon, are fundamentally dif-

ferent from the common garnet family of minerals in which sil-

icon is always in tetrahedral coordination" [Ringwood, 1967,

p.258]. The density increase over the pyroxene → garnet

---

*The Roman numeral superscripts indicate coordination number.

Garnet

transformation is about 10% [Ringwood, 1969, p. 406]. Because
of the high pressures and temperatures required for synthesis,
garnet-transformed pyroxenes will not be readily available in
amounts necessary for ultrasonic experiments. So perhaps the
partial octahedral coordination of the silicon may be under-
stood through a combination of analogue studies, namely,
ordinary garnets and six-coordinated silica analogues such as
rutile-GeO_2.

Ultrasonic measurements on garnet in this country have
been limited. Verma [1960] measured the room condition elas-
tic constants of an almandine-pyrope garnet and a spessartite-
almandine garnet. (Table IV.1 is a reminder list of common
end member names of natural garnets and synthetic or rare-
earth garnets as well as their chemical formulas.) Soga
[1967] measured the pressure and temperature dependence of the
elastic constants of another almandine-pyrope garnet. In
Russia Ryzhova et al. [1966] ultrasonically measured the
elastic constants of a number of natural garnets. Several
synthetic garnet measurements and older determinations of
garnets of unspecified composition exist [see the compilation
by Simmons and Wang, 1971].

Garnet

A. Sample description.

Table IV.2 lists the chemical analyses, densities, and mean atomic weights of the present garnet and others considered in this chapter. The analysis of Verma's spessartite-almandine garnet and the present one agree in all oxides to 1.5 weight percent. The present garnet was purchased from the International Mineral Corp., 44 Maiden Lane, New York, New York, as a cut stone (Fig. IV.2a) with Brazil as its likely source of origin. Its original weight was 7.58 g. After X-ray orientation, it appeared as in Fig. IV.2b and its weight was 1.865 g. Only the {110}-faces were polished. The path length was 6.217 mm. Verma's garnet was obtained from the Harvard collection with Brazil as its origin. His [110]-path length was 8.79 mm.

The hydrostatically determined density of the present spessartite-almandine garnet was 4.2374 g/cm^3 while the X-ray density was 4.2597 g/cm^3. An average value of 4.249 g/cm^3 was used in the determination of the elastic constants.

A mean atomic weight of 25.0 was calculated directly from the chemical analysis while $\bar{M}$ from the approximate chemical formula (based on the ideal 12 oxygens in the garnet formula) was 24.7. There is a deficiency of cations compared to the number expected for 12 oxygens (Σ cations = 7.95 versus ideal Σ = 8.00).

Garnet

It is worth emphasizing the optical purity of the present garnet sample. Under a microscope with a strong light source, the garnet transmits like a medium red glass with absolutely no visible flows or inclusions. By way of contrast, Soga's almandine sample contained five volume percent ilmenite inclusions [Takahashi and Liu, 1970].

Garnet

B. Experimental method and results.

The elastic constants of the spessartite-almandine gar-
net were measured to 5 kb at room temperature (20 °C) by the
pulse-echo-overlap technique [Papadakis, 1967; Chung et al.,
1969]. The garnet was oriented to 1/2° with a Laue back-
reflection camera in the [110] and [100]-directions. However,
only the {110}-faces were optically polished flat and parallel
to 10^{-4} in/in by the A.D. Jones Optical Works of Burlington,
Mass. In this direction there exist three independent pure
modes which yield $C_L = 1/2 (C_{11} + C_{12} + 2C_{44})$, $C_S = 1/2 (C_{11} -
C_{12})$, and C_{44}. Then $C_{11} = C_L + (C_S - C_{44})$ and $C_{12} = C_L - C_S -
C_{44}$. The path length in the [110]-direction was 6.217 mm.

The measurements were made at 20 MHz with coaxially
plated X-cut and AC-cut quartz transducers. At this frequency
the echo train was modulated by guided-wave modes. However,
no particular difficulties occurred if early echoes were
used. The C_{ij} are considered to be accurate to 0.5% and the
$\partial C_{ij}/\partial P$ accurate to 5%.

The results of the single crystal measurements are
tabulated in Table IV.3 and calculated aggregate properties
in Table IV.4. No bounds for the aggregate property deriva-
tives are implied. However, because of the very small anisot-
ropy of velocities in single crystal garnet, the averages are
determined fairly well. The raw frequency versus pressure

Garnet

data were fitted by a least squares linear relation. The derivative of the "effective elastic constant" [Thurston, 1965] was obtained either by computing the elastic constant C_{ij} at different pressures and finding the slope, or by differentiating the expression

$$C_{ij} = 4 \, \rho \, l^2 \, f^2 \qquad \text{(Eqn. IV.1)}$$

where ρ = density

l = path length

f = reciprocal round trip travel time

with respect to pressure and evaluating it at P = 0. No distinction between adiabatic and isothermal bulk modulus was made in calculating $\partial C_{ij}/\partial P$ since the difference does not effect the result within the stated 5% accuracy.

Garnet

C. Comparison with other garnets.

1. Ultrasonic measurements on natural garnets.

Tabulated in Table IV.5 are the elastic constants of the present study, garnets 1 and 2 of Verma [1960], the almandine-pyrope of Soga [1967], and the grossularite of Ryzhova et al. [1966]. The immediate conclusion to be drawn from the first four garnets in the upper half of the table is that all four of the natural garnets are very similar in their room condition elastic behavior. All variations are within 2%. Grossularite is an exception as calcium-rich compounds tend to be [Simmons, 1964].

The comparison of the pressure derivative values of the present garnet with Soga's almandine-pyrope is shown in the bottom half of Table IV.5. My value of the bulk modulus pressure derivative is $\partial K/\partial P = 5.0$ compared to Soga's $\partial K/\partial P = 5.4$, an 8% difference. Such a difference is not particularly significant considering the compositional and possible quality difference between the samples. The derivatives of the shear moduli C_S and C_{44} are about 1.5. No shear instabilities are indicated.

Garnet

2. Isothermal compression measurements on pyrope-almandine

garnets.

The bulk modulus of four garnets in the pyrope-almandine

series, including the end members, were recently determined

from isothermal X-ray measurements up to pressures of 300 kb

by Takahashi and Liu [1970]. The end-member pyrope and

almandine samples were laboratory synthesized. A natural

pyrope isolated from a Roberts Victor Mine eclogite and Soga's

[1967] natural almandine were the other two garnet samples.

The microprobe analysis for the natural pyrope is given in

Table IV.2.

The volume compression V/V_O versus pressure data were

least-squares fit to a third order Birch-Murnaghan equation

where the zero pressure isothermal bulk modulus K_O and its

pressure derivative $K_O' = (\partial K/\partial P)_{P=0}$ were the variable para-

meters. Takahashi and Liu fitted their data once by allowing

both K_O and K_O' to be adjustable and then fitted their data

again by fixing $K_O' = 5.45$ (Soga's ultrasonic value) and only

allowing K_O to be adjustable. The two parameter fit yielded

values of K_O 10 to 15% higher than K_O obtained with K_O' fixed

at 5.45. Because the latter analysis yielded a K_O value for

Soga's almandine within 1% of the ultrasonic value, Takahashi

and Liu considered the $K_O' = 5.45$ fit to be most reliable for

all four garnets. The results are tabulated in Table IV.6.

3. Ultrasonic measurements on synthetic garnets.

Tabulated in Table IV.7 are the elastic constants of the present spessartite-almandine along with several synthetic or rare-earth garnets. A large range of densities ($4.24 < \rho < 7.10$ g/cm^3) and mean atomic weights ($24 < \overline{M} < 51$) is represented. The four synthetic garnets YIG, YGaG, EuIG, and GdGaG have values of $\rho/\overline{M}$ close to 0.14. YAG has $\rho/\overline{M} = 0.153$, while grossularite has $\rho/\overline{M} = 0.161$ and spessartite-almandine has $\rho/\overline{M} = 0.17$. Since both YIG and GdGaG have exactly the same $\rho/\overline{M} = 0.14$ but different values of the seismic parameter $\phi = K/\rho$, they cannot both satisfy the seismic equation of state [D.L. Anderson, 1967].

One might wonder about the effect of electronic structure (both orbital and spin) on the elastic properties. Several of the synthetic garnets are ferrimagnetic (indicated in Table IV.7) and show magnetostriction. The elastic constants might show a change in value upon application of a magnetic field below saturation. This change in elastic constants is known as the ΔE-effect and is due to interaction of the elastic field with the magnetic domain structure [see, for example, Bozorth, 1951]. Thus the tabulated constants may not represent purely elastic behavior. Of the magnetic garnets tabulated, the EuIG and YIG measurements were made in a demagnetized state [Bateman, 1966]. No mention of the magnetic state was made in the GdGaG paper [Graham and Chang, 1970].

Garnet

The pressure derivative values for YIG were calculated from the complete set of third-order elastic constants given by Eastman [1966]. The YIG sample was magnetically saturated to eliminate magnetostrictive effects under pressure. The value of $(\partial K/\partial P)_{YIG} = 4.6$ is 10% lower than for spessartite-almandine, but is in the usual range for oxides and silicates.

Besides magnetic effects the different electronic structures may be responsible for deviations from general relations between elastic properties and cell volume. Thus trivalent yttrium, iron, gadolinium, and gallium have valence electronic configurations $4p^6$, $3d^5$, $4f^7$, and $3d^{10}$, respectively.

Garnet

4. Crystal chemical considerations.

In some sense the parameter $\rho/\overline{M}$ does normalize wide variations in the individual parameters ρ and $\overline{M}$. When the normalization is expected to be reliably true within a particular <u>structural</u> <u>family</u> (namely, the garnets) will be investigated in this section. The parameter $\rho/\overline{M}$ within a structural family is inversely proportional to the unit cell volume. Tables of effective ionic radii may be used to indicate the relative sizes of the ions occupying the different sites in the crystal structure. The site radii for the natural and synthetic garnets of Tables IV.5, IV.6, and IV.7 are shown in Table IV.8. In addition, site radii are shown for garnet-transformed $MgSiO_3$ and garnet-transformed bronzite. As indicated in the introduction, garnet-$MgSiO_3$ has the structural formula $Mg_3^{VIII}(Mg,Si)^{VI}Si_3^{IV}O_{12}$. Garnet-transformed aluminous pyroxenes will also contain some Al^{3+} in the VI-coordinated site. The radius of the ion occupying this $\underline{B}$ or octahedral site for these transformed garnets is taken to be the formula number average of the individual ions. Thus the $\underline{B}$-site radius in garnet-$MgSiO_3$ is the simple average of the radii of Mg^{2+} and Si^{4+} appropriate to 6-fold coordination. All the effective ionic radii are taken from Shannon and Prewitt [1969] and are based on $r(^{VI}O^{2-}) = 1.40 \overset{\circ}{A}$. The radius for 8-coordinated Fe^{2+} is estimated by assuming that the ratios $r(^{VIII}Fe^{2+})/r(^{VI}Fe^{2+})$ and $r(^{VIII}Mn^{2+})/r(^{VI}Mn^{2+})$ are equal.

Garnet

The natural and synthetic garnets separate into two
groups on the basis of different reciprocal volumes per ion.
(Recall that the reciprocal volume per ion is proportional to
$\rho/\overline{M}$.) The difference is due to the much smaller size of the
Si^{4+} ion in the C-site and to the somewhat smaller size of the
Mg^{2+}, Mn^{2+}, or Fe^{2+} ions in the A-site compared to the tran-
sition or rare earth ions. Within each group there occurs a
misfit. The Ca^{2+} occupying the A-site in grossularite is
notably larger than in any of the other natural garnets. And
the Al^{3+} occupying the C-site in YAG is notably smaller than
in any of the other synthetic garnets. These ionic size
differences also mean values of $\rho/\overline{M}$ distinctly different
from other members of the group. For the purpose of the pre-
sent discussion, no particular attempt will be made to fit
these two garnets into their respective groups except to note
that when the relative ratios of the ions in the different
sites change appreciably, the resulting relative distortions
in the coordination polyhedra may lead to elastic anomalies
not predicted from a universal equation of state [see also
D.L. Anderson, 1969]. It turns out that YAG fits in nicely
with the other synthetic garnets when an inverse Φ versus $\overline{M}$
relationship is considered.

Garnet

5. Seismic Φ - density - mean atomic weight relations.

Universal equations of state such as O.L. Anderson's and Nafe's [1965] relation [also O.L. Anderson, 1966] and D.L. Anderson's [1967] seismic equation of state relate the mean volume per ion pair $2\overline{M}/\rho$ (or its reciprocal) to the bulk modulus K (or the seismic parameter $\Phi = K/\rho$). In terms of Φ the two equations may be expressed as follows:

D.L. Anderson $\qquad \Phi = A_1 \ (\rho/\overline{M})^n \qquad\qquad$ (Eqn. IV.2)

O.L. Anderson $\qquad \Phi = (A_2/\overline{M}) \ (\rho/\overline{M})^{K'_o - 1} \qquad$ (Eqn. IV.3)

$\qquad$ where $\quad A_1, \ A_2, \ n$ = constants

$\qquad\qquad\qquad\qquad \Phi$ = seismic parameter

$\qquad\qquad\qquad\qquad \rho$ = density

$\qquad\qquad\qquad\qquad \overline{M}$ = mean atomic weight

$\qquad\qquad\qquad\qquad K'_o = (\partial K/\partial P)_{P=0}$

The exponent $\underline{n}$ in D.L. Anderson's equation is close to 3 as determined by fitting the equation to "31 selected minerals and rocks." When n = 3 the equation implies K'_o = 4. O.L. Anderson's equation then becomes identical to D.L. Anderson's equation for K'_o = 4 and compounds of equal mean atomic weight $\overline{M}$. Except for these special conditions the two relations predict different behavior. In particular, for all the natural garnets where $\rho/\overline{M}$ is essentially constant, Eqn. IV.2 predicts equal values of Φ whereas Eqn. IV.3 predicts Φ to be inversely proportional to $\overline{M}$. The inverse proportionality of

Garnet

Φ and $\overline{M}$ in garnets from Eqn. IV.3 was pointed out by
Takahashi and Liu [1970] and was satisfied by their isothermal
compression data for the pyrope-almandine series. If all the
garnet data including the synthetic garnets are plotted ac-
cording to Φ <u>versus</u> $1/\overline{M}$, the garnets again separate into two
groups (Fig. IV.3). Within each group (except grossularite)
the data follow the Φ <u>versus</u> $1/\overline{M}$ proportionality fairly well.
Note that within the two groups $\rho/\overline{M}$ is being treated as a
constant. For the synthetic garnets $\rho/\overline{M}$ varies up to 10%.
If the variations in $\rho/\overline{M}$ are taken into account by either
Eqn. IV.2 or IV.3, the fit to the data becomes considerably
poorer. In Fig. IV.3 all the data points (except grossularite)
are within 5% of the fitted lines. Most points are within 2%.
Two conclusions are indicated by the plotted data in terms of
the crystal chemical discussion of the previous section.

a. Within the isostructural garnet family neither D.L. Ander-
son's relation (Eqn. IV.2) nor O.L. Anderson's relation (Eqn.
IV.3) fit all the data. The different <u>A</u>:<u>B</u>:<u>C</u> site-radii in-
fluence Φ in a way not predicted from a cell volume dependence.

b. However, the plausible condition is that if garnets have
equal values of $\rho/\overline{M}$ <u>and</u> have ions of equal radii in the in-
dividual coordination sites, then they satisfy the inverse
proportionality between Φ and $\overline{M}$ derived from O.L. Anderson's
relation (Eqn. IV.3).

Garnet

6. Garnet-MgSiO$_3$.

If a density increase of 10% over pyroxene-MgSiO$_3$ is

assumed, the density of garnet-MgSiO$_3$ is 3.52 g/cm^3, the mean

atomic weight is 20.08, and $\rho/\overline{M}$ = 0.175. Compare these values

to pyrope, Mg$_3$Al$_2$Si$_3$O$_{12}$. The density of pyrope is 3.56 g/cm^3,

the mean atomic weight is 20.16, and $\rho/\overline{M}$ = 0.177. Not only

is the cell volume for garnet-MgSiO$_3$ the same as for pyrope

and the other natural garnets, but also the radii of the

cations in the three sites are the same (see Table IV.8).

Recall that the $\underline{B}$-site radius of garnet-MgSiO$_3$ is the average

of the Mg^{2+} and Si^{4+} radii when both are in 6-fold coordina-

tion. That the effective radii of the three cation sites are

nearly the same for pyrope and garnet-MgSiO$_3$ is consistent

with their nearly equal values for $\rho/\overline{M}$.

So the elastic properties of pyrope and garnet-MgSiO$_3$

will probably be the same (shown also in Table IV.8). Though

the discussion has so far concentrated on Φ, the justifica-

tion for also estimating values for V$_p$ (compressional wave

velocity) and V$_s$ (shear wave velocity) comes from noting in

Table IV.5 that the ratio V$_p$/V$_s$ for the ultrasonically

measured natural garnets is fairly constant.

Since the single crystal elastic constants of ortho-

pyroxene-bronzite have been determined [Kumazawa, 1969], the

estimated values for a garnet-transformed bronzite have also

been tabulated in Table IV.8. Note that iron substitution

Garnet

into garnet-transformed pyroxenes does not affect the cell

volume or individual coordination site radii just as it does

not in the pyrope-almandine series. Hence the elastic

parameters may be determined from the inverse Φ versus $\overline{M}$

proportionality.

Garnet

D. Garnet's role in the mantle.

The relative proportion of mantle compounds in the garnet structure is not well-determined at present. Ringwood's estimate of 14 weight percent of pyrope-rich garnet in the 150 to 250 km region of the upper mantle was mentioned in the introduction to this chapter. For greater depths high pressure phase studies show different transformation possibilities. Though emphasis has been placed in this chapter on estimating the elastic properties of $MgSiO_3$ transformed into the garnet structure, this transformation has not been observed directly but rather is inferred from Ringwood's studies [reviewed in Ringwood, 1970] on $MgSiO_3$:10% Al_2O_3, $MnSiO_3$, $CaGeO_3$, and $CdGeO_3$. Direct transformation of $MgSiO_3$ into the garnet structure must occur at pressures greater than 200 kb. By such pressures competing modes of transformation are:

$$MgSiO_3 \rightarrow MgO + SiO_2 \text{ (stishovite)}$$

$$MgSiO_3 \rightarrow MgSiO_3 \text{ (ilmenite)}.$$
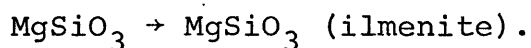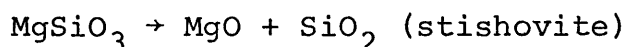
The presence of Al_2O_3 as aluminous pyroxene alters the situation since the aluminous pyroxenes transform into the garnet structure at lower pressures.

Garnet

Does the seismic data provide evidence for the

pyroxene → garnet transformation occurring in the earth's

mantle? First, some laboratory data must be considered.

$MgSiO_3$ forming a garnet solid solution with pyrope is indi-

cated by the sharp increase in lattice parameter of garnet

crystallized from $MgSiO_3$:10% Al_2O_3 glass at 100 kb (see

Fig. IV.4 after Ringwood, 1967). The magnitude of the

velocity change over the pyroxene → garnet transformation may

be obtained from the single crystal elastic constants of

bronzite [Kumazawa, 1969] and the estimated values for the

velocities of bronzite transformed into the garnet structure

shown in Table IV.8. The Hill averages for the single cystal

bronzite are compared with the estimated garnet-bronzite

values

Pyroxene-
bronzite $\quad V_p = 7.84$ km/sec $\qquad V_s = 4.74$ km/sec

Garnet-
bronzite $\quad V_p = 9.32$ km/sec $\qquad V_s = 5.22$ km/sec

The value of Φ changes from 31.5 km^2/sec^2 to 50.5 km^2/sec^2

(estimated) over the pyroxene → garnet transition in bronzite.

Garnet

A density increase of 10% is thus matched by an increase
of 20% in V_p and an increase of 10% in V_s. A 20% increase
in V_p accompanying a 10% increase in density was found by
Mizutani et al. [1970] for the olivine → spinel transition
in Fe_2SiO_4.

Ringwood in 1967 placed the pyroxene → garnet transforma-
tion at a depth of 350 km after correcting the 900 °C con-
ditions of Fig. IV.4 to 1500 °C (the 2500 °C temperature on
p. 260 of his paper must be a misprint). He stated that
"some seismologists now suspect that the rapid increase of
seismic velocity marking the beginning of the transition
zone occurs around 17 or 18°, or a depth of about 350 km."
Since that time compressional wave discontinuities have been
found by looking for reflectors. Whitcomb and D.L. Anderson
[1970] found a P'P' reflector at 280 km but none at 440 km.
Simpson et al. [1971] separated the 360 km discontinuity into
ones at 280 km and 440 km. It seems reasonable then to as-
sociate the 280 km discontinuity with Ringwood's aluminous
pyroxene to garnet transformation, as Whitcomb and D.L.
Anderson have done.

The magnitude of the velocity discontinuity is dependent
upon the amount of the pyroxene component in the upper mantle.
Ringwood's [1970, p. 140] estimate for pyrolite is about

Garnet

25 weight percent orthopyroxene. The resulting seismic dis-
continuities would be about 0.4 km/sec for V_p and 0.1 km/sec
for V_s. Thus there is little chance for resolving the dis-
continuity from shear velocity profiles and only a slight
chance from compressional velocity profiles. Perhaps the ar-
gument so far used may be reversed so that the magnitude of
the discontinuity becomes a broad band estimator of the
pyroxene component.

Garnet

References

Anderson, D.L., A seismic equation of state, Geophys. J., 13, 9-30, 1967.

Anderson, D.L., Bulk modulus-density systematics, J. Geophys. Res., 74, 3857-3864, 1969.

Anderson, O.L., A proposed law of corresponding states for oxide compounds, J. Geophys. Res., 71, 4963-4971, 1966.

Anderson, O.L., and J.E. Nafe, The bulk modulus-volume relationship for oxide compounds and related geophysical problems, J. Geophys. Res., 70, 3951-3963, 1965.

Bateman, T.B., Elastic moduli of single-crystal europium iron garnet and yttrium iron garnet, J. Appl. Phys., 37, 2194-2195, 1966.

Bozorth, R.M., Ferromagnetism, 968 pp., Van Nostrand, New York, 1951.

Chung, D.H., D.J. Silversmith, and B.B. Chick, A modified ultrasonic pulse-echo-overlap method for determining sound velocities and attenuation of solids, Rev. Sci. Inst., 40, 718-720, 1969.

Deer, W.A., R.A. Howie, and J. Zussman, Rock-Forming Minerals, Vol. 1, Ortho- and Ring Silicates, 333 pp., Longmans, London, 1962.

Eastman, D.E., Measurement of third-order elastic moduli of yttrium iron garnet, J. Appl. Phys., 37, 2312-2316, 1966.

Garnet

Graham, L.J., and R. Chang, Elastic moduli of single-crystal gadolinium gallium garnet, J. Appl. Phys., 41, 2247-2248, 1970.

Kumazawa, M., The elastic constants of single-crystal orthopyroxene, J. Geophys. Res., 74, 5973-5980, 1969.

Mizutani, H., Y. Hamano, Y. Ida, and S. Akimoto, Compressional-wave velocities of fayalite, Fe_2SiO_4 spinel, and coesite, J. Geophys. Res., 75, 2741-2747, 1970.

Papadakis, E.P., Ultrasonic phase velocity by the pulse-echo-overlap method incorporating diffraction phase corrections, J. Acoust. Soc. Am., 42, 1045-1951, 1967.

Ringwood, A.E., The pyroxene-garnet transformation in the earth's mantle, Earth Planet. Sci. Letters, 2, 255-263, 1967.

Ringwood, A.E., Phase transformations in the mantle, Earth Planet. Sci. Letters, 5, 401-412, 1969.

Ringwood, A.E., Phase transformations and the constitution of the mantle, Phys. Earth Planet. Interiors, 3, 109-155, 1970.

Ryzhova, T.V., L.M. Reshchikova, and K.S. Aleksandrov, Elastic properties of rock-forming minerals, Izv. Solid Earth Physics, English Transl., no. 7, 447-450, 1966.

Shannon, R.D., and C.T. Prewitt, Effective ionic radii in oxides and fluorides, Acta Cryst., B25, 925-946, 1969.

Simmons, G., Velocity of compressional waves in various minerals at pressures up to 10 kilobars, J. Geophys. Res., 69, 1117-1121, 1964.

Garnet

Simmons, G., and H. Wang, Single Crystal Elastic Constants and

Calculated Aggregate Properties: A Handbook, 370 pp., MIT

Press, Cambridge, 1971.

Simpson, D.W., C. Wright, and J.R. Cleary, Double discontinuity

in the upper mantle, Nature, 231, 201-203, 1971.

Soga, N., Elastic constants of garnet under pressure and tem-

perature, J. Geophys. Res., 72, 4227-4234, 1967.

Spencer, E.G., R.T. Denton, T.B. Bateman, W.B. Snow, and L.G.

Van Uitert, J. Appl. Phys., 34, 3059-3060, 1963.

Takahashi, T., and L. Liu, Compression of ferromagnesian gar-

nets and the effect of solid solutions on the bulk modulus,

J. Geophys. Res., 75, 5757-5766, 1970.

Thurston, R.N., Effective elastic coefficients for wave pro-

pagation in crystals under stress, J. Acoust. Soc. Am., 37,

348-356, 1965. Erratum, J. Acoust. Soc. Am., 37, 1147, 1965.

Verma, R.K., Elasticity of some high-density crystals, J. Geo-

phys. Res., 65, 757-766, 1960.

Whitcomb, J.H., and D.L. Anderson, Reflection of P'P' seismic

waves from discontinuities in the mantle, J. Geophys. Res.,

75, 5713-5728, 1970.

Table IV.1

Garnet end-member compositions.

[see Deer et al., 1962, Vol. 1, pp. 77-112]

Natural garnet end members	General formula: $A_3^{2+}B_2^{3+}C_3^{4+}O_{12}$ $(A_3^{VIII}B_2^{VI}C_3^{IV}O_{12})$
Almandine	$Fe_3^{2+}Al_2Si_3O_{12}$
Andradite	$Ca_3Fe_2^{3+}Si_3O_{12}$
Grossular	$Ca_3Al_2Si_3O_{12}$
Pyrope	$Mg_3Al_2Si_3O_{12}$
Spessartite	$Mn_3Al_2Si_3O_{12}$
Uvarovite	$Ca_3Cr_2Si_3O_{12}$

Roman numeral superscripts indicate coordination number.

Table IV.1 (continued)

Synthetic or rare earth garnets	General formula: $A_3^{3+} B_2^{3+} B_3^{3+} O_{12} = A_3^{3+} B_5^{3+} O_{12}$
Yttrium Aluminum Garnet (YAG)	$Y_3^{3+} Al_5 O_{12}$
Yttrium Iron Garnet (YIG)	$Y_3 Fe_5^{3+} O_{12}$
Yttrium Gallium Garnet (YGaG)	$Y_3 Ga_5^{3+} O_{12}$
Gadolinium Gallium Garnet (GdGaG)	$Gd_3 Ga_5 O_{12}$
Erbium Aluminum Garnet (ErAlG)	$Er_3 Al_5 O_{12}$
Europium Iron Garnet (EuIG)	$Eu_3 Fe_5 O_{12}$
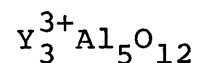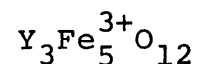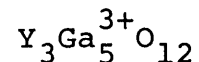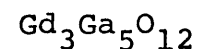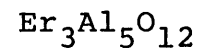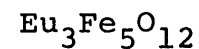
The B and C of the general formula for natural garnets is now the same ion. The synthetic garnets may be thought of as the result of charge-coupled substitution between the A and C sites.

Table IV.2

Garnet chemical analyses (wt. %), densities, and mean atomic weights.

Oxide	Present Study*	Verma Garnet 1 [1960]	Verma Garnet 2 [1960]	Soga [1967]	Takahashi and Liu [1970]
SiO_2	36.4	35.4	36.3	37.62	41.59
TiO_2	---	---	---	0.01	0.31
Al_2O_3	20.6	21.0	21.0	21.44	21.29
Total Fe as FeO	19.4	19.1	37.1	33.15	16.15
MnO	22.3	23.8	0.4	1.10	0.25
MgO	---	0.05	3.6	5.07	16.37
CaO	0.3	0.44	1.5	1.10	3.39
	99.0	99.79	99.9	99.49	99.35

*Microprobe analysis by A. Reid of the NASA Manned Spacecraft Center, Houston, Texas.

ρ, g/cm^3	4.249	4.247	4.183	4.1602	3.81
a_o, Å	11.5445	11.56	11.52	11.531	11.521
$\overline{M}$	24.9	24.9	24.3	23.8	21.9

(continued)

Table IV.2

Garnet chemical analyses (wt. %), densities, and mean atomic weights.

(continued)

Sample	Approximate chemical formula	Name
Present study:	$3(Mn_{54}Fe_{46})O:Al_2O_3:3SiO_2$	Spessartite-almandine
Verma Garnet 1:	$3.(Mn_{55}Fe_{45})O:Al_2O_3:3SiO_2$	Spessartite-almandine
Verma Garnet 2:	$3(Fe_{81}Mg_{14}Ca_5)O:Al_2O_3:3SiO_2$	(Natural) almandine
Soga	$3(Fe_{76}Mg_{21}Ca_3)O:Al_2O_3:3SiO_2$	(Natural) almandine
Takahashi & Liu	$3(Mg_{60}Fe_{31}Ca_9)O:Al_2O_3:3SiO_2$	(Natural) pyrope

Table IV.3

Spessartite-almandine single crystal elastic constants

	11	12	44
C_{ij}	3.085	1.123	0.948
$\partial C_{ij}/\partial P$	7.15	3.85	1.30
S_{ij}	0.4023	-0.1074	1.0549
$\partial S_{ij}/\partial P$	-0.746	0.112	-1.45

$$\frac{\partial S}{\partial P} = -S \frac{\partial C}{\partial P} S$$

Symbol	Unit	Pressure derivative
C_{ij}, elastic stiffnesses	Mb	None
S_{ij}, elastic compliances	Mb^{-1}	Mb^{-2}

Table IV.4

Spessartite-almandine calculated

aggregate elastic constants.

Zero pressure aggregate constants						
E	μ	σ	K	β	V_s	V_p
2.443	0.961	0.271	1.777	0.563	4.756	8.484

Aggregate pressure derivatives						
$\partial E/\partial P$	$\partial\mu/\partial P$	$\partial\sigma/\partial P$	$\partial K/\partial P$	$\partial\beta/\partial P$	$\partial V_s/\partial P$	$\partial V_p/\partial P$
4.13	1.44	2.51	4.95	-1.57	2.22	7.14

No distinction is made between the different methods of averaging the single crystal elastic constants since they all give the same results.

Symbol	Unit	Pressure derivative $(\partial/\partial P)$ unit
E, Young's modulus	Mb	None
μ, Shear modulus	Mb	None
σ, Poisson's ratio	None	Mb^{-1}
K, Bulk modulus	Mb	None
β, Compressibility	Mb^{-1}	Mb^{-2}
V_s, Shear velocity	km/sec	(km/sec)/Mb
V_p, Compressional velocity	km/sec	(km/sec)/Mb

Table IV.5

Natural garnets: ultrasonic measurements.

Elastic constants

Garnet	ρ	$\overline{M}$	K	c_S	c_L	c_{11}	c_{12}	c_{44}	V_p	V_s	V_p/V_s
Present study	4.249	24.9	1.777	0.981	3.052	3.085	1.123	0.948	8.484	4.756	1.784
Verma 1	4.247	24.9	1.756	0.988	3.037	3.073	1.097	0.952	8.466	4.770	1.775
Verma 2	4.183	24.3	1.765	0.962	3.030	3.048	1.123	0.944	8.515	4.769	1.785
Soga	4.160	23.8	1.770	0.968	3.020	3.062	1.125	0.927	8.531	4.762	1.791
Grossularite	3.598	22.4	1.504	0.970	2.724	2.798	0.857	0.896	8.723	5.071	1.720

Elastic constant pressure derivatives $(\partial/\partial P)$

Garnet	ρ	$\overline{M}$	K	c_S	c_L	c_{11}	c_{12}	c_{44}	V_p	V_s	V_p/V_s
Present study	4.249	24.9	4.95	1.65	6.80	7.15	3.85	1.30	7.14	2.22	-----
Soga	4.160	23.8	5.43	1.54	7.25	7.48	4.41	1.31	7.87	2.18	-----

Symbol	Unit	Pressure derivative $(\partial/\partial P)$ unit
c_{ij}, elastic stiffnesses	Mb	None
K, bulk modulus	Mb	None
V_p, compressional velocity	km/sec	(km/sec)/Mb
V_s, shear velocity	km/sec	(km/sec)/Mb
ρ, density	g/cm^3	Not used
$\overline{M}$, mean atomic weight	g/mole/atom	Not used

$$c_S = 1/2 \ (c_{11} - c_{12}) \qquad c_L = 1/2 \ (c_{11} + c_{12} + 2c_{44})$$

Table IV.6

Pyrope-almandine garnets: isothermal compression measurements.

[Takahashi and Liu, 1970]

Garnet	ρ (g/cm^3)	$\overline{M}$ $\frac{\text{(g/mole)}}{\text{Atom}}$	K (Mb)	Φ (km/sec)
Pyrope	3.564	20.2	1.90	53.3
Natural pyrope	3.81	21.9	1.77	46.5
Natural almandine (Soga's)	4.16	23.8	1.73	41.6
Almandine	4.312	24.9	1.68	39.0

Table IV.7

Elastic constants of synthetic garnets.

Garnet	Magnetic?	ρ	M̄	K	C_s	C_L	C_{11}	C_{12}	C_{44}	V_p	V_s	V_p/V_s	Ref.
						Elastic constants							
Sp-Alm	No	4.25	24.9	1.777	0.981	3.052	3.085	1.123	0.948	8.484	4.756	1.784	(1)
YAG	No	4.55	29.7	1.849	1.112	3.370	3.332	1.107	1.150	8.596	4.994	1.721	(2)
YIG	Yes	5.17	36.9	1.631	0.787	2.659	2.680	1.106	0.766	7.177	3.870	1.855	(3)
YGaG	No	5.79	40.4	1.750	0.865	2.993	2.903	1.173	0.955	7.166	3.982	1.800	(2)
EuIG	Yes	6.28	46.4	1.550	0.720	2.552	2.510	1.070	0.762	6.364	3.444	1.848	(3)
GdGaG	Yes	7.09	50.6	1.720	0.854	2.908	2.859	1.151	0.903	6.393	3.529	1.812	(4)
						Elastic constant pressure derivatives $(\partial/\partial P)$							
Sp-Alm	No	4.25	24.9	4.95	1.65	6.80	7.15	3.85	1.30	7.14	2.22	-----	(1)
YIG	Yes	5.17	36.9	4.60	1.20	6.42	6.21	3.80	1.41	6.39	2.11	-----	(5)

References	Symbol	Unit	Pressure derivative $(\partial/\partial P)$ unit
1. Present study.	C_{ij}, elastic stiffnesses	Mb	None
2. Spencer et al., 1963.	K, bulk modulus	Mb	None
3. Bateman, 1966.	V_p, compressional velocity	km/sec	(km/sec)/Mb
4. Graham & Chang, 1970.	V_s, shear velocity	km/sec	(km/sec)/Mb
5. Eastman, 1966	ρ, density	g/cm³	Not used
	M̄, mean atomic weight	g/mole/atom	Not used

$$C_S = 1/2\ (C_{11} - C_{12}) \qquad C_L = 1/2\ (C_{11} + C_{12} + 2C_{44})$$

Table IV.8

Effective ionic radii of garnet sites and some
estimated elastic properties of unmeasured garnets.

Garnet	ρ (g/cm^3)	$\bar{M}$ $\frac{g/mole}{atom}$	$\rho/\bar{M}$ $\frac{mole \cdot atom}{cm^3}$	A-site radius (Å)	B-site radius (Å)	C-site radius (Å)	Φ (km/sec)^2	V_p (km/sec)	V_s (km/sec)
Present study	4.25	24.9	0.171	0.89	0.53	0.26	41.8	8.48	4.76
Grossularite	3.60	22.4	0.161	1.12	0.53	0.26	41.8	8.72	5.07
Pyrope	3.56	20.2	0.176	0.89	0.53	0.26	53.3	(9.60)	(5.38)
Natural Pyrope	3.81	21.9	0.174	0.87	0.53	0.26	46.5	(8.94)	(5.01)
Natural Almandine	4.16	23.8	0.175	0.87	0.53	0.26	42.5	8.53	4.76
Almandine	4.31	24.9	0.173	0.85	0.53	0.26	39.0	(8.19)	(4.59)
YAG	4.55	29.7	0.153	1.015	0.53	0.39	40.6	8.60	4.99
YIG	5.17	36.9	0.140	1.015	0.55	0.49	31.2	7.17	3.89
YGaG	5.79	40.4	0.143	1.015	0.62	0.47	30.2	7.17	3.98
EuIG	6.28	46.4	0.136	1.07	0.55	0.49	24.7	6.36	3.44
GdGaG	7.09	50.6	0.140	1.06	0.62	0.47	24.3	6.39	3.53
Garnet-MgSiO$_3$	(3.52)	20.1	(0.175)	0.89	0.56	0.26	(53.0)	(9.55)	(5.35)
Garnet-Bronzite*	(3.67)	21.1	(0.174)	0.88	0.56	0.26	(50.5)	(9.32)	(5.22)

*Bronzite (84.5% enstatite) = $(Mg_{84.5}Fe_{15.5})SiO_3$

Parentheses around values in the table indicate estimated values.

Garnet

Figure Captions

Fig. IV.1. Garnet structure showing the different coordina-
tion polyhedra [taken from Deer et al., 1962, Vol. 1, p. 79].

Fig. IV.2. Sketches of garnet sample before and after cutting.

Fig. IV.3. Φ versus $1/\overline{M}$ proportionality for natural and
synthetic garnets.

Fig. IV.4. Lattice parameter versus pressure for garnets
crystallized from $MgSiO_3$:10% Al_2O_3. Around 100 kb the
$MgSiO_3$ transforms into the garnet structure and forms a
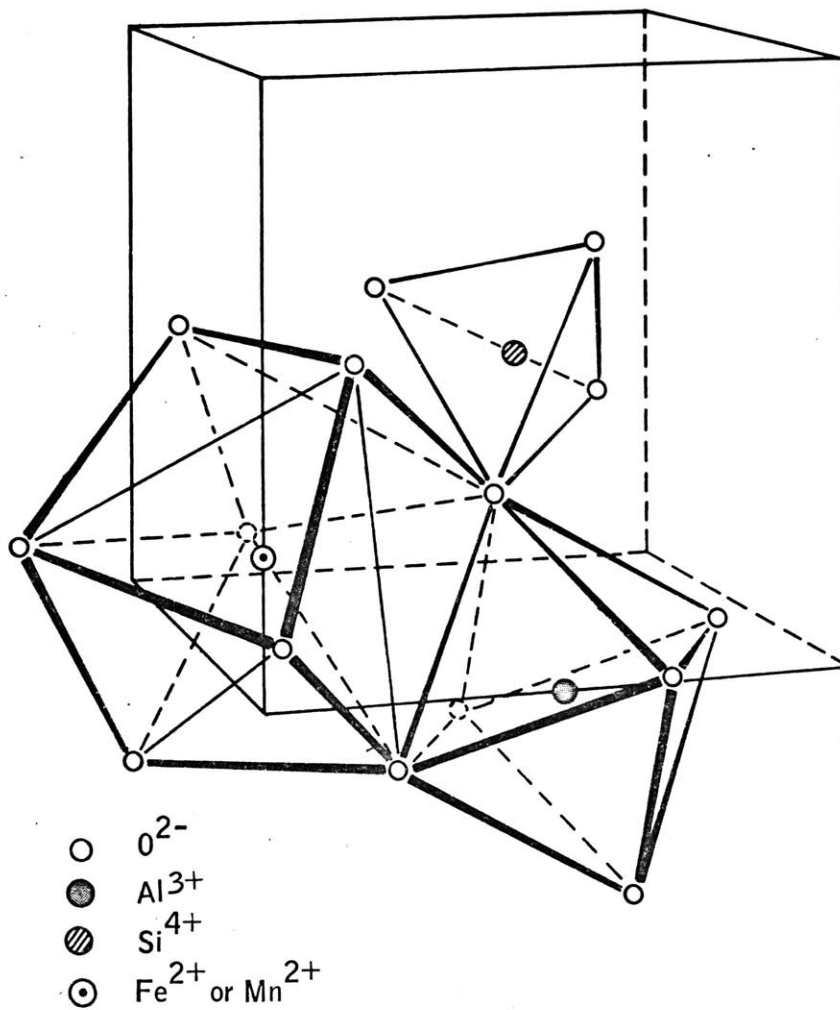solid solution with pyrope [after Ringwood, 1967].

O O^{2-}
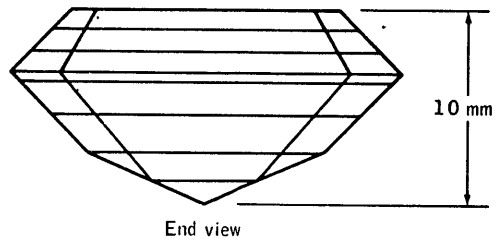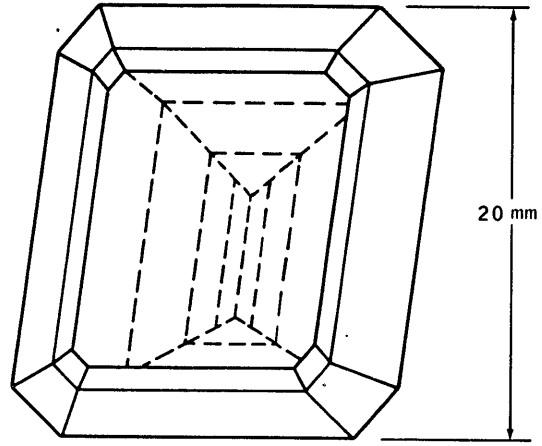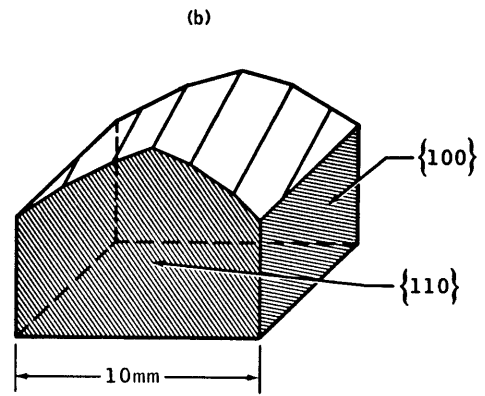
◉ Al^{3+}

◍ Si^{4+}

⊙ Fe^{2+} or Mn^{2+}

Fig. IV.1

20 mm

(a)

(b)

10 mm

End view

{100}

{110}

10mm

Fig. IV.2

Fig. IV.3

MgSiO$_3$. 10 percent Al$_2$O$_3$
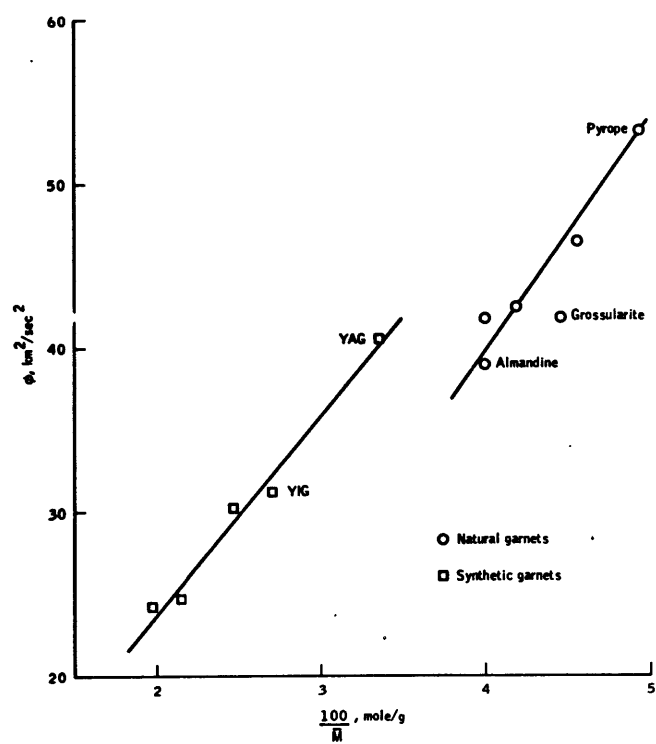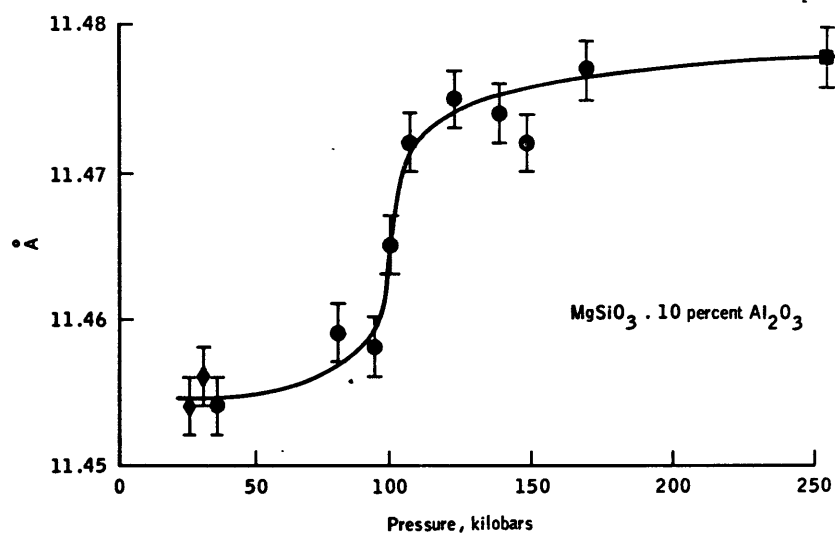
Fig. IV.4

Summary

V. Summary.

The elasticity of high-pressure mantle phases may be

characterized by measurements on crystal chemically similar

compounds. Analogue compounds available as single crystals

yield the most reliable elastic constant data.

A. Spinel.

The $C_S = 1/2$ $(C_{11} - C_{12})$ shear modulus pressure deriva-

tive of pleonaste is slightly negative. Though the pressure

derivative of C_S in $MgO:2.6Al_2O_3$ is positive, it is small in

magnitude. Small shear moduli pressure derivatives are

characteristic of the spinel structure. The weak shear modes

imply a low kinetic barrier to phase transformations and

diffusion. The decrease in C_S with iron substitution due to

Jahn-Teller relaxation indicates that for iron-rich spinels

an electronic instability is superposed on the structural

weakness.

Pleonaste and hercynite belong to the $MgAl_2O_4$ - $FeAl_2O_4$

series. The series is a particularly good analogue to the

Mg_2SiO_4 - Fe_2SiO_4 series in the spinel phase. The molar vol-

umes, densities, and mean atomic weights are exactly similar

for $(Mg_{1-x}Fe_x)Al_2O_4$ and $(Mg_{1-z}Fe_z)_2SiO_4$ when $z = x/2$. Lines

for compressional velocity V_p and shear velocity V_S as a

function of mean atomic weight are determined by the new

pleonaste and hercynite elastic constant data. Application

Summary

of the data to the question of iron content change in the
transition zone leads to inconclusive results. An increase
in iron content is indicated by the V_p data while no increase
is indicated by the V_s data.

B. Rutile.

Germanium dioxide and germanates are good crystal chemi-
cal analogues to silica and silicates. The bulk modulus
pressure derivative $\partial K/\partial P$ of rutile-structure GeO_2 is about
6.2, a value higher than most other oxides and silicates.
Since rutile-TiO_2 has a value of $\partial K/\partial P$ equal to 6.8, it is
likely that $\partial K/\partial P$ for stishovite is between 6 and 7. Both
rutile-GeO_2 and TiO_2 are elastically anisotropic and both
display a weak C_S-mode.

The seismic parameter Φ of stishovite is not well-deter-
mined at present. The use of Φ(stishovite) in a molar
averaging scheme to deduce the FeO and SiO_2 content of the
lower mantle contains inconsistencies. There is no strong
evidence for enrichment of either component in the lower
mantle.

C. Garnet.

Ultrasonic and static compression elastic constant data
exist for both natural garnets and synthetic garnets. Within
each group of garnets the unit cell volumes are nearly the

Summary

same and the ions occupying the different coordination sites
have similar sizes. Then within each group the seismic
parameter Φ is inversely proportional to the mean atomic
weight $\bar{M}$.

The elastic velocities of garnet-transformed $MgSiO_3$ may
be estimated from the inverse proportionality between Φ and $\bar{M}$.
The velocity change over the pyroxene $\rightarrow$ garnet transformation
is estimated to be 20% for compressional velocity V_p and 10%
for shear velocity V_s.

Procedure

Appendix A: Experimental procedure.

In this appendix I describe my experimental procedure. The documentation may be useful to someone in the future making similar measurements or for any evaluation of my results.   At present some differences between ultrasonic laboratories seem to exist on values for the pressure derivatives of elastic constants.   The values are sensitive to experimental procedure.   A section is devoted to discussing ambiguities that occurred in the pulse-echo-overlap method of measurement.

A.   X-ray orientation and polishing.

The crystals were cut and oriented by a standard Laue back-reflection X-ray method in the MIT Crystal Physics Laboratory.   A crystal was mounted on a goniometer aligned with the X-ray beam.   A Polaroid camera (Type 57 film) was between the sample and the beam.   After exposure the angular distances (both horizontal and vertical) between the center of the beam and a point of symmetry on the film were determined by overlaying a Greninger chart on the film [see, for example, Cullity, 1956].   The Greninger chart is a graphical display of the coordinate transformation between the back-scattered X-rays and the flat film plane.   Fig. A.1 is an example of an oriented {100}-face with the Greninger chart shown for scale.   The goniometer was adjusted over several

Procedure

exposures until the center of the beam and the desired sym-
metry axis nearly coincided. Since the Greninger chart
translated angles into distances on the film, the goniometer
could be adjusted until orientation within 1/2° was assured.
The goniometer was then taken off the X-ray track and slid
into a track perpendicular to a diamond saw blade whose
thickness was about 0.020" . Two parallel cuts were made
and the alignment of the blade was checked by placing the
crystal on the end of a machined rod with double-stick tape
and taking a final Laue picture.

Extremely small samples could be accurately oriented.
For example, I oriented and cut a pair of {100}-faces and
a pair of {110}-faces on an $FeAl_2O_4$ crystal 4 × 4 × 10 mm
(Fig. II.2, Chapter II).

Accurate ultrasonic measurements required sample faces
to be optically polished flat and parallel to 10^{-4} in/in.
I could not do a good enough job with simple holding jigs
and hence had it commercially done by the A.D. Jones Optical
Works in Burlington, Mass. They charged $150 per pair of
faces.

Procedure

B.   Transducers and bonding.

Coaxially plated one-quarter inch X-cut and AC-cut
quartz transducers generated compressional and shear waves,
respectively. They were purchased from the Valpey-Fisher
Corp., Holliston, Mass. with resonant frequencies of 10 or
20 MHz (±1%) and with third-overtone polish. The shear wave
polarization (±1°) was marked by a flat to which the par-
ticle motion was perpendicular.

A 50/50 mixture (by volume) of pthalic anhydride and
glycerin was used as the bonding material for pressure runs
and an epoxy (Tra-bond 2101, Tra-Con, Inc., Medford, Mass.)
was used for shear wave temperature runs. Methylene chloride
was the epoxy stripping agent. A few small drops of the
pthalic anhydride and glycerin mixture were heated on the
sample under an infrared lamp until it flowed quite readily.
It was spread thinly and uniformly over the sample face with
copper wire before the transducer was "wrung" on with a Q-tip.
The pthalic anhydride and glycerin mixture was not dissolved
by the pressure fluid of petroleum ether so that both shear
and compressional waves could be transmitted. An epoxy
bond was cured for at least 2 hours at 80 °C and it remained
hard to 100 °C whereas a thermosetting bond became too soft
to maintain a good shear signal.

Procedure

The crystal sample with transducer was then placed in a cylindrical holder with a spring-loaded pin making electrical contact with the center spot of the coaxial transducer (Fig. A.2). The entire assembly was grounded and placed directly into either the pressure vessel or oven.

Procedure

C. Ultrasonic equipment.

The elastic constants were determined by measuring the velocity of plane compressional or shear waves in specific propagation directions. Since sample lengths were 5 to 10 mm and velocities were 5 to 10 mm/μsec (1 mm/μsec = 1 km/sec), round trip travel times were 1 to 4 μsec. I measured these travel times by the pulse-echo-overlap method developed by Papadakis [1964, 1967]. The particular modification in our laboratory enabled the simultaneous measurement of travel time and attenuation [Chung et al., 1969], but attenuation was not a part of my study.

I only briefly describe the principles of the technique since it is covered in detail by Papdakis and Chung et al. A block diagram of the equipment, as I used it, is shown in Fig. A.3. An rf-pulse whose rf-frequency was tuned to the resonance or overtone of the transducer was applied to the transducer. The same transducer was used also for receiving successive echoes which have travelled the length of the specimen and back. A typical echo-train is shown in Fig. A.4a. A rough idea of the travel time in the sample was obtained by using the oscilloscope's calibrated time base and noting the distance between successive echoes on the screen grid. The actual measurement was made by intensifying any two echoes

Procedure

and sweeping the X-axis of the oscilloscope at just the reciprocal of the travel time between the echoes. Only the intensified echoes were displayed on the oscilloscope face. The X-axis sweep rate was controlled by a sinusoidal frequency generator. Thus when the triggering frequency was the reciprocal of the travel time, successive sweeps of the electron beam presented a stable image of the two echoes with their rf-cycles in synchronization (Fig. A.4b). The frequency was read directly on a digital counter and was the raw datum of the experiment.

All my measurements were made with $f_o = 1/T$ (where T is the travel time) between 100 kHz and 1 MHz. Rf-pulses from the Arenberg pulsed oscillator had a repetition rate $f_o/100$ and were in synchronism with all the echoes. Using a division factor of 100 in the single crystals kept only one pulse train in the crystal at a time, i.e., all the echoes from the input pulse died away before the next pulse occurred. The synchronism between the main pulse and echoes was necessary for a stable display of the individual echoes when the oscilloscope was swept at the reciprocal of the travel time.

Procedure

D. Ambiguities in the measurements.

While making my measurements, I found ambiguities which could limit the accuracy of the frequency determination as a function of pressure or temperature. These ambiguities were especially significant for the short path length and high-velocity crystals with which I worked. I discuss the following difficulties, several of which are related: (1) Guided-wave modes (2) Cyclic mismatches (3) Changes of transducer resonance with pressure or temperature (4) Incomplete damping of one echo before the next (5) Trigger delay between channels in dual channel operation (6) Shear wave polarization mis-orientation.

1. Guided-wave modes.

In my samples one pair of parallel faces nearly always had another pair perpendicular to them (see Figs. II.1, II.2, III.3, and IV.2 for sample shapes). Thus, besides the reflection at the end of the wave path, there existed multiple side-wall reflections. When the side-wall reflections were in phase, a guided-wave mode resonance occurred. The resonance appeared as a modulation on the envelope of the wave train (Fig. A.5). Without the effect the echoes should have decayed exponentially. The nodal minima and build up again in amplitude indicated that energy was being fed in by the

Procedure

"free oscillations" which were of longer period than the time between successive echoes. Also side-wall reflections could lead to spurious echoes in the oscilloscope display.

The guided-wave modes could affect measurements in two ways if a pair of echoes near a node was chosen. First, phasing effects near a node might alter the proper cyclic match [Papadakis, 1969; also discussed in the next section D.2]. Second, the strong phasing near a node was a function of pressure and temperature and hence might lead to incorrect coefficients for the elastic constants.

The solution of the problem was to stay away from nodal points and to work preferably with the first and second or second and third echoes. Another help was to use the slightly higher frequency of 30 MHz rather than 20 MHz so that less beam energy was diffracted to the parallel side-walls. A careful study of the effects of phasing near nodal points on the pressure and temperature derivatives of the elastic constants would be useful.

2. Cyclic mismatch.

A big error (2 to 5%) in the travel time determination occurs if the overlapping of two echoes is off by one or more cycles. It is not reliable to merely match the "leading edge" of the pulse nor to match peak half-cycle with peak half-cycle. The maximum peaks of two adjacent echoes are

Procedure

often displaced one cycle apart because part of the energy of each cycle of the first echo is delayed by the transducer upon reflection at that interface, and makes its appearance in a subsequent cycle of the second echo [Papadakis, 1969].

Papadakis [1967, 1969] described two methods of determining the proper cyclic matching in the pulse-echo-overlap technique. The first method is based on the McSkimin criterion and the second is based on a video-pulse-matching method. These methods will be discussed in turn.

a. McSkimin criterion.

The basis of the McSkimin criterion or method [McSkimin, 1962] is to measure the travel time both at the resonant frequency of the transducer and at a frequency 10% lower for different cyclic matches. The travel time T is given by

$$T = p\delta - \frac{p\gamma}{360\ f} + \frac{n}{f} \qquad \text{(Eqn. A.1)}$$

where δ = true round trip travel time

p = number of round trips between echoes used

γ = phase angle upon reflection at the specimen-transducer interface

f = rf frequency

n = number of cycles of mismatch.

Procedure

Then denote the measurements at resonance by the subscript R and denote the measurements at $0.9 f_R$ by the subscript L.

$$\Delta T = \frac{1}{f_L}\left(n - \frac{p\gamma_L}{360}\right) - \frac{1}{f_R}\left(n - \frac{p\gamma_R}{360}\right) \qquad \text{(Eqn. A.2)}$$

where $\Delta T \equiv T_L - T_R$.

For a thin bond $\gamma_R << \gamma_L$ [see calculations by McSkimin, 1961, Table I, p. 15]. Then

$$\Delta T \simeq \left(0.111\, n - \frac{p\gamma_L}{324}\right)\frac{1}{f_R} \, . \qquad \text{(Eqn. A.3)}$$

Eqn. A.3 is the basic equation to be interpreted for the condition $n = 0$, i.e., no cyclic mismatch. Putting $n = 0$ in Eqn. A.3 yields $\Delta T(n=0) < 0$. So a necessary condition for proper cyclic matching is that $\Delta T < 0$. But note that for any $n < 0$, $\Delta T < 0$. Therefore, the condition $\Delta T < 0$ is not a sufficient condition for proper cyclic matching. Also note from Eqn. A.3 that for some $n \geq 1$, ΔT will be greater than zero. Then consider the following theorem.

For adjacent echoes in high density ($\rho > 3$ g/cm^3) - high elasticity ($V_p > 7$ km/sec, $V_s > 4$ km/sec) crystals, $\Delta T > 0$ whenever $n \geq 1$. Thus the proper cyclic match occurs at the last negative ΔT just before it turns positive, i.e., at the smallest negative ΔT in magnitude.

Procedure

Call the result of the theorem the "crossover condition."
It is illustrated by an example for a shear mode in garnet
(Fig. A.6 and Table A.1).

The assumptions of adjacent echoes, high density, and
high elasticity are important. For example, the crossover
condition is not always true for fused quartz [Papadakis,
1967]. Also examination of Eqn. A.3 shows that for some
p > 1 (several round trips between echoes), $\Delta T < 0$ for
n = 1.

The justification for the crossover condition is now
given. The assumption of a high density - high elasticity
crystal is immediately translated into a high value for the
acoustic impedance $Z = \rho V$ where ρ is the density and V
is the compressional or shear velocity. The assumption
of adjacent echoes sets p = 1 in Eqn. A.3. Then in order for
ΔT to be greater than zero for n = 1, γ_L must be less than
36°. To satisfy $\gamma_L < 36°$ for X-cut quartz transducers, the
impedance Z should be greater than about 20 [McSkimin and
Andreatch, 1962, Fig. 11, p.614]. For Y-cut quartz transducers,
Z should be greater than about 10 [McSkimin and Andreatch,
1962, Fig. 13, p.614]. Then for high density ($\rho > 3$ g/cm^3) -
high elasticity ($V_p > 7$ km/sec, $V_s > 4$ km/sec) crystals,
the cyclic match condition occurs at the last negative ΔT
before it turns positive.

b. Video-pulse-matching method.

Ambiguities still occurred, however, in determining the sign of ΔT in the course of an actual experiment. Changing the rf-frequency changed the pulse shape so the match at 0.9 f_R became uncertain. Furthermore, guided-wave effects could introduce spurious ΔT measurements. Proper cyclic matching was then determined by Papadakis' [1969] video-pulse-matching method. A video or square pulse rather than an rf-pulse was used for the electrical input to the transducer. In terms of the block diagram (Fig. A.3) a Velonex pulse generator was substituted for the Arenberg pulsed oscillator. The pulse had an amplitude of about 200 V and its width was 0.1 μsec. Because of the finite bandwidth of the transducer resonance, its spectrum was broad enough to encompass both the sharp phase fluctuation near a node and the large region of little fluctuation.

The first echo had the trident shape seen also in rock velocity measurements in which a square pulse input is used. The second echo had a portion of energy from each half cycle shifted one cycle because of delay in the transducer. The proper cyclic match was made as in Fig. A.7. The earlier of the two large peaks in the second echo was aligned with the maximum peak in the first echo. When the rf-pulse was substituted back for the square pulse, only a very minor adjustment in the reciprocal travel-time frequency was necessary;

Procedure

the proper cyclic match had already been effected.

An experiment of possible interest would be to test the effect of a one cycle mismatch on the measured pressure or temperature coefficients. Would the effect be large or small?

3. Changes of transducer resonance with pressure or temperature.

The transducer was bonded directly to the sample for both the pressure and temperature runs. As a result the transducer's resonant frequency will change slightly during a run [less than 1% over either 5 kb or 100 °C, McSkimin and Andreatch, 1962].

For the $n = 0$ condition and symbols as in Eqn. A.1,

$$\frac{\delta_o}{\delta} = \frac{\dfrac{T_o}{p} + \dfrac{\gamma_o}{360 \, f_o}}{\dfrac{T}{p} + \dfrac{\gamma}{360 \, f}} \qquad \text{(Eqn. A.4)}$$

Variables with a subscript zero refer to values at room conditions and unsubscripted variables refer to values at some pressure or temperature. Since $\dfrac{\gamma}{360 \, f} \ll \dfrac{T}{p}$, Eqn. A.4 becomes

Procedure

$$\frac{\delta_o}{\delta} = \frac{T_o}{T} \left[1 + \frac{P\gamma_o}{360\ f_o T_o} \left(1 - \frac{\frac{\gamma}{\gamma_o}}{\frac{f}{f_o}\frac{T}{T_o}} \right) \right] \qquad \text{(Eqn. A.5)}$$

What error results for not taking into account the change

in transducer resonance? That is, what is the magnitude of

$\frac{P\gamma_o}{360\ f_o T_o}$? For typical values ($\gamma_o = 10°$, $f_o = 20$ MHz,

$T_o = 1$ μsec) , the error in travel time is about 0.5%.

Then the error in the pressure or temperature derivatives

of the elastic constants is about 1 to 2%.

4. Incomplete damping of one echo before the next.

The incomplete damping of one echo before the next

arrived was quite a problem for a few compressional wave

modes (see Fig. A.8 for an example). The input rf-pulse had

a width of about 1/2 μsec, but returned echoes had a width

of about 1 μsec. Because of the short path lengths in the

crystals, some travel times were 1.1 μsec and caused the

blending of echoes. In addition side-wall reflections

could clutter returned echoes. The presence of a high noise

level resulted in phase shifts equivalent to an uncertainty

of 0.3% in the velocity. What was unknown was the relative

change in these phase shifts as a function of pressure or

temperature. The blending of echoes was probably the major

source of error and was a consequence of having small samples.

On the basis of cross checks from different modes, the

accuracy of pressure and temperature derivatives was about

5 and 10%, respectively.

5.   Trigger delay between channels in dual channel operation.

     Chung et al. [1969] mentioned a dual channel mode of

operation in which the oscilloscope sweep was on an alternate

mode. The amplitudes of the intensified echoes could then be

adjusted individually. I found that dual channel operation

could lead to a minor ambiguity. Because the triggering

levels of the two channels were not calibrated, a phase

lag or lead was introduced.

6.   Shear wave polarization misorientation.

     The shear wave polarization was aligned by eye to within

1 or 2°. A small misorientation meant that a minor amount

of energy would be propagated with the velocity of the shear

mode 90° to the one desired (assuming nondegenerate shear

modes). The second mode was never detected in the echo

train.

Procedure

7.   Summary of ambiguities.

The main source of error was a high background noise

level due to insufficient echo damping. The existence of

side-wall reflections contributed to spurious noise. Guided-

wave modes caused no problem if echoes away from nodes were

chosen. Cyclic mismatches could be avoided either by an

analysis of the McSkimin criterion or by video-pulse-matching.

The change in transducer resonant frequency as a function of

pressure or temperature could be neglected. Single channel

operation was preferred. The accuracy of zero pressure,

room temperature elastic constants was 0.5%. Pressure and

temperature derivatives were 5 and 10%, respectively.

Procedure

E. Reduction of raw data.

1. Pressure data.

The reciprocal travel-time frequency $f = 1/T$ where
T is the travel time was linear with pressure P. The raw
data were represented by a least squares line

$$\frac{f}{f_o} = 1 + b P \qquad \text{(Eqn. A.6)}$$

where b =   least squares slope

and f_o =   least squares zero pressure frequency.

(Note that the symbol f_o no longer refers to the rf-frequency
as in the previous section.)

The elastic constant C_{ij} is given by:

$$C_{ij} = \rho \, (2 \frac{p}{m} 1 \, f)^2 \qquad \text{(Eqn. A.7)}$$

where ρ =   density

     1 =   sample path length

     p =   number of round trips between
            echoes used

     m =   integer multiple of reciprocal
            of travel time; m/f = travel time
            between echoes used

     f =   some multiple m of $1/T$

Procedure

Then

$$\frac{\partial C_{ij}}{\partial P} = (\chi - 2\beta + 2b) \; C_{ij}^{o} \qquad \text{(Eqn. A.8)}$$

where χ = volume compressibility, kb^{-1}

β = linear compressibility in propagation direction, kb^{-1}

b = slope of $\frac{f}{f_o}$ versus P line, kb^{-1}

C_{ij}^{o} = elastic constant at zero pressure, kb .

2. Temperature data.

For temperature runs the elastic constant C_{ij} is given by:

$$C_{ij}(T) = \rho_o \; (2 \, \frac{p}{m} \, l_o \, f(T))^2 \; [1 + (2\alpha_1 - \alpha_V)\Delta T] \qquad \text{(Eqn. A.9)}$$

where α_V = volume thermal expansion, $°C^{-1}$

α_1 = linear thermal expansion in propagation direction, $°C^{-1}$

A least squares fit for the coefficient $\partial C_{ij}/\partial T$ was then made on the C_{ij} as a function of T.

Procedure

F.   Pressure system.

   Pressure runs were made to 5 kb in a standard liquid-medium (petroleum ether) pressure system (Fig. A.9).   A cylindrical hydraulic ram pushed a piston of smaller area into the vessel so that pressure behind the ram was intensified by the ratio of the areas.   The top seal was an O-ring and the bottom seal was an O-ring and brass retaining ring assembly.

   Pressures were read both on a calibrated Heise gauge and on a digital voltmeter.   The digital voltmeter recorded the output of a linear bridge amplifier [Philbrick Researches, Inc., 1966, section III.80] in which the gain was linear with the resistance change in a manganin coil (Fig. A.10).   The amplifier was calibrated so that 1 mV = 1 bar.   The pressure in the vessel could be held to ±2 bar for periods of thirty minutes.   Readings were taken at 500 bar intervals every twenty minutes to allow the vessel to equilibrate to room temperature (20 °C).

Procedure

G.   Temperature system.

A non-inductively wound tubular oven was used to 100 °C
for temperature runs.   The sample holder was directly inserted
into a brass tube in the oven.   Mullite was plugged into the
ends as an insulator.   Temperature could be maintained to
±0.2 °C simply by allowing the sample to equilibrate twenty
minutes for some fixed current value in the oven windings.
The temperature was read on a potentiometer with a copper-
constantan thermocouple in contact with the sample.   The
thermocouple junction was shielded from direct radiation from
the windings.   The temperature corresponding to a thermocouple
voltage was determined from a quadratic fit to standard
emf tables:

$$T = -0.2135 + 25.4442\ E - 0.4918\ E^2 \qquad \text{(Eqn. A.10)}$$

where   T = temperature in °C

E = copper-constantan thermocouple emf in mV

The formula fitted the tables to within 0.1 °C.

The most difficult problem in making temperature measure-
ments was in maintaining a good bond between the sample and
the transducer.   Above 100 °C an epoxy bond was not very
satisfactory, so this was the upper temperature limit used.
The 20 to 100 °C temperature range provided just about the
same changes in elastic constants as did the 0 to 5 kb pressure
range.

Procedure

H. Density determination.

Since an elastic constant C_{ij} is the product of a density and a velocity squared, accurate density determinations were necessary. Both hydrostatic weighing and X-ray densities were measured. Agreement between the two was within 0.3 to 0.5%. The hydrostatic weighings were made in the MIT Crystal Physics Laboratory with ethylene bromide $(C_2H_4Br_2)$ as the immersion fluid. The apparatus was described in Smakula and Sils [1955].

Procedure

References

Chung, D.H., D.J. Silversmith, and B.B. Chick, A modified
ultrasonic pulse-echo-overlap method for determining sound
velocities and attenuation of solids, Rev. Sci. Inst., 40,
718-720, 1969.

Cullity, B.D., Elements of X-ray Diffraction, 514 pp.,
Addison-Wesley, Reading, Mass., 1956.

McSkimin, H.J., Pulse superposition method for measuring
ultrasonic wave velocities in solids, J. Acoust. Soc. Am.,
33, 12-16, 1961.

McSkimin, H.J., and P. Andreatch, Analysis of the pulse
superposition method for measuring ultrasonic wave velocities
as a function of temperature and pressure, J. Acoust. Soc.
Am., 34, 609-615, 1962.

Papadakis, E.P., Ultrasonic attenuation and velocity in
three transformation products in steel, J. Appl. Phys., 35,
1474-1482, 1964.

Papadakis, E.P., Ultrasonic phase velocity by the pulse-echo-
overlap method incorporating diffraction phase corrections,
J. Acoust. Soc. Am., 42, 1045-1051, 1967.

Papadakis, E.P., Effect of multimode guided-wave propagation
on ultrasonic phase velocity measurements: problem and
remedy, J. Acoust. Soc. Am., 45, 1547-1555, 1969.

Procedure

Philbrick Researches, Inc., <u>Applications</u> <u>Manual</u> <u>for</u> <u>Computing</u>
<u>Amplifiers</u> <u>for</u> <u>Modelling</u>, <u>Measuring</u>, <u>Manipulating</u> <u>and</u> <u>Much</u>
<u>Else</u>, 115 pp., Nimrod Press, Boston, 1966.

Smakula, A., and V. Sils, Precision density determination of
large single crystals by hydrostatic weighing, <u>Phys</u>. <u>Rev</u>.,
<u>99</u>, 1744-1746, 1955.

Table A.1

Experimental test of cross-over condition for shear mode S[1$\bar{1}$0] in [110]-direction in garnet.

	p=1				p=2		
n	T_L	T_R	ΔT	n	T_L	T_R	ΔT
-3	2.42547	2.43751	-0.01204	-	--	--	--
-2	2.47868	2.48765	-0.00897	-2	5.06660	5.07472	-0.00812
-1	2.53216	2.53765	-0.00549	-1	5.11941	5.12474	-0.00533
0	2.58591	2.58754	-0.00163	0	5.17239	5.17504	-0.00265
+1	2.63967	2.63759	+0.00208	+1	5.22561	5.22529	+0.00032
+2	2.69306	2.68814	+0.00492	+2	5.27880	5.27568	+0.00312
+3	2.74679	2.73804	+0.00875	+3	5.33219	5.32629	+0.00590
-	--	--	--	+4	5.38561	5.37709	+0.00852

Table A.1 (continued)

Experimental test of cross-over condition for shear mode

S[1$\bar{1}$0] in [110]-direction in garnet.

The subscript L refers to echo-overlap readings taken at a carrier frequency 10%
below resonance R.

$$T = \text{travel time in sample, } \mu\text{sec}$$

$$\Delta T = T_L - T_R, \quad \mu\text{sec}$$

$$n = \text{number of cycles of mismatch}$$

The results are plotted in Fig. A.6.

p=1 refers to one round trip in the sample and

p=2 refers to two round trips in the sample.

Procedure

Figure Captions

Fig. A.1. Laue back-reflection photograph showing four-fold axis of symmetry in pleonaste. The center of the X-ray beam is indicated by the intersection of the horizontal and vertical line segments connecting the four black spots or fiducial points. The center of symmetry is indicated by the intersection of the line segments connecting Laue spots related by inversion symmetry. When the two points of intersection are one, orientation is perfect. The scale for misorientation is indicated by the Greninger chart.

Fig. A.2. Schematic of assembly for making electrical contact with a coaxially-plated transducer.

Fig. A.3. Block diagram of ultrasonic equipment [after Chung et al., 1969]. (1) Hewlett-Packard model 606B signal generator (2) Hewlett-Packard model 524L electronic counter (3) Airtech model DD-103 decade divider (4) General Radio model 1217-C unit pulse generator (5) Arenberg model PG-650C pulsed oscillator (6) Matec model 5-30 MHz broad band receiver (7) Matec model 2470 attenuation recorder with double delay strobe (8) Tektronix model 546 oscilloscope.

Procedure

Fig. A.4.   (a) Typical pulse-echo train.   The picture is for

a shear wave polarized in the [1$\bar{1}$0]-direction and propagating

in the [110]-direction in garnet.   The time base is 10 μsec/

cm.   (b) Overlap of two echoes.

Fig. A.5.   Guided-wave mode effect appearing as modulation of

the echo train envelope.   The picture is for a shear wave

polarized in the [1$\bar{1}$0]-direction and propagating in the

[110]-direction in GeO_2.   The time base 20 μsec/cm.

Fig. A.6.   Crossover condition for proper cyclic matching.

Plotted are the experimentally determined $\Delta T = T_L - T_R$

versus the number of cycles of mismatch n for p = 1 and

p = 2.   The ΔT values are for a shear wave polarized in the

[001]-direction and propagating in the [110]-direction in

garnet.   Note that in accord with Eqn. A.3, ΔT is smaller

for p = 2 than for p = 1.   If the cross plotted at n = 1

had been very slightly negative, application of the smallest-

negative-ΔT-in-magnitude criterion would have lead to a one

cycle mismatch.   However, for p = 1 (adjacent echoes) in a

high acoustic impedance crystal, the distinction is quite

clear.

Fig. A.7.   Proper cyclic-match overlap for video-pulse-
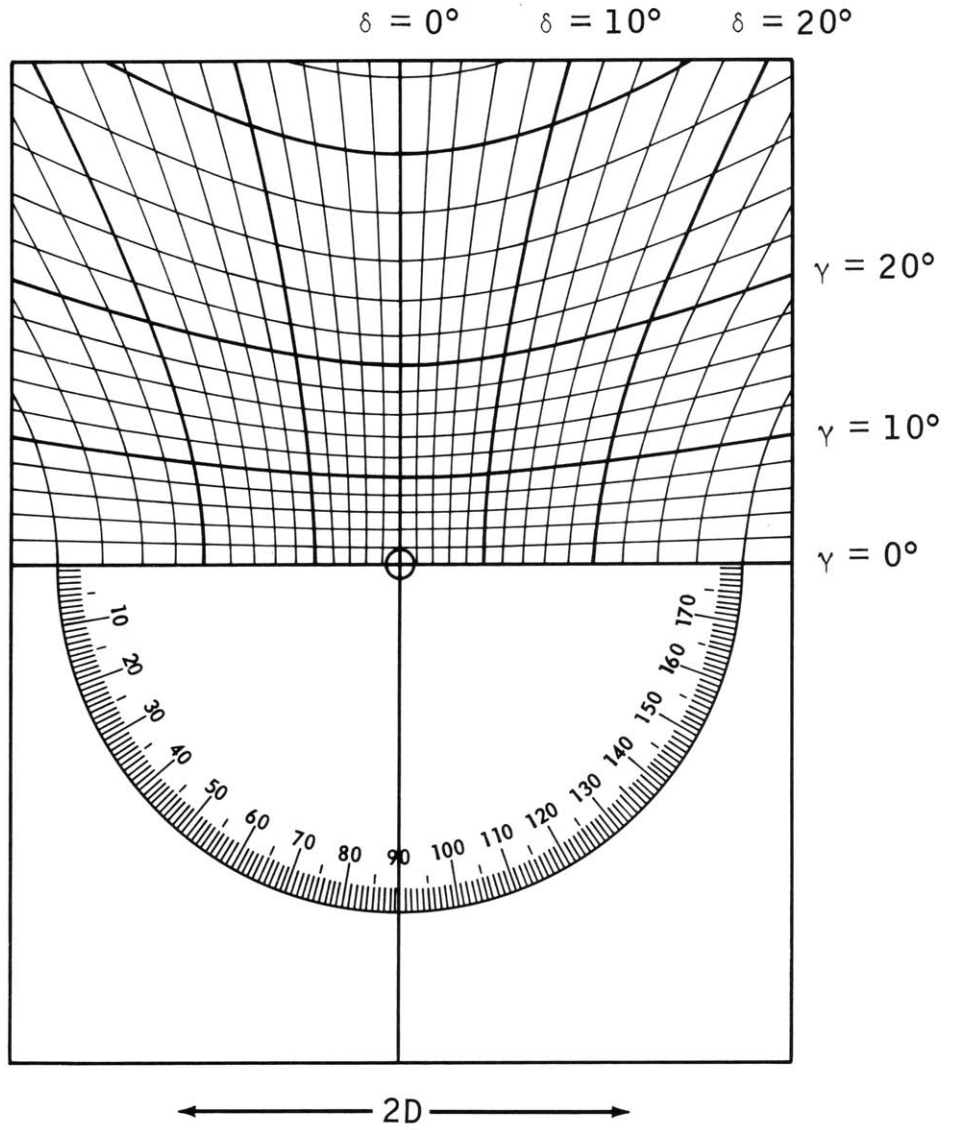
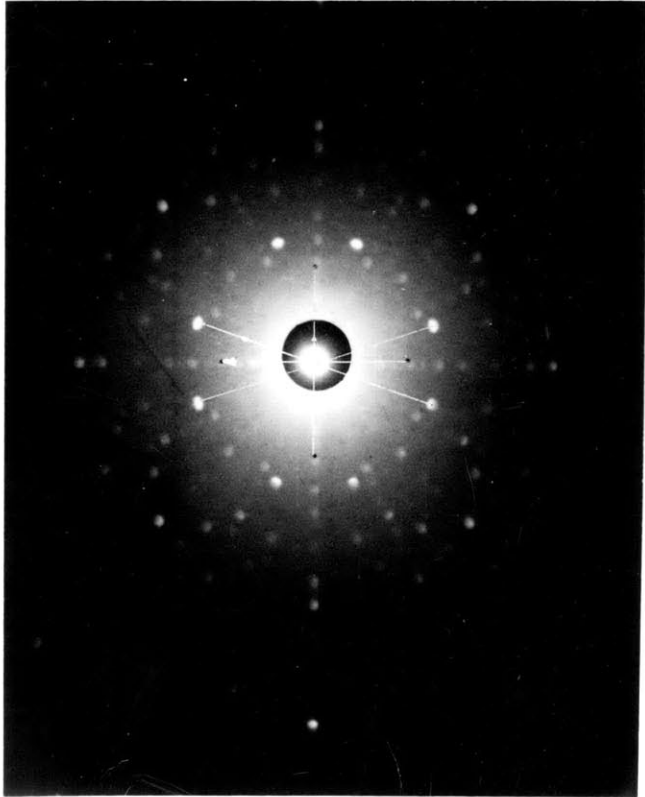matching method [after Papadakis, 1969, p. 1553].

Procedure

Fig. A.8. Incomplete damping of one echo before the next

arrived. The picture is for a compressional wave propagating

in the [100]-direction in pleonaste. The time base is

2 μsec/cm.

Fig. A.9. Schematic of pressure system.

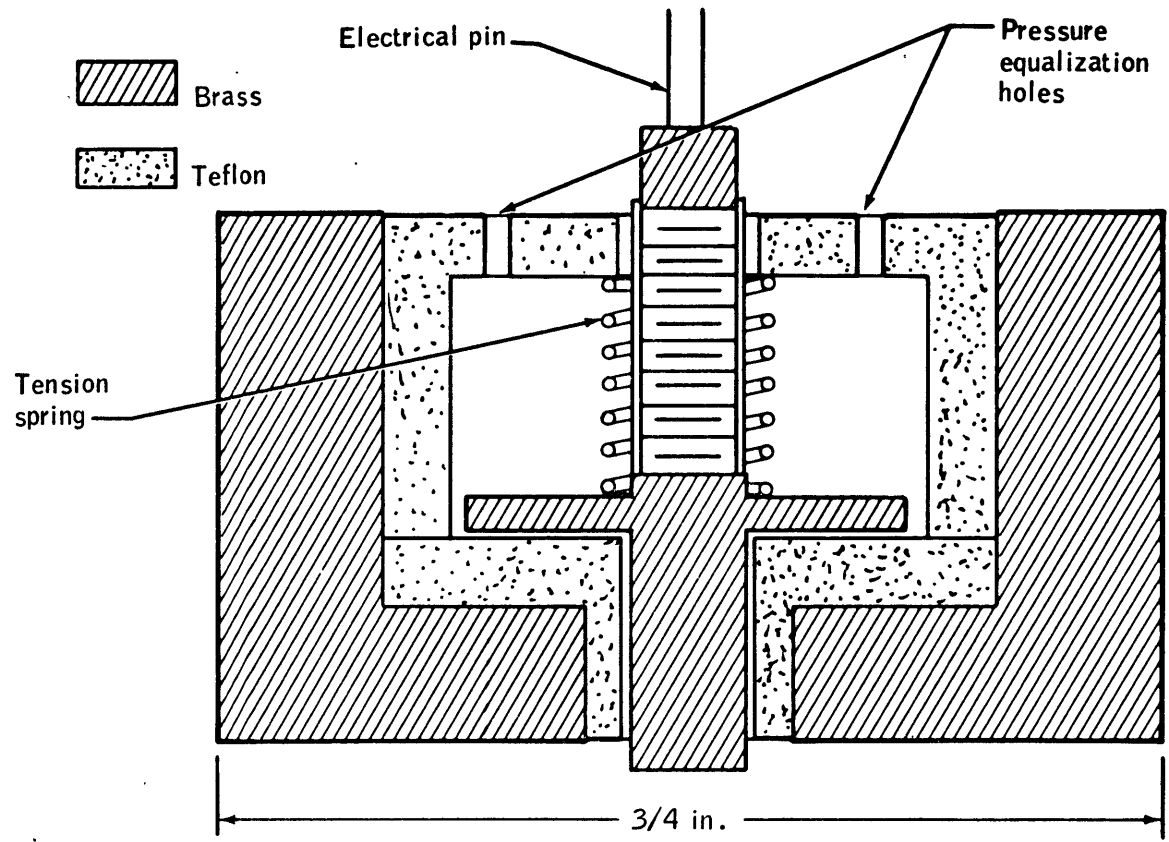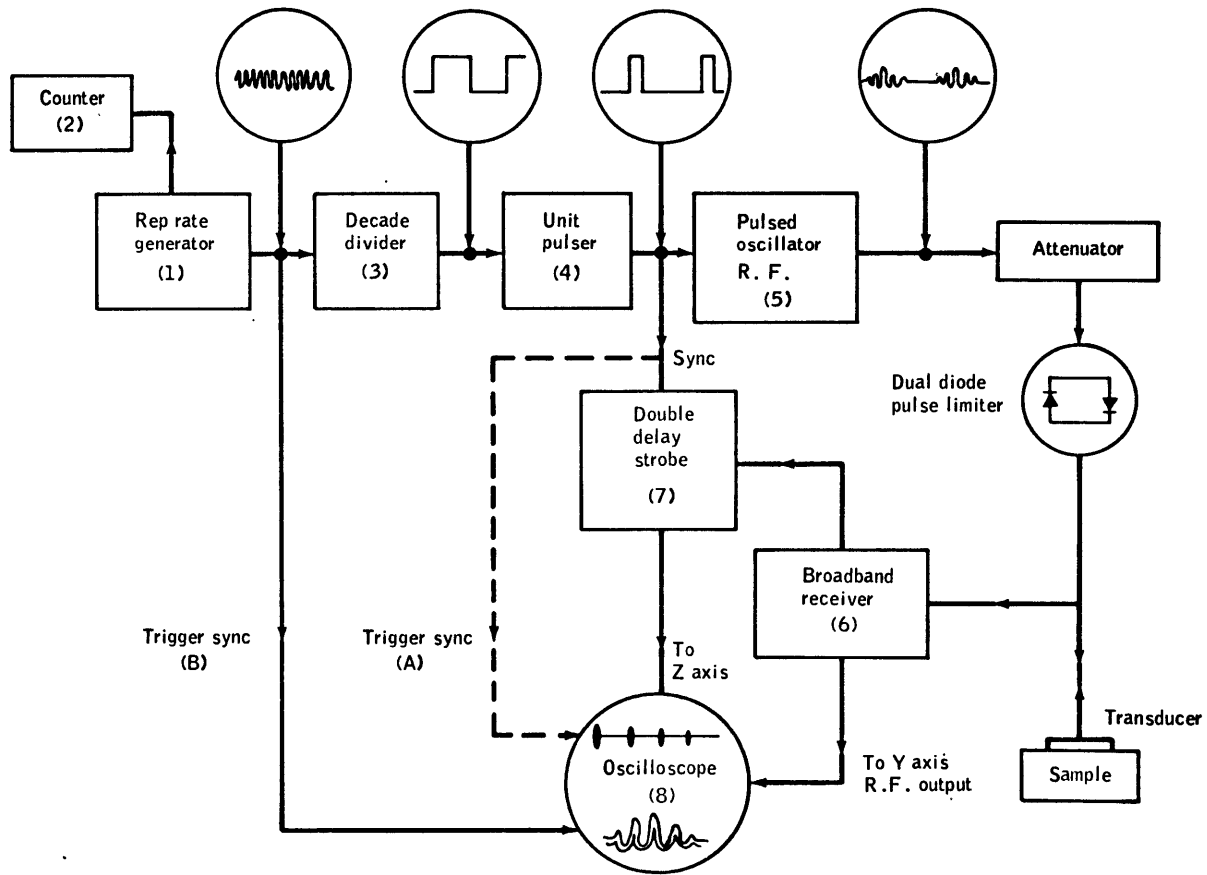Fig. A.10. Schematic of manganin pressure sensor.

Fig. A.1

Fig. A.2

Brass

Teflon

Electrical pin

Pressure
equalization
holes

Tension
spring

3/4 in.

Fig. A.3

(a)
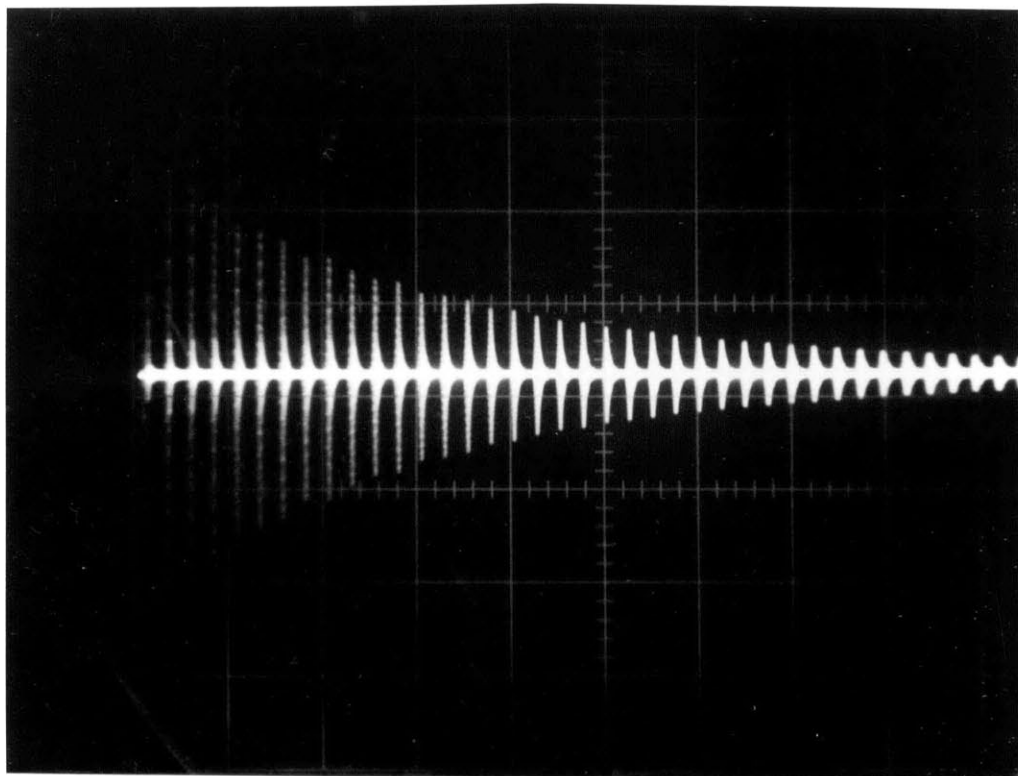
(b)
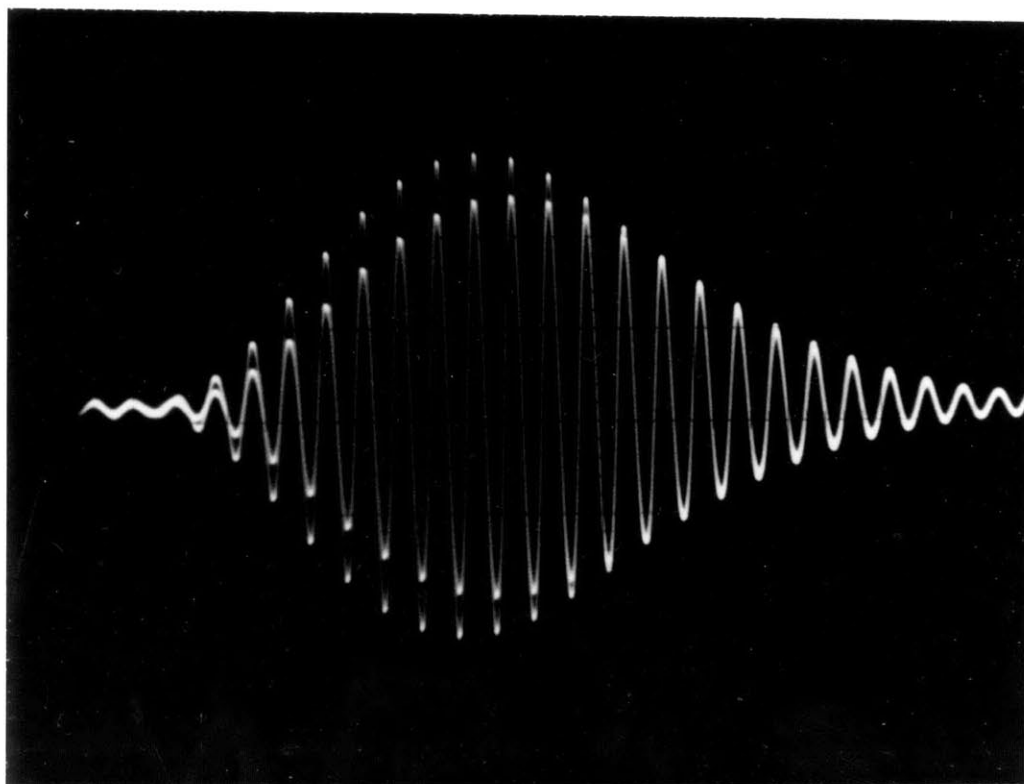
Fig. A.4
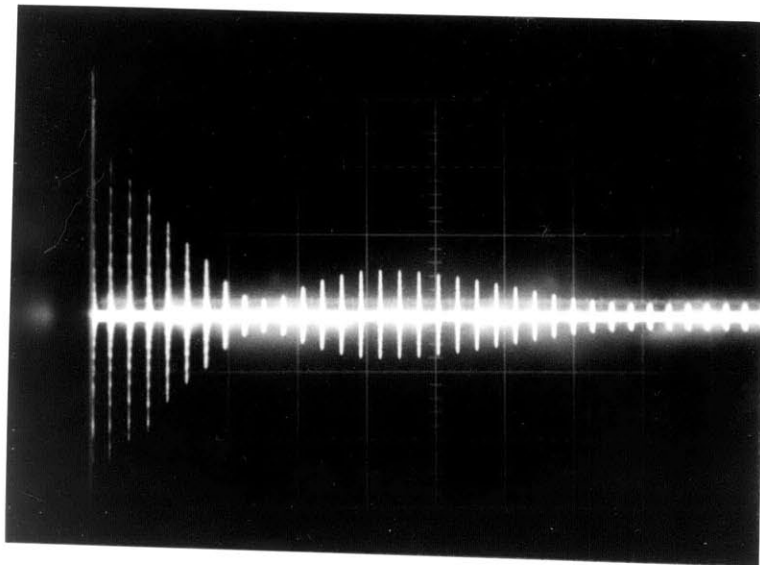
Fig. A.5
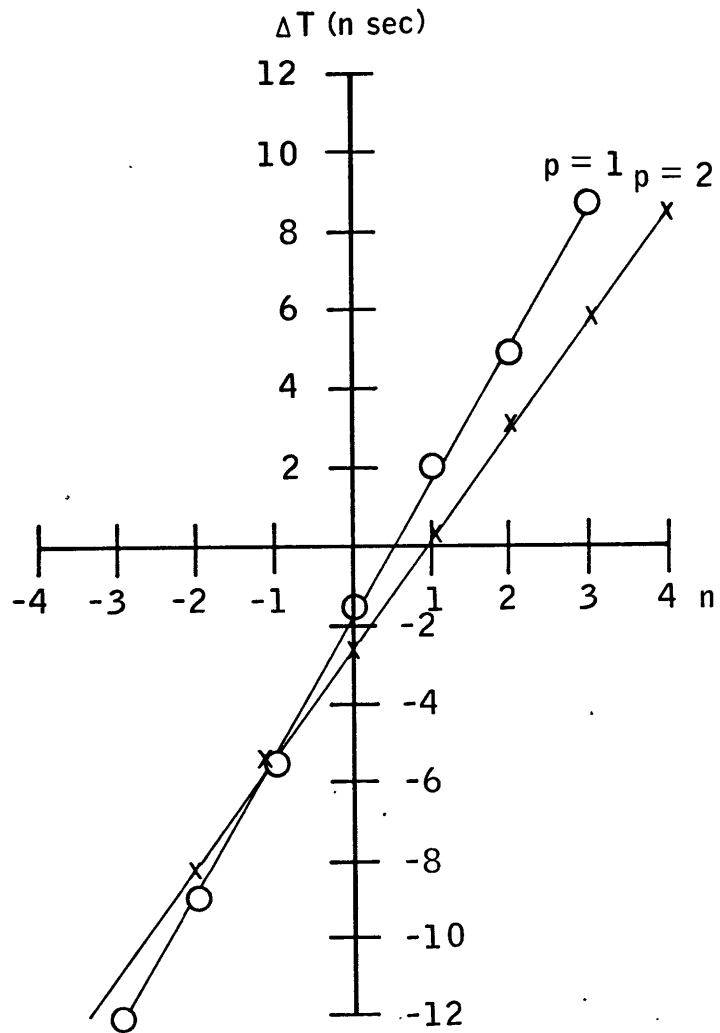
Fig. A.6
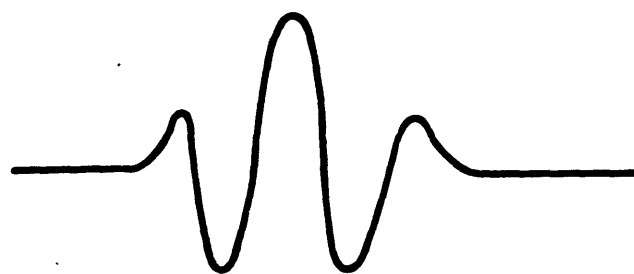
First echo

Second echo
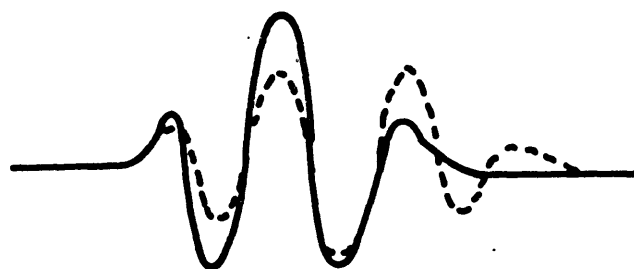
Proper overlap

Fig. A.7

Fig. A.8

HEISE
0-7500

BARS

0-2000

BARS

HIGH
PRESSURE
VESSEL

HI-P
VALVE

DUMP
VALVE

DUMP

VALVE

AIR LINE
VALVE

HYDRAU-
LIC
CYLINDER

OIL RESERVOIR

PET. ETHER RESERVOIR

AIR
PUMP

HAND
PUMP
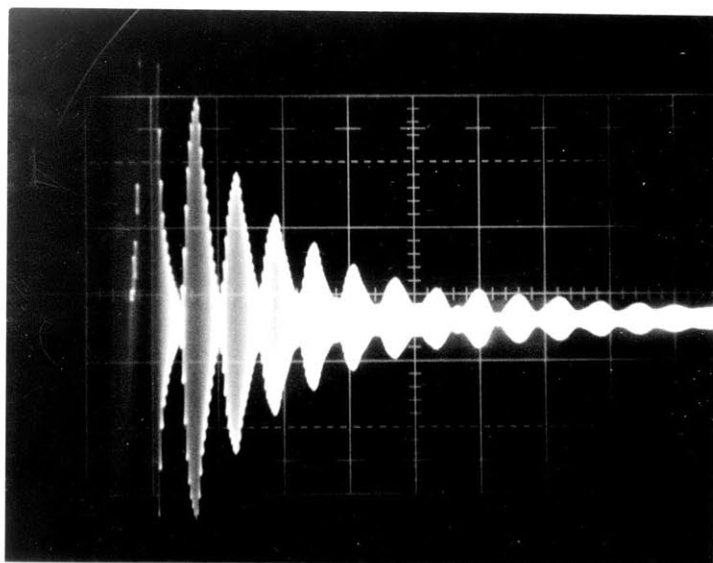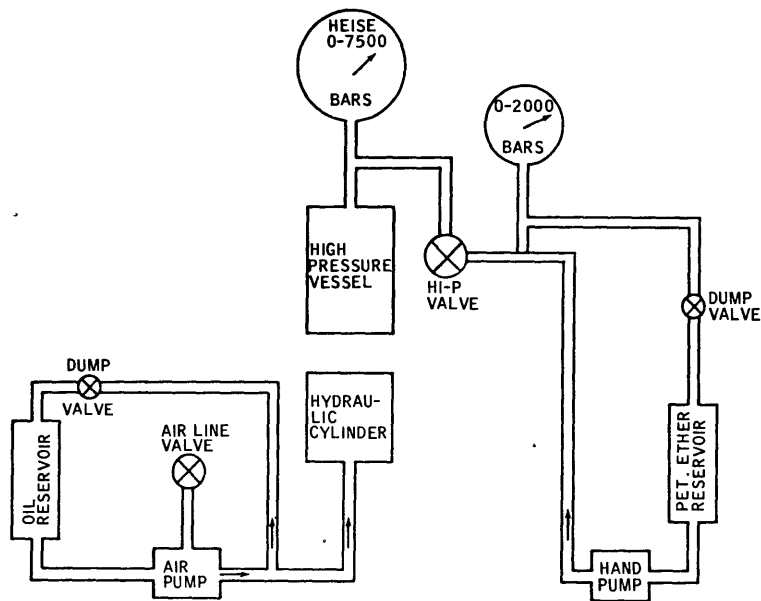
Fig. A.9

Fig. A.10
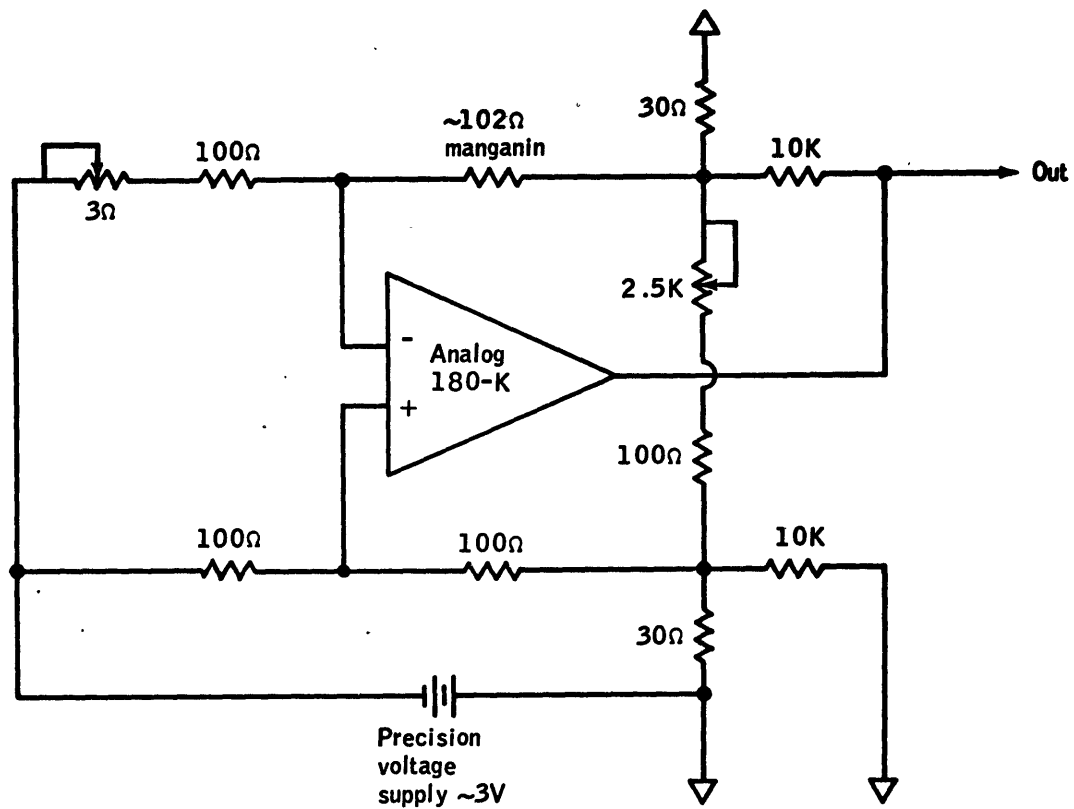
Pressure data

Appendix B: Least squares fits to pressure data.

For any pressure run the individual frequency readings at different pressures were least squares fit to a straight line. The slope of the least squares line $\frac{f}{f_o} = 1 + bP$ is given in Tables B.1, B.2, and B.3 for the individual pressure runs in pleonaste, GeO_2, and spessartite-almandine, respectively. The standard deviation of the slope is also given.

Table B.1

Pleonaste least squares fits to raw pressure data. $\dfrac{f}{f_o} = 1 + bP$

Mode	Direction	Polarization	Elastic constant	Path length	Number of data points	b, Mb^{-1}	σ_b, Mb^{-1}	$\partial C_{ij}/\partial P$
L	[110]	---	C_L	6.645	19	0.760	0.008	6.08
L	[110]	---	C_L	6.645	9	0.728	0.025	5.86
T	[110]	[1$\bar{1}$0]	C_S	6.645	20	-0.084	0.002	0.00
T	[110]	[1$\bar{1}$0]	C_S	6.645	19	-0.167	0.013	-0.09
T	[110]	[001]	C_{44}	6.645	9	0.153	0.002	0.69
T	[110]	[001]	C_{44}	6.645	10	0.194	0.003	0.80
T	[100]	Any	C_{44}	4.933	14	0.179	0.012	0.76
L	[100]	---	C_{11}	4.933	17	0.808	0.010	4.82
L	[100]	---	C_{11}	4.933	21	0.783	0.008	4.69

σ_b = standard deviation of b, $\quad C_L = 1/2 \, (C_{11} + C_{12} + 2C_{44})$, $\quad C_S = 1/2 \, (C_{11} - C_{12})$

L = longitudinal $\qquad$ T = transverse

Table B.2

GeO$_2$ least squares fits to raw pressure data. $\quad \dfrac{f}{f_o} = 1 + bP$

Mode	Direction	Polarization	Elastic constant	Path length	Number of data points	b, Mb^{-1}	σ_b, Mb^{-1}	$\partial C_{ij}/\partial P$
L	[110]	---	C_{L_1}	9.5225	24	1.084	0.006	11.61
L	[110]	---	C_{L_1}	9.5225	23	1.085	0.006	11.62
T	[110]	[1$\bar{1}$0]	C_S	9.5225	23	-0.508	0.004	-0.71
T	[110]	[1$\bar{1}$0]	C_S	9.5225	11	-0.543	0.006	-0.76
T	[110]	[1$\bar{1}$0]	C_S	9.5225	15	-0.442	0.008	-0.61
T	[110]	[001]	C_{44}	9.5225	21	0.514	0.004	1.76
T	[1$\dot{1}$0]	[001]	C_{44}	9.5225	23	0.529	0.004	1.81
T	[001]	Any	C_{44}	6.7686	22	0.399	0.004	1.73
T	[100]	[001]	C_{44}	6.8669	12	0.537	0.004	1.83
L	[001]	---	C_{33}	6.7686	23	0.380	0.003	6.20
L	[001]	---	C_{33}	6.7686	19	0.435	0.008	6.86
L	[001]	---	C_{33}	6.7686	15	0.468	0.018	7.26
L	[001]	---	C_{33}	6.7686	16	0.403	0.007	6.48

(continued)

Mode	Direc-tion	Polari-zation	Elastic constant	Path length	Number points	b	σ_b	$\partial C_{ij}/\partial P$
L	[001]	---	C_{33}	6.7686	13	0.391	0.007	6.33
L	[100]	---	C_{11}	6.8669	13	0.857	0.011	5.97
L	[100]	---	C_{11}	6.8669	11	0.991	0.013	6.90
L	[100]	---	C_{11}	6.8669	13	0.951	0.009	6.64
T	[100]	[010]	C_{66}	6.8669	16	0.762	0.006	4.10
T	[100]	[010]	C_{66}	6.8669	11	0.762	0.007	4.10
T	[101]	[10$\bar{1}$]	C_{T_2}	4.9878	14	0.529	0.004	1.60
T	[101]	[10$\bar{1}$]	C_{T_2}	4.9878	18	0.490	0.009	1.49
L	[101]	---	C_{L_2}	4.9878	15	0.628	0.041	7.16

σ_b = standard deviation of b, $C_{L_1} = 1/2 \ (C_{11} + C_{12} + 2C_{66})$, $C_S = 1/2 \ (C_{11} - C_{12})$

$C_{L_2} = A + B$, $C_{T_2} = A - B$ where $A = 1/4 \ (C_{11} + C_{33} + 2C_{44})$

and $B = 1/4 \ [(C_{11} - C_{33})^2 + 4 \ (C_{13} + C_{44})^2]^{1/2}$

L = longitudinal   T = transverse

Table B.3

Garnet least squares fits to raw pressure data. $\frac{f}{f_o} = 1 + bP$

Mode	Direction	Polarization	Elastic constant	Path length	Number of data points	b, Mb^{-1}	σ_b, Mb^{-1}	$\partial C_{ij}/\partial P$
L	[110]	---	C_L	6.217	16	0.984	0.008	6.59
L	[110]	---	C_L	6.217	16	1.023	0.009	6.82
L	[110]	---	C_L	6.217	16	1.048	0.017	6.95
T	[110]	[1$\bar{1}$0]	C_S	6.217	15	0.759	0.004	1.68
T	[110]	[1$\bar{1}$0]	C_S	6.217	17	0.741	0.003	1.64
T	[$\bar{1}$10]	[001]	C_{44}	6.217	14	0.585	0.004	1.29
T	[110]	[001]	C_{44}	6.217	16	0.584	0.002	1.28

σ_b = standard deviation of b, $C_L = 1/2\ (C_{11} + C_{12} + 2C_{44})$, $C_S = 1/2\ (C_{11} - C_{12})$.

L = longitudinal   T = transverse

Biographical Note

Birth date and place: 14 September 1946 in Shanghai, China.

Marital status: Married with one child.

Education:

Grade	School	Location	Years	Degree
K-2	Union Hill	Boulder, Colo.	1951-1954	-----
3	Leal	Urbana, Ill.	1954-1955	-----
4-6	Wiley	Urbana, Ill.	1955-1958	-----
7-9	University High	Urbana, Ill.	1958-1960	-----
10-12	Wisconsin High	Madison, Wisc.	1960-1963	-----
13-16	U. Wisconsin	Madison, Wisc.	1963-1966	B.A.
17-18	Harvard U.	Cambridge, Mass.	1966-1968	A.M.
19-21	MIT	Cambridge, Mass.	1968-1971	Ph.D.

Summer jobs:

Title	Description	Institution	Location	Year
Physicist	X-ray analyzed glass samples	Corning Glass Works	Corning, New York	1966
Instructor	Taught elementary calculus	Corning Community College	Corning, New York	1967

Teaching assistantships: Physics of the Earth (1970)
Planetary Physics and Chemistry (1971)

Fellowships: NSF (1966-1968), NDEA (1968-1970)
Chevron (1970-1971)

Honorary societies: Phi Beta Kappa (1966), Sigma Xi (1969)

Co-authored publications:

On the calculation of the seismic parameter ϕ at high pressure and high temperatures, J. Geophys. Res., 75, 5113-5120, 1970.

The elastic constants of an iron-bearing spinel--$(Mg_{75}Fe_{25})Al_2O_4$ (abstract), Trans. Am. Geophys. Union, 52, 358, 1971.

Single Crystal Elastic Constants and Calculated Aggregate Properties: A Handbook, 2nd edition, 370 pp., MIT Press, Cambridge, 1971.

Elastic properties of Apollo 12 rocks, in Proceedings of the Second Lunar Science Conference, Vol. 3, edited by A. A. Levinson, MIT Press, Cambridge, 1971, in press.